Syracuse University

SURFACE

Dissertations - ALL   SURFACE

December 2015

Characterization and Chemical Kinetic Analysis of the Ignition of Representative Conventional and Bio-Derived Fuels

Mazen Eldeeb
Syracuse University

Follow this and additional works at: https://surface.syr.edu/etd

Part of the Engineering Commons

ABSTRACT

Fossil fuels are the main energy source in the world. However, they are responsible for negative environmental impacts, such as global climate change and rising sea levels. Biofuels are an environmentally friendly alternative which can substitute fossil fuels without major engine modifications, especially in the transportation sector. Furans, a class of biofuels, are considered as possible alternative fuels for SI engines. They can be produced from sugars, derived from non-food biomass sources. This thesis is a contribution to fundamental characterization of their combustion properties.

Reactivity trends in furan combustion are established through ignition delay measurements of selected furans; 2,5-dimethyl furan (DMF), 2-methyl furan (2-MF), and furan. The isomer effect on the ignition of alkylated furans is also investigated to understand the general trends between dimethyl and ethyl isomers of cyclic fuel components. Since near term use of biofuels involves blends with fossil fuels, the relative ignition behavior of the least reactive furan, DMF, the gasoline surrogate, *iso*-octane, and their blends, is investigated. Experiments are carried out in a shock tube, a reactor that can generate instantaneous high temperature and pressure conditions by means of reflected shock wave, leading to chemical reactions and subsequent ignition of a test mixture of fuel and oxidizer.

Experimental results are compared with chemical kinetic model simulations and the models are analyzed to gain insight on leading chemical pathways. The experimental results for furans and *iso*-octane are compared to the most recent chemical kinetic models of each fuel and a combined DMF/iso-octane model is developed for the analysis of fuel blend combustion. The

new blend model is used to clarify the chemical interactions during ignition of fuel blends.

The thesis also considers the ignition of saturated furans. In this respect the ignition behavior of tetrahydrofuran (THF) and methyl tetrahydrofuran (MTHF) is investigated to establish relative reactivity trends. The results are put into context by comparing with the unsaturated furan, 2-MF.

Cyclic fuel components of non-biofuel nature are considered. The high-temperature auto-ignition delay times of dimethyl and ethyl isomers of cyclohexane are carried out behind reflected shock waves to establish reactivity differences between these dimethyl and ethyl isomers, which could further be explored in chemical kinetic modeling. The study is designed to test whether the observed trend is indicative of general reactivity differences between dimethyl and ethyl isomers of cyclic hydrocarbons, oxygenated or non-oxygenated. The ignition delay times of ECH are compared to model predictions to test the model performance. The pronounced differences in the high-temperature ignition delay times of these isomers are clearly established using the shock tube technique and motivate further mechanistic explorations of distinguishing reaction pathways, without necessarily invoking the more complex low-temperature chemistry.

With regards to model reduction, the existing Alternate Species Elimination (ASE) model reduction method is employed for the reduction of recently reported *iso*-octane and n-heptane models. The ASE approach is expanded into a stochastic species sampling approach, referred to as the Stochastic Species Elimination (SSE) method. The SSE method allows for a linear reduction process, and involves new features leading to reduced computational resource requirements, compared to the standard ASE method. Larger systems, such as the recent literature model of n-octanol, are approached with the SSE method with multiple species sampling, which allows for a less time consuming model reduction process. Resulting skeletal models are shown to adequately predict ignition delay times as well as flame propagation, compared to the predictions of the detailed models.

The work advances understanding of biofuel combustion. The established reactivity trends between the various fuels investigated in this work is of great importance to transportation fuel technology. The resulting experimental data sets are expected to fill the gap in the understanding of furans and gasoline combustion. The combined DMF/*iso*-octane model is a main contribution that allows for better insight into the combustion chemistry of furans, *iso*-octane, and their blends. Further, the proposed SSE model reduction method contributes to the use of combustion chemistry in practical combustion analysis in the form of cost-effective reduced models.

Characterization and Chemical Kinetic Analysis of the Ignition of Representative Conventional and Bio-Derived Fuels

by

Mazen A. Eldeeb

B.S., Cairo University, 2008

M.S., Cairo University, 2010

D I S S E R T A T I O N

Submitted in partial fulfillment of the requirements for the degree of

Doctor of Philosophy in *Mechanical Engineering*

Syracuse University

December 2015

Acknowledgment

I am greatly indebted to my advisor, Dr. Benjamin Akih-Kumgeh, for all the support he has given me during my doctoral studies. Dr. Akih-Kumgeh has been an excellent mentor to have. His dedication, perseverance and unwavering integrity are simply infectious. His belief in enabling young researchers to address challenging problems has helped me to develop a unique perspective of looking at the problems encountered in combustion science and engineering. Because of his guidance, I am a better researcher now than three years ago.

I wish to thank the members of my dissertation committee: Prof. Jeonmin Ahn, Prof. Jesse Bond, Prof. Thong Dang, Dr. Shalabh Maroo, and Prof. Jianshun Zhang for generously offering their time, support, guidance and good will throughout the preparation and review of this document.

I also owe great gratitude to the professors at Syracuse University: Prof. H. E. Khalifa for his continued interest in my academic progress during my time at SU. I thank Prof. John Dannenhoffer for showing genuine interest in addressing any issues I might have during my first semester at SU. I thank Prof Alan J. Levy for his continuous encouragement and appreciation of my efforts as a student and a teaching assistant. I thank Dr. Shalabh Maroo again for treating me very respectfully during my time as a teaching assistant.

I'm also indebted to all my friends and lab mates at the Thermodynamics and Combustion Lab, who have given me much support. I would like to thank Nathan Peters, for being a good friend and constantly taking interest in my work and progress. I would like also to thank

Contents

Appendices 134

List of Figures

List of Tables

To my fuel...

To Noha...

To my spark...

To Eyad...

Introduction and literature review

1.1   Background and motivation

Fossil fuels are the main energy source in the world; they account for about 82% of the global energy consumption [1]. However, they also account for 57% of the greenhouse gas emissions [2], which are responsible for global climate change and rising sea levels. One of the main challenges to the society is the development of affordable and environmentally friendly energy sources to replace fossil fuels in the future. One promising alternative is the use of biofuels, which can substitute fossil fuels without major modifications to the present engine technology. Moreover, they have significantly lower greenhouse gas emissions than fossil fuels, because of CO_2 recycling through agricultural activities. These properties promote biofuels as alternative fuels, especially in the transportation sector which accounts for 21% of the global energy consumption [1]. Therefore, the fundamental combustion properties of biofuels need to be explored with the purpose of developing and validating detailed and reduced chemical kinetic models. Fuel-flexible combustion technology is advanced through validated scientific models which can be used for computer-aided development of novel combustion engines, ultimately aimed at the development of clean and efficient transportation systems, as shown in Figure 1.1.
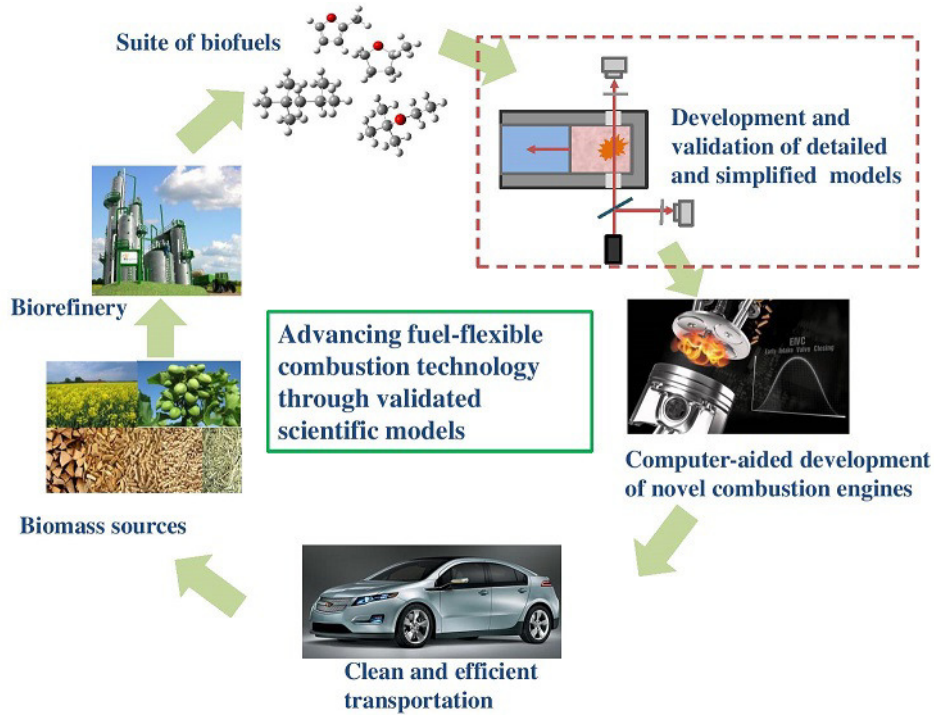
Figure 1.1: A schematic of the process of advancing flexible-fuel technology.

Among biofuels are alcohols, biodiesels, and furans. In transportation systems, spark ignition (SI) engines are the most dominant technology worldwide. Alcohols are the most widely-used biofuels for SI engines, due to the established fuel processing infrastructure and also their resistance to engine knock. Ethanol has a research octane number (RON) of 110 [3], but a low energy density of 20 MJ/L. Bio-alcohols as first-generation biofuels are mostly produced from food sources such as corn. Moreover, biofuels with higher energy densities and higher resistance to undesirable engine knock are needed. A class of bio-derived fuels known as furans is considered as good alternative fuels for SI engines. They have a potential for mass production from sugars that are derived from second-generation biomass [4–7], and they also possess favorable combustion properties. The production process of 2,5-dimethyl furan (DMF) and 2-methyl furan (2-MF) from fructose presented by Román-Leshkov et al. [4] is illustrated in Figure 1.2. Compared to ethanol, the furan, 2,5-dimethyl furan (DMF), has a higher energy density of 30 MJ/L, and it is shown to have better knock resistance with an RON of 119.
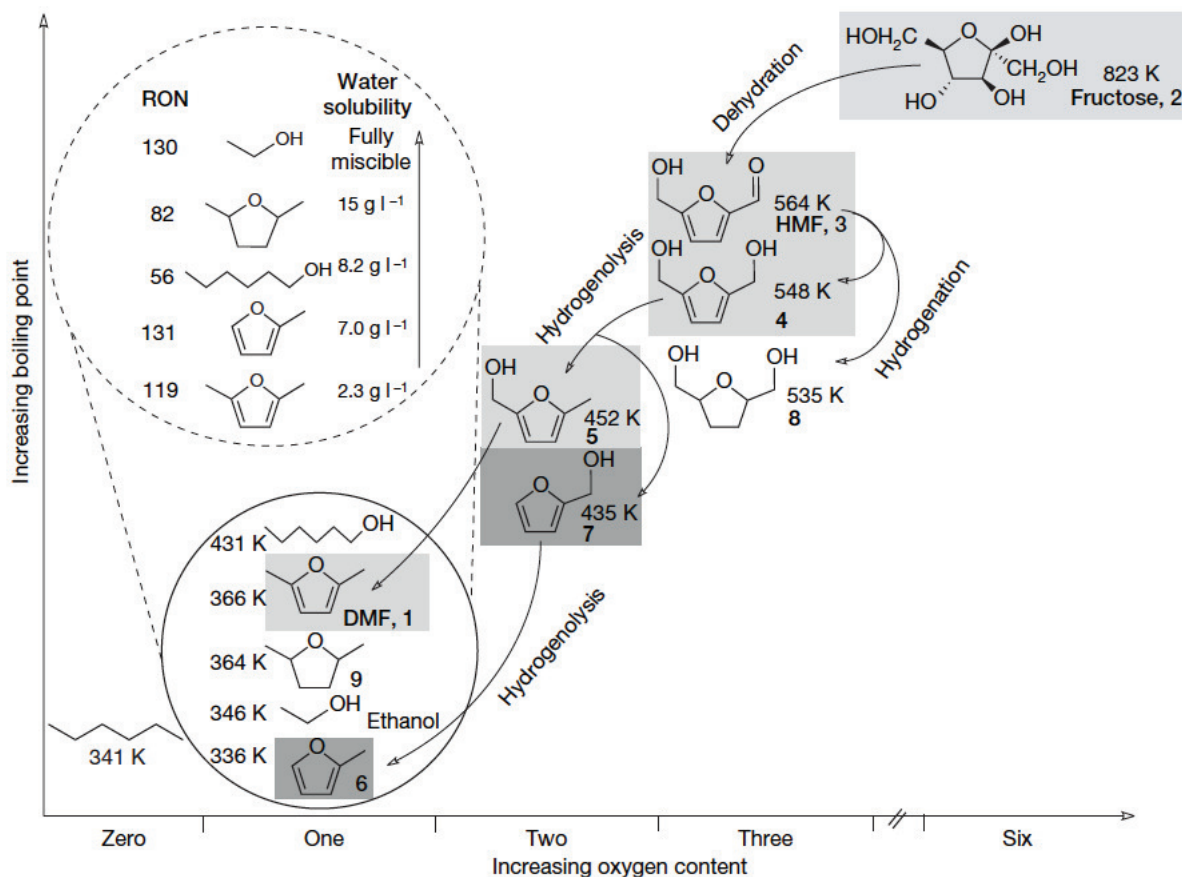
Figure 1.2: A schematic for the production of 2,5-dimethyl furan (DMF), 2-methyl furan (2-MF), and other biofuels from fructose as reported by Román-Leshkov et al. [4].

As a result of these attractive features, there is need to explore and quantify the fundamental combustion properties of furans. These properties include ignition behavior, flame propagation velocity, and species concentration profiles during combustion. Moreover, it is important to compare the reactivity of furans with that of conventional gasoline to assess the feasibility of furans as replacement or additive to gasoline. Further studies of furans and gasoline blends are also needed. These results are made more general if they lead to the development of predictive models.

A number of factors control the combustion process, such as fuel injection, vaporization, and mixing; but the major controlling factor is the chemical kinetics of the processes. Combustion chemistry can be characterized through ignition delay time studies, which can establish fuel

reactivity trends and validate proposed models. The delay times are generally measured using shock tubes and rapid compression machines. The rapid compression machine (RCM) is a compression device with a pneumatically driven piston assembly that rapidly compresses a fuel-oxidizer mixture in a reaction chamber. The rapid compression brings the mixture to high temperature and pressure conditions; suited for ignition delay time investigation [8]. Rapid compression machines provide long test duration and are mostly used for autoignition investigations in the temperature range of 600–1100 K [8]. A drawback of RCM is the pressure and temperature drop over the test time due to heat loss and mechanical relaxation, which increases uncertainty in the final thermodynamic conditions. More widely used, especially for high temperature ignition is the shock tube.

The shock tube can be used to study a variety of high temperature phenomena. It consists of tube segments separated into driver and test sections by a diaphragm. For ignition studies, the fuel-oxidizer mixture is introduced into the driven (test) section at low pressure, while the driver section is pressurized with a low molecular weight gas, such as helium, until the pressure difference is enough to burst the diaphragm. A shock wave is formed and it compresses the test mixture, bringing it to high temperature and pressure conditions. The test gas is brought to even higher temperature and pressure when the shock wave reflects from the endwall [9]. Unlike the RCM, heat loss from shock tube surface is minimal, since there is very limited flow and the typical test time is too short for molecular heat diffusion to the cold walls [9]. Shock tubes are mostly used to investigate ignition delay times at temperatures above 1000 K, but can also access lower temperatures by skillful control of the wave processes through driver gas choice.

Historically, shock tubes have been used to investigate the ignition behavior of conventional gasoline. Since gasoline is a complex fuel, its ignition behavior can be studied by means of a surrogate, such as *iso*-octane. This surrogate has been extensively studied, and the ignition data has been used to develop chemical kinetic models, which continue to be improved. The

most recent model of *iso*-octane, a representative gasoline surrogate, predicts ignition delay time to an accuracy that is within a factor of 2 [10]. With the recent interest in alternative fuels, the fundamental combustion studies are extended to the study of biofuels. Short-term implementation of biofuels is mainly achieved through blending with conventional gasoline. The combustion characterization of such fuel blends is also needed.

As a promising class of biofuels, the combustion behavior of furans have been investigated. Ignition studies of these fuels have focused on individual cases. Since the choice of engine fuels is mostly focused on relative properties, it is important to carry out systematic comparative studies to establish fuel reactivity trends. These established trends will also inform the improvement of existing chemical kinetic models [11–14]. The most up-to-date model of DMF by Somers et al. [12] predicts ignition delay times to within 20% but deviations of 60% can be seen at other conditions. The blending effect on the ignition behavior of furans and gasoline is yet to be explored, especially with respect to the blending effect on reactivity and knock resistance. Also, the difficulty in the chemical kinetic modeling of cyclic compound needs to be addressed. The existing chemical kinetic models of alkanes are not yet sufficiently accurate although they perform better than those of cyclic compounds. The differences in reactivity revealed by ignition studies of these compounds can be used for further understanding and modeling.

The development of detailed and reduced chemical kinetic models is a main area of combustion research; necessitated by the fact that these models more accurately describe the chemical kinetics of the combustion processes than global reaction models. Developing chemical kinetic models is supported by experimental characterization of fundamental combustion properties. Modeling efforts have also expanded owing to the need for combustion models of emerging fuels such as biofuels, as well as the need for improved predictive capability of existing chemical kinetic models. One difficulty associated with using existing chemical kinetic models for computational combustion is the large size of these models. The models

often contain thousands of reactions among hundreds or thousands of species, leading to higher computational resource requirements.

Detailed chemical kinetic models are validated against a variety of combustion characterization experiments. These include flow reactor, shock tube ignition and pyrolysis experiments, as well as 1D laminar premixed and non premixed flame propagation. The measurements are compared with model predictions to validate the said models. Such validated chemical kinetic models couple with fluid transport equations to simulate combustion. Practically, computational requirements are increased in turbulent chemically reactive flows. Therefore, skeletal models are needed, with fewer species and yet a predictive capability comparable with that of detailed models. A higher level of reduction can be achieved with further techniques such as lumping [15–17].

From the above, continuous efforts on developing mechanism reduction methods are ongoing to enable researchers in the combustion field to obtain reduced models efficiently without the need for extensive knowledge of chemical kinetic modeling. Most of the existing methods minimized the need for detailed chemical kinetic knowledge. However, a few research groups have the knowledge of the algorithmic skill set necessary for model reduction. Nonetheless, some reduction criteria and species choices are informed by chemical kinetic knowledge.

In summary, biofuels are needed as an environmentally friendly alternative to replace fossil fuels in the transportation sector. Furans, a class of second-generation biofuels, are considered as candidates for use as SI engines fuels or additives to gasoline. The combustion properties of furans need to be characterized to aid the development of chemical kinetic models of this class of biofuels. Moreover, chemical kinetic models are often large and need to be reduced to skeletal versions to reduce the computational requirements for combustion simulations while preserving the predictive capability. This thesis seeks to contribute to addressing these challenges.

1.2   Literature review

The review below assesses the current state of the combustion characterization of furans represented by DMF, 2-methyl furan (2-MF), furan, and tetrahydrofurans. The review also includes efforts on the characterization of gasoline surrogates represented by *iso*-octane. Moreover, the review considers literature work on cycloalkanes such as ethylcyclohexane and dimethylcyclohexane as well. The gaps noted in the review lead to the objectives of this work. It focuses on ignition delay measurements and chemical kinetic modeling of the selected fuels. Chemical kinetic model reduction work is also considered.

Combustion characterization of furans and gasoline surrogates

Fundamental combustion research focusing on SI engine fuels is complicated by the fact that practical fuels are a complex mixture of hydrocarbons such as *n*-alkanes, branched alkanes, and aromatics. Initially, characterization of gasoline combustion focused on empirical system level tests, using parameters such as research and motor octane numbers [18–21]. With the advent of combustion science, chemical kinetics is a more advanced theory that captures ignition and flame phenomena encountered during gasoline combustion [22]. The development of comprehensive chemical kinetic mechanisms is not sufficiently advanced to depend only on theory; it depends on fundamental experimental data which serve as validation targets of proposed models. As a result, ignition delay times have been investigated for various gasoline mixtures in several shock tube studies [22–25]. To overcome problems posed by the complexity of gasoline, fundamental investigations have used representative fuel molecules for gasoline. An example is *iso*-octane or a mixture of *iso*-octane and *n*-heptane as primary reference fuels.

Similar to the experimental and modeling studies of gasoline surrogate combustion; biofuels have been investigated. As shown in [26–28], the existing studies mostly focus on low carbon alcohols, such as ethanol, *n*-butanol, and *iso*-pentanol, with an increasing interest in furans. Fundamental combustion properties of biofuels have been studied, including ignition delay

times. For instance, ignition behavior of butanol isomers has been investigated in a number of shock tube studies [29–33], whose data sets were the base for several chemical kinetic models [29, 30, 32, 34].

In line with the increased interest in furans, The use of furans as alternative SI engine fuels or fuel additives has been assessed in several studies [3, 35–42]. The results of engine studies highlight the possibility of using furans in current SI engines without major modifications. It is claimed that furan combustion offers better knock resistance and lower emissions of NO_x, HC, and particulate matter (PM) than gasoline and other well established biofuels such as bio-ethanol.

Auto ignition of furans has been also investigated in the literature. Sirjean et al. [13] presented shock tube ignition delay measurements of $DMF/O_2/Ar$ mixtures at pressures of 1.0 and 4.0 atm, over a temperature range of 1300–1831 K, and at equivalence ratios of 0.5–1.5. A detailed chemical kinetic model was also proposed, with generally good agreement between model predictions and experiment. Somers et al. [12] presented an improved model, comparing its performance with another set of ignition delay times for $DMF/O_2/Ar$ mixtures at equivalence ratios of 0.5–2.0, temperatures from 1350 to 1800 K, and pressures of 1, 20, and 80 atm. The ignition data sets, based on sidewall ignition measurement, show good agreement with the kinetic model presented, whereas the previous model by Sirjean et al. [13], which was validated using data based on endwall ignition measurements, predicts longer ignition delay times. The model by Somers et al. [12] incorporates the furan sub chemistry presented in the work of Sirjean et al. [13] into an existing chemical kinetic model for small hydrocarbons.

In addition to DMF, the ignition behavior of other furans has been investigated. For instance, 2-MF was studied by Somers et al. [14] and Wei et al. [43]. Somers et al. [14] measured ignition delay times of $2-MF/O_2/Ar$ mixtures at equivalence ratios of 0.5, 1.0 and 2.0 and pressure of 1 atm over a temperature range of 1200–1800 K. They also presented a chemical kinetic model with good prediction performance against their experimental data. The other

high temperature ignition data by Wei et al. [43] at pressures up to 10.65 bar, have been compared to the model by Somers et al. [14] showing good agreement at lower pressures. However, the model under-predicts ignition delay at higher pressures as shown in a study by Uygun et al. [44] for stoichiometric 2-MF/air mixtures at 40 atm. However, the study also showed that the model over-predicts ignition delay times at lower temperatures.

With respect to furan ignition, an initial study was conducted by Wei et al. [45] at temperatures of 1320–1880 K, and pressures of 1.2–10.4 atm for dilute mixtures with equivalence ratios of 0.5–2.0. The data showed fairly good agreement with a previous chemical kinetic model by Tian et al. [11], although the model under-predicts ignition delay times of lean mixtures at lower temperatures.

The saturated furans, tetrahydrofurans, are equally attractive as fuel additives or pure fuels. Although not as extensively studied as DMF and 2-MF, there are increasingly more research activities on their computational and experimental characterizations [44, 46–48]. While the number of ignition investigations of furans is increasing, few studies focus on structure-activity trends.

Comparative ignition investigation is needed to establish a relative reactivity trend, which provides greater insight into the combustion behavior of furans and supports chemical kinetic modeling. Isomer effects on the reactivity of furans also need to be evaluated. The DMF isomer of interest here is 2-ethyl furan (2-EF, C_6H_8O); which is hypothesized to be more reactive. A recent study by Sudholt et al. [49] presented bond dissociation energies (BDEs) of various furans, including 2-EF. However, it is not known how these differences translate to quantifiable differences in homogenous ignition of 2-EF and DMF. The prediction accuracy of the current models for furans still needs improvement, including thorough review and update of the kinetic parameters of the most important reactions.

The second group of interest is gasoline surrogates, represented in this work by *iso*-octane.

The ignition of *iso*-octane has been extensively investigated in the literature, yielding sets of ignition data over a wide range of shock tube conditions, as reviewed by Pitz and Mueller [50]. Fieweger et al. [51] measured *iso*-octane ignition delay times at pressures of about 13 and 40 atm and equivalence ratios of 0.5, 1.0, and 2.0. Generally, ignition delay times decrease with increasing temperature. For some fuels, a temperature range exists where the delay time increases with temperatures. This reversed temperature sensitivity and fuel reactivity is termed the Negative Temperature Coefficient (NTC) behavior. NTC behavior was observed during *iso*-octane ignition at pressures above 40 atm; the slope of the NTC was more pronounced as the equivalence ratio increased. Another study by Davidson et al. [52] compared ignition delay times of *iso*-octane/air mixtures at 50 atm and equivalence ratios of 0.5 and 1.0 with the previous study by Fieweger et al. [51], showing excellent agreement. Shen et al. [53] also investigated shock tube ignition of *iso*-octane/O_2/Ar mixtures at temperatures of 868–1750 K, pressures of 1–58 atm, and equivalence ratios of 1.0, 0.5, and 0.25, showing good agreement with previous literature data, with some disagreement at lower temperatures for lean mixtures. Mixtures in which the oxidizer consisted of argon and oxygen had 20% shorter ignition delay times than those for which the oxidizer was air.

Ignition behavior of *iso*-octane has also been investigated in a number of studies focusing on other hydrocarbon systems, such as the study by Akih-Kumgeh and Bergthorson [54] which provided data at 10 atm while focusing on methyl formate ignition. Rapid compression machines (RCM) ignition data have also been presented in various studies [55, 56].

In addition to ignition and other combustion property measurements, detailed chemical kinetic models for *iso*-octane have been developed. The shock tube data by Fieweger et al. [51] were used in the development of the first major kinetic model by Curran et al. [57]; and later models by Ranzi et al. [58], as well as the most recently updated model by Mehl et al. [10]. These models predict various combustion properties to a varying degree of success. Ignition predictions using the more comprehensive model by Mehl et al. [10] are generally

within a factor of 2.

Another group of interest, cyclohexanes, are key components in transportation fuels. Similar to aromatics, their proportion in fuels is often quoted without specification of the make up with respect to their individual molecular structures. It is of interest to identify the isomer effect on the reactivity of cyclohexane. The mono alkylated cyclohexanes have been the subject of many experimental and modeling studies [59–63], resulting in shock tube and rapid compression machine ignition data sets and models with varying degree of prediction abilities. The study by Hong et al. [63] includes species concentration profiles aimed at linking observed ignition delay trends to the role of key radicals such as OH. Ignition delay times of methyl and ethyl cyclohexane and air mixtures have been investigated by Vanderover and Oehlschlaeger [64], showing that ignition delay times of methyl cyclohexane are longer than those of ethyl cyclohexane. However, studies including dimethyl cyclohexanes have not been reported.

Direct comparison of ignition delay times of gasoline surrogates such as *iso*-octane and furanic fuels has not been carried out. This is crucial for further model development and for practical applications in fuel-flexible engines. Moreover, the effect of blending these two groups need to be investigated to determine if there are indeed pronounced differences in the reactivity.

In addition to the efforts on the chemical kinetic modeling of individual fuels, a number of researchers have developed models of the chemistry of multi-surrogate fuel mixtures. Li et al. [65] developed a chemical kinetic model for blends of primary reference fuels (PRF). Other studies on the modeling of PRF were presented in [66, 67]. Klotz et al. [68] developed a chemical kinetic model for high temperature combustion of toluene-butane blends. Another work by Farrell et al. [69] presented a chemical kinetic model for diesel surrogate mixtures. With respect to gasoline mixtures, several chemical kinetic models have been developed [10, 25, 70, 71] based on the available combustion experiments [22–25], with the most up-to-date model being that by Mehl et al. [10].

Other efforts focused on modeling combustion chemistry of blends of gasoline surrogates with other compounds. Curran et al. [72] presented a chemical kinetic model for blends of n-heptane, a representative diesel fuel, with oxygenated fuels such as methanol, ethanol, and dimethyl ether (DME). Ra et al. [73] has presented an extended PRF model which includes submechanisms for other compounds including ethanol, DMF, toluene, and cyclohexane. However, despite the increased research activities on the chemical kinetic modeling of fuel blend combustion, there is no work on the modeling of the combustion of blends of gasoline surrogate and the emerging furan. Such models are needed to investigate the effect of pathway interactions of both classes of fuels on the ignition behavior of their blends.

Chemical kinetic model reduction

With respect to chemical kinetic model reduction, various mechanism reduction methods have been employed to obtain skeletal models. One of the most widely used methods is the Directed Relations Graph (DRG) [74] method, in which the important species to be retained are identified by their direct influence on a chosen target species, most commonly the fuel, during combustion process simulations. Other variants of the DRG method have been used in the literature, including error propagation analysis (DRGEP) [75] and species sensitivity analysis (DRGASA) [76, 77], a combination of both DRGEP and DRGASA (DRGEPSA) [78], as well as the recent DRG with expert knowledge (DRGX) [79]. A number of studies on DRG-based reduction of large chemical kinetic models for biodiesel surrogates [80–87], as well as gasoline surrogates [88], has been presented.

Other mechanism reduction approaches have been proposed and utilized in the literature, such as the elemental flux analysis method [89, 90]. This method depends on the calculation of the fluxes of different atoms between species for all the reactions containing the species in question. The sum of the fluxes for the species is compared to a user-set threshold to decide whether to retain or remove the species. This method has been utilized for on-the-fly reduction [91], where the simulation is divided into discrete time steps and for each time step

a reduced mechanism is generated. Moreover, further research activities continue to explore the development of new mechanism reduction methods. These include the path flux analysis method proposed by Sun et al. [92], a modification of the method of Necessity Analysis by Karadeniz et al. [93], and modifications to the Principal Component Analysis by Esposito and Chelliah [94]. Most recently, Zhao et al. [95] have proposed the Betweenness Centrality (BC) method for mechanism reduction. It utilizes the nodal fluxes as well as the nodal relative positions in the network to obtain a ranked species list based on the quantified relative species importance, which is claimed to lead to high predictive capability in combustion simulations.

A more straightforward model reduction approach, the Alternate Species Elimination (ASE) method, has been adopted by Akih-Kumgeh and Bergthorson [96], and used in different studies [97–99]. The ASE method is based on species sensitivity analysis, which aims to identify the species that are indispensable for the simulation of a given combustion property, such as ignition delay time. This is achieved by evaluating the effect of excluding reactions containing a given species on the prediction of a combustion property of interest. The ASE method is ultimately aimed at reducing the number of the system's dimensions through the elimination of any species to which the transition from an unburnt state to a burnt state is not sensitive. The ASE method is most conveniently performed using the CANTERA [100] software package. It enables the user to easily eliminate reactions containing the species to be examined through the "setMultiplier" i.e. reaction rate multiplier is set to zero. Moreover, CANTERA can be integrated into MATLAB, which enables the automation of the ASE reduction method.

The ASE has attractive features that the method needs further development. Firstly, the DRG methods are based on averaged direct influence coefficients from approximately 1000 different conditions of pressure, temperature, equivalence ratio, as well as different time steps [74], which leads to a reduced mechanism that can be used for virtually any possible condition. On the other hand, the ASE method targets three conditions and assumes generalized behavior

of the reduced model. Secondly, even though the ASE method yields good skeletal models in terms of predictive capability, the computational cost of implementing the ASE method is relatively high. The suppression of each of the species in the model is followed by an ignition delay time simulation with a full-sized model. For large mechanisms, this means hundreds or thousands of ignition delay time simulations per ASE run. Finally, the ASE method depends on the order by which chemical species are placed in the mechanism to be reduced. Implementation of a stochastic based ASE reduction approach with fewer simulations would improve the ease of model reduction through species elimination.

1.3   Scope and objectives of this work

From the literature review, a number of gaps and open questions have been identified. First, the relative ignition behavior of furan and alkylated furans has not yet been established, although the ignition delay times of the individual fuels have been studied. The reactivity trends can be established through direct comparison of ignition delay times of these fuels at similar conditions. Moreover, the ignition behavior of the DMF isomer, 2-EF, has not been studied. Ignition delay measurements of 2-EF are needed in order to explore the isomer effect on alkylated furan combustion. This could provide further insight on the isomer effect on the combustion of cyclic compounds in general. Moreover, comparative ignition behavior of furans, gasoline surrogates, and their blends has not been investigated, which is important for further model development and for engine applications. With respect to chemical kinetic modeling, the predictions of existing models of furans and gasoline surrogates need further improvement, guided by extended experimental data. Further, existing furan and gasoline models are not capable of simulating combustion behavior of fuel blends. A combined model needs to be developed to enable the chemical kinetic analysis of blending effect on the combustion of furans and gasoline surrogates. This thesis seeks to address these problems. Specifically, this work seeks to:

■ Establish chemical structure-reactivity trends in furans based on ignition behavior. The fuels investigated are the unsaturated furans DMF, 2-MF, 2-EF, and furan, as well as the saturated furans tetrahydrofuran (THF) and methyltetrahydrofuran (MTHF).

■ Establish the relative ignition behavior and blending effect of the furan, DMF, and the gasoline surrogate, *iso*-octane, and assemble a chemical kinetic model for blends.

■ Use observed trends in DMF and 2-EF ignition to explore reactivity trends in ring compounds with alkyl branches.

■ Contribute to model reduction through development and testing of a mechanism reduction method based on stochastic species elimination.

The constraints for the experimental studies are carefully chosen to reveal reactivity trends and blending effects. The combustion process of a generic fuel can be represented as follows:

$$\text{Fuel} + \nu(\text{O}_2 + D\ \text{N}_2) \rightarrow \text{products} \tag{1.1}$$

where ν is the number of moles of oxygen needed for complete combustion of one mole of fuel, or the stoichiometric coefficient, and D is the ratio of the number of moles of the diluent gas (e.g. N_2 or Ar) to the number of moles of oxygen, or simply called the dilution.

The material covered in this thesis is divided into four sections. The first part deals with the ignition investigations of furans as a representative group of biofuels. Relative ignition delay times are first measured for furans, represented by DMF, 2-MF, and furan; at similar equivalence ratios, ϕ, ratio of argon to oxygen, D, and nominal pressure, p, over a range of temperatures, T. Moreover, ignition delay times of 2-EF are measured and compared with DMF ignition data to establish the structural effect on ignition of ethyl and dimethyl furans with same molecular composition. Ignition delay data are compared to predictions of furan models by Somers et al. [12] and Sirjean et al. [13]. These models incorporate the kinetics of furan, 2-MF, and DMF. Species sensitivity and reaction pathway analyses are performed to provide further mechanistic insight on the chemical pathways responsible for the observed relative reactivity trends.

The second part is the measurements of ignition delay times of DMF and *iso*-octane to quantify differences in their reactivities. Further, to determine kinetic interations in fuel blends, ignition delay measurements are carried out using mixture of equal liquid volumes of DMF and *iso*-octane. Ignition data of the pure fuels are compared with their respective model predictions and a combined chemical kinetic model for DMF and *iso*-octane combustion is

developed, starting from the *iso*-octane model by Mehl et al. [10] and the DMF model by Somers et al. [12]. Modifications are applied to combined model to improve the agreement with the current and previous ignition data. Reaction pathway analysis and species sensitivity analysis are performed to gain more insight on the governing chemical kinetics.

The third part of this work deals with the ignition studies of other bio-derived and conventional cyclic compounds. Firstly, ignition behavior of the saturated furans, tetrahydrofurans, is investigated through ignition delay measurements for THF and MTHF. The results are put in the broader context of furan reactivity by comparing with the ignition data of 2-MF. Ignition data of tetrahydrofurans are compared with predictions of the recently published tetrahydrofurans model by Moshammer et al. [47]. Secondly, the effect of molecular structure on ignition propensity for dimethyl and ethyl isomers of cyclohexane, DMCH and ECH, is investigated and further compared with the ignition data of the dimethyl and ethyl isomers of furan, DMF and 2-EF. The experimental ignition delay time measurements of ECH are compared with the predictions of the surrogate fuel model, JetSurF2.0 [101]. The ignition data of DMCH are used to constrain a chemical kinetic model developed by our research collaborators. The experimental results present an opportunity to further explore mechanistic pathways and rate processes controlling the oxidation of cyclic hydrocarbons of relevance to combustion systems.

The final part of this work deals with the development of reduced chemical kinetic models from detailed models of various surrogate fuels. These reduced models are also referred to as skeletal models in this work. The existing Alternate Species Elimination (ASE) [97] model reduction method is employed for the reduction of recently reported *iso*-octane model version 3 by Mehl et al. [102] and *n*-heptane model version 3.1 by Mehl et al. [10]. The ASE approach is extended to a stochastic species sampling approach, identified as the Stochastic Species Elimination (SSE) method. The SSE method allows for a linear reduction process, and involves dynamic mechanism sizing and dynamic threshold determination. This leads to

reduced computational resource requirements, compared to the standard ASE method. The SSE method also features the possibility of real-time observation of reduction progress, which provides the user with more freedom to stop the reduction process at a user-defined reduction level. Larger models, such as the recent literature model of *n*-octanol (1281 species, 5537 reactions) by Cai et al. [103], are approached with a multi species sampling SSE method, which allows for time-efficient model reduction process. Resulting reduced models are compared with original large versions with respect to ignition delay times and flame propagation properties.

The chemical structure of the investigated fuels is shown in Figure 1.3, as discussed previously in the literature review.

furan   2,5-dimethyl furan   2-ethyl furan

tetrahydrofuran   2-methyltetrahydrofuran   2-methyl furan

iso-octane   1,3-dimethyl cyclohexane   ethyl cyclohexane
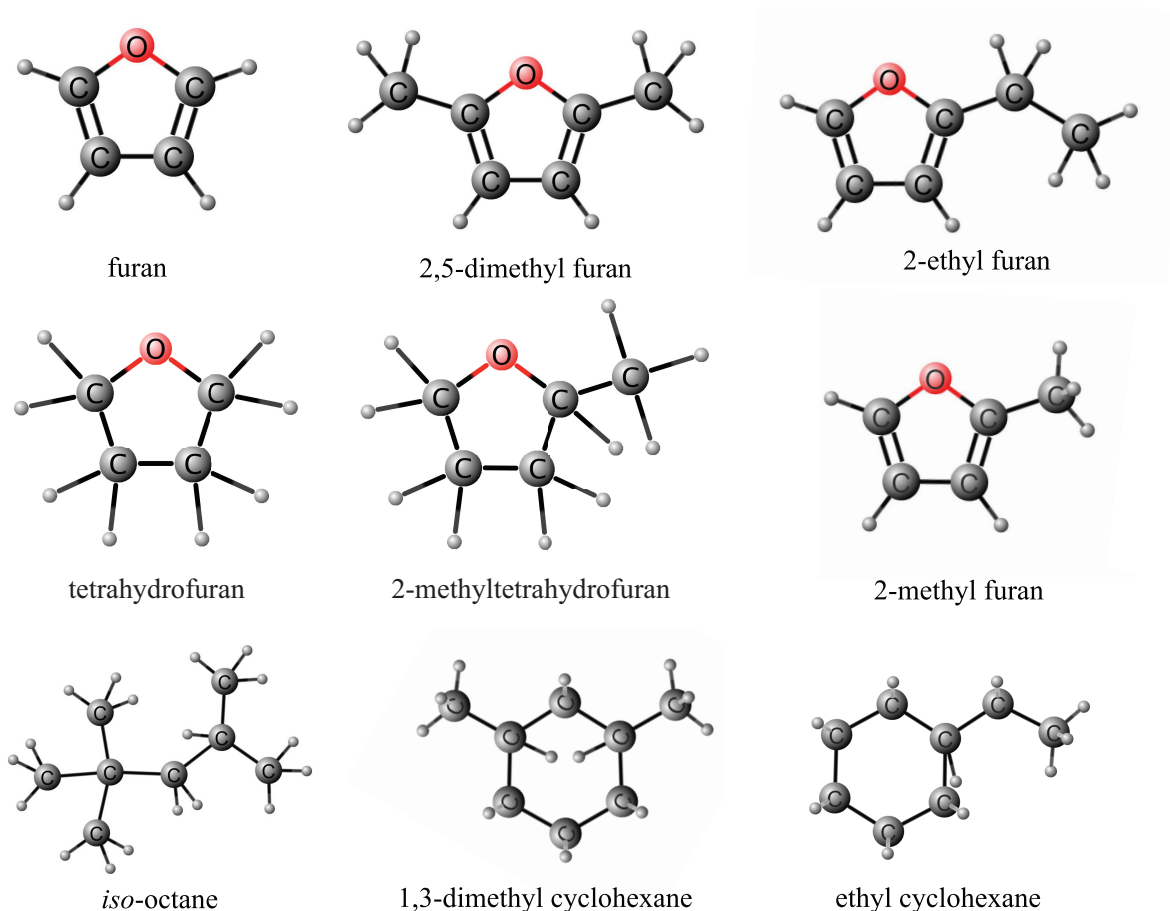
Figure 1.3: Chemical structure of the investigated fuels.

From an organizational perspective, the thesis is divided into six chapters. Chapter two

presents the experimental method used in this work. The focus is on the shock tube technique as used in high temperature chemical kinetics. The associated gas dynamics, instrumentation, data acquisition and processing are highlighted. Experimental uncertainties are then discussed. Finally, the experimental setup and procedure are described.

Chapter three presents the approach used to analyze chemical kinetic models. First, the analysis of homogeneous constant volume reactor is presented. Then, the chemical kinetic model reduction methods and simulation approach are explained. The discussion includes the existing Alternate Species Elimination (ASE) method [97] and the modified version, Stochastic Species Elimination (SSE) method.

Chapter four includes shock tube ignition delay studies of various fuels, as well as chemical kinetic simulations and analysis. The first section focuses on the comparative ignition trends of the furans DMF, 2-MF and furan. The second section demonstrates the ignition study of DMF, a representative furan, and *iso*-octane, a representative gasoline surrogate, as well as blends of these pure fuels. The development of a combined *iso*-octane/DMF model is also presented in this section. The third section includes ignition investigation of the saturated furans, tetrahydrofurans, represented by THF and MTHF, as well as comparative reactivity trends of MTHF and 2-MF. Finally, the fourth section presents a comparative ignition study of cyclohexanes, represented by DMCH and ECH.

Chapter five focuses on the development of skeletal chemical kinetic models using model reduction methods. The chapter shows the chemical kinetic model reduction process for various surrogate fuels, such as *iso*-octane and *n*-heptane, using both ASE and SSE reduction methods. Another modification of the SSE, referred to as multi-species sampling, is then demonstrated in the process of obtaining reduced versions of the larger detailed model of *n*-octanol. Chapter six presents an overall conclusion and outlook of this work.

Noteworthy is that chapter 4 contains work that appeared in references [104–108]. The

candidate is first author of these publications. Chapter 4 also contains work that is currently under review by the Proceedings of the Combustion Institute and the International Journal of Chemical Kinetics. Chapters 3 and 5 include work that is currently being prepared for publication.

Experimental method

In this chapter, the shock tube technique as used in high temperature chemical kinetics is presented. The experimental setup and procedure are then described. The data acquisition and processing procedures are demonstrated. This chapter concludes with a discussion on the experimental uncertainties associated with the shock tube reactor.

2.1 Shock tube technique

The shock tube is one of the most widely used experimental devices in high temperature gas dynamics and chemical kinetics, as demonstrated in a number of review articles [9, 109–112]. It is used to generate instantaneous high temperature and pressure conditions, which induce chemical reactions and lead to subsequent ignition of a test mixture of fuel and oxidizer. The tube consists of two tube sections separated by a diaphragm, as shown in Figure 2.1a. The driver section is pressurized with an inert low molecular weight gas, such as helium, and the driven section is filled with the combustible test gas at low pressure, as shown in Figure 2.1a. When the diaphragm ruptures, a shock wave moves into the driven section and instantaneously heats and pressurizes the test gas, as shown in Figure 2.1b. When the shock reaches the endwall, it reflects and travels through the previously heated gas, further increasing the temperature and pressure [112], as shown in Figure 2.1c. The region behind

the reflected shock wave is of interest for ignition observation; it is necessary to determine the pressure and temperature of the gas in this region.
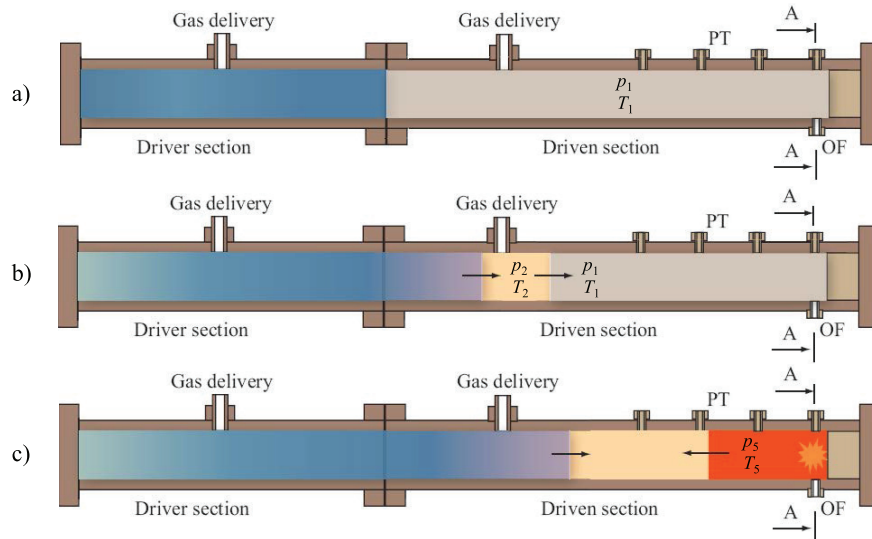
Figure 2.1: A schematic of shock tube and stages of the ignition experiment. a) Shock tube filled with driver and test gases, b) Post diaphragm rupture, c) Post shock reflection.

Figure 2.2 shows Schlieren images of the shock wave propagation in the shock tube facility used in this work through a special optical access located near the endwall. Figure 2.2a shows the propagation of the incident shock front from right to left. In Figure 2.2b, the shock wave reflects from the endwall and travels from left to right. The pressure increase in the reflected shock compared to that of the incident shock is visible in Figures 2.2a and 2.2b. Finally, Figure 2.2c shows the ignition event of the test mixture.
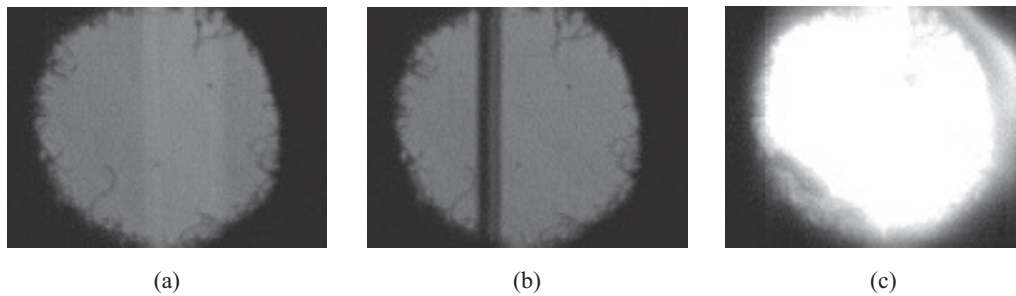
Figure 2.2: Schlieren images of a representative shock tube experiment. a) Incident shock wave propagation from right to left, b) Reflected shock wave propagation from left to right, c) Ignition event.
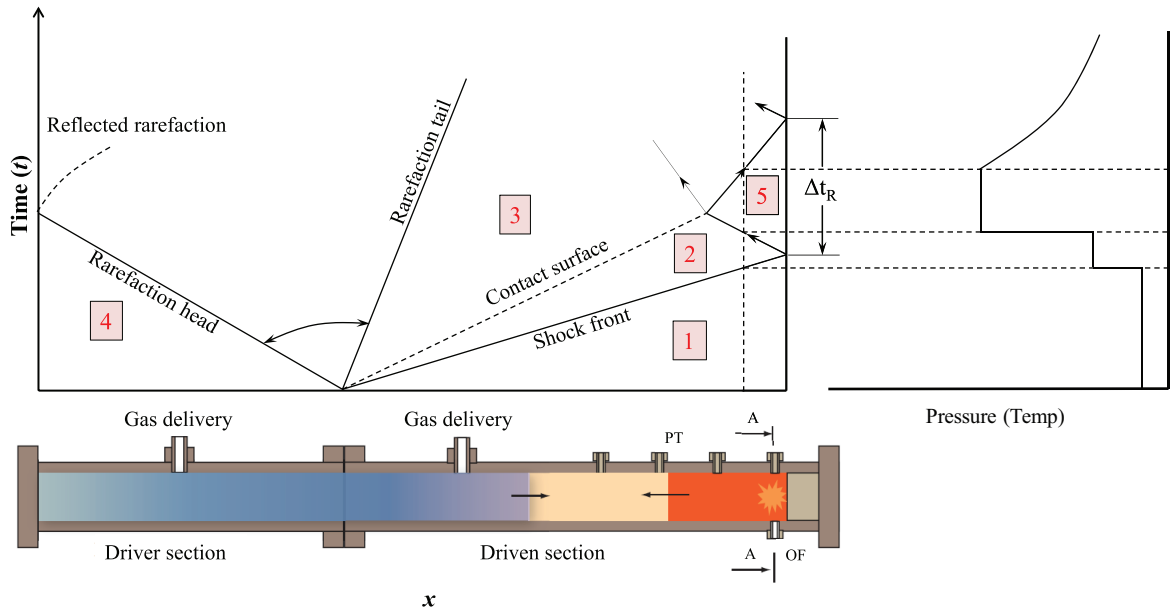
Figure 2.3: x–t diagram of shock tube operation with gases at various states, and temperature and pressure traces at a location near the endwall. (1) Unshocked test gas, (2) Shocked gas, (3) Driver gas behind contact surface, (4) Driver gas at the state prior to diaphragm rupture, (5) Test gas behind reflected shock wave.

Figure 2.3 shows the pressure and temperature traces at a location near the endwall of the shock tube. The figure shows that the gas near the endwall is initially at low pressure and temperature. When the incident shock wave passes, the test gas is subjected to a step in pressure and temperature. The incident shock then reflects from the endwall, and the resulting reflected shock wave subjects the test gas to another temperature step. The time scale of the gas heating process is microseconds to milliseconds, and therefore heat losses and molecular diffusion through the cold wall of the shock tube cannot make contributions.

Figure 2.3 also shows an x–t diagram of the shock tube, indicating the location of various wave fronts at a given time, t, from the rupture of the diaphragm. Zone 1 represents the undisturbed test gas at low pressure and temperature. Zone 4 represents the driver gas at a relatively high pressure and room temperature. Zone 2 contains the gas behind the incident shock wave, processed to a higher temperature and pressure of the test gas. Zone 3 represents the driver gas transported into the driven section with the same pressure as the shocked test

gas. The zone of interest in ignition delay studies is zone 5, which is behind the reflected shock wave; a zone of hot, stagnant gas at uniform high pressure, p_5, and temperature, T_5.

When the reflected shock wave meets the contact surface, as shown in Figure 2.3, the interaction results in a reflected disturbance, in the form of an expansion wave or a shock wave, as well as a transmitted shock wave. Upon the interaction of the reflected shock wave with the contact surface, equality of static pressure and velocity before and after the contact surface must continue to be satisfied, despite the sudden change in the speed of sound at the contact surface. In the case of a sudden fall in the speed of sound, the reflected shock Mach number and pressure increase upon passing the contact surface. As a result, the static pressure behind the contact surface becomes higher than in front of it. To restore static pressure equality, a reflected shock is generated from the contact surface toward the endwall. On the other hand, if the speed of sound increases at the contact surface, the reflected shock Mach number decreases on passing the contact surface, and therefore a reflected expansion wave is generated to compensate for the pressure inequality [113].

The observation time is a critical parameter and it limits the temperature range over which ignition delay times can be observed using a shock tube. For a tube with a sufficiently long driver section, it is the time interval between the reflection of incident shock wave and the arrival of the reflected wave from the contact surface, as shown in Figure 2.3. The typical test time for a shock tube is approximately 2 ms, which can be extended up to 10 ms with contact surface modification through driver gas composition. This is useful for measuring ignition delay times at temperatures below 1000 K [110].

To enable comparison of experimental observations with simulations of a homogeneous reactor, the conditions established behind the reflected shock wave (zone 5) need to be known accurately. It would be preferable to measure p_5 and T_5. While p_5 can be measured; T_5 cannot be easily quantified because of the short duration it lasts. As a result, T_5 is inferred from the gas dynamic model of a one-dimensional shock wave. Assuming that the flow is approximately

one-dimensional, and the gases are ideal, the continuity, momentum, and energy equations

across the shock wave are [109]:

$$\rho_1 u_1 = \rho_2 u_2 \tag{2.1}$$

$$p_1 + \rho_1 u_1{}^2 = p_2 + \rho_2 u_2{}^2 \tag{2.2}$$

$$h_1 + \frac{1}{2} u_1{}^2 = h_2 + \frac{1}{2} u_2{}^2 \tag{2.3}$$

where ρ is the mass density, u is the velocity, h is the specific enthalpy, and p is the pressure.

The properties are those of the ideal gas mixtures. The indices 1 and 2 refer to the unshocked

gas and the shocked gas behind the incident shock wave, respectively. A closed form solution

for T_5 can be obtained, if we assume constant specific heat. The pressure and temperature

ratios across the shock wave can be obtained from the following shock relations [109]:

$$\frac{p_2}{p_1} = \frac{2\gamma M_1{}^2 - (\gamma - 1)}{\gamma + 1} \tag{2.4}$$

$$\frac{T_2}{T_1} = \frac{\left(\gamma M_1{}^2 - \frac{\gamma-1}{2}\right)\left(\frac{\gamma-1}{2} M_1{}^2 + 1\right)}{\left(\frac{\gamma+1}{2}\right)^2 M_1{}^2} \tag{2.5}$$

where T_1 and p_1 are the temperature and pressure of the unshocked test gas, T_2 and p_2 are

the temperature and pressure behind the incident shock wave as shown in Figure 2.1c, γ is

the specific heat ratio, and M_1 is the incident shock Mach number.

Similarly, $\frac{p_5}{p_2}$ and $\frac{T_5}{T_2}$ can be calculated, and hence state 2 is eliminated to obtain the following

relations [109]:

$$\frac{p_5}{p_1} = \left[\frac{2\gamma M_1{}^2 - (\gamma - 1)}{\gamma + 1}\right]\left[\frac{(3\gamma - 1) M_1{}^2 - 2(\gamma - 1)}{(\gamma - 1) M_1{}^2 + 2}\right] \tag{2.6}$$

$$\frac{T_5}{T_1} = \frac{\left[2(\gamma - 1) M_1{}^2 + (3 - \gamma)\right]\left[(3\gamma - 1) M_1{}^2 - 2(\gamma - 1)\right]}{(\gamma + 1)^2 M_1{}^2} \tag{2.7}$$

where T_5 and p_5 are the temperature and pressure behind the reflected shock wave as shown

in Figure 2.1d. Hence, the temperature and pressure of the test section can be calculated if

the shock Mach number and the initial conditions of the driven gas are known.

The relations presented above are obtained by assuming constant specific heats, which is not the case, especially when polyatomic gases are involved. To account for the variation of specific heats with temperature, a different approach is followed. Using the initial guess from ideal gas calculations [109], equations (2.1) – (2.3) are solved implicitly, to get T_2 and p_2 from which T_5 and p_5 can be obtained by further considering the reflected shock wave equation. The temperature dependence of specific heat is accounted for through the NASA polynomials for constant pressure specific heat (c_p), enthalpy (h), and entropy (s), which have the form:

$$\frac{c_p}{R} = a_1 + a_2T + a_3T^2 + a_4T^3 + a_5T^4 \tag{2.8}$$

$$\frac{h}{RT} = a_1 + \frac{a_2}{2}T + \frac{a_3}{3}T^2 + \frac{a_4}{4}T^3 + \frac{a_5}{5}T^4 + \frac{a_6}{T} \tag{2.9}$$

$$\frac{s}{RT} = a_1 \ln T + a_2T + \frac{a_3}{2}T^2 + \frac{a_4}{3}T^3 + \frac{a_5}{4}T^4 + a_7 \tag{2.10}$$

where the coefficients a_1 to a_7 are supplied for each species in NASA thermodynamic files. Two sets of coefficients are provided for low-temperature and high-temperature ranges. The input data for the system of equations are the initial species concentrations, pressure, and temperature of the test mixture, as well as the shock velocity.

The one dimensional approach demonstrated above is valid assuming a potential flow, which neglects the effect of the boundary layer in real cases. The viscous effects are significant. Viscous boundary layer is formed as the shock wave propagates, which leads to modification of the flow behind the shock wave. The shock wave slows down due to the energy dissipation associated with this viscous layers. The shock velocity decreases downstream. The available observation time depends on the distance between the incident shock wave and the contact surface. For inviscid flow in the shock tube, the shock wave and the contact surface propagate at constant velocities with a higher velocity on the shock wave. Consequently, the separation between the incident shock front and the contact surface increases with increasing driven section length. This longer separation between the waves leads to an increased observation

time since the distance reflected shock wave covers before interaction with the contact surface increases. It is important also that the driver section is long enough to avoid observation time limitation by the reflected expansion wave.

2.2   Experimental setup and procedure

The experimental work in this thesis is carried out in a newly constructed shock tube facility. For the majority of this work, the stainless steel shock tube consists of a 4.0 m driven (test) section and a 2.7 m driver section. Recently, it has been extended to a total length of about 9.0 m with a 6.0 m driven section. The inner diameter of the mechanically polished tube is 10 cm. Research grade samples of furan, 2-MF, DMF, *iso*-octane, THF, MTHF, DMCH, ECH (Sigma-Aldrich, at least 99%), and 2-EF (Sigma-Aldrich, 97%) are used. The oxygen, argon, nitrogen, and helium used are ultra high purity gases (Airgas, > 99.999%).

In the current facility, the ignition delay experiment is preceded by gaseous mixture preparation. Fuel mixtures are prepared according to pre-defined compositions using the method of partial pressures. Special care and precautions are necessary in the process of mixture preparation as the fuels investigated in this study are liquid fuels. For this purpose, the mixtures are prepared in a 150 L mixing tank equipped with ball valves to control the delivery of gases and fuel. The tank is first evacuated using a rotary vacuum pump (Edwards, RV12). The mixture components are then delivered to the mixing tank to set pressures using a 1000-Torr high-precision MKS Baratron pressure transducer accurate to 0.12% of reading. The fuel is introduced using a gas-tight syringe and it immediately vaporizes. The target partial pressure of the fuels are kept below 50% of the their room temperature vapor pressures to prevent condensation. Oxygen is then added, based on the required equivalence ratio, ϕ, and the diluent gas is finally added to obtain the desired argon/oxygen ratio, D. Oxygen and diluent gas addition is performed slowly to prevent local fuel condensation. The mixture is then left for at least 14 hours to homogenize.

Ignition delay experimental realizations start with the placement of a polycarbonate diaphragm of appropriate thickness between the driver and driven sections of the shock tube. The two sections of the shock tube are then vacuumed out to ultimate pressures of 2×10^{-3} mbar.

The leak rate of the shock tube facility used in this work is regularly checked and found to be consistently less than 1 Pa/min. Moreover, similar ignition results were obtained in tests performed at time durations ranging from a few minutes up to one hour from the introduction of the fuel mixture into the test section. For low initial pressure studies, residual air in the tube is minimized by first flushing the tube with the test gas mixture. The driven section is then filled with the test mixture to a pressure likely to produce target p_5; based on empirical calculations obtained from calibration and validation experiments. The test section fill pressure depends on the driver gas pressure, diaphragm thickness, and the required post-reflected pressure and temperature of the experiment.

After the test section is filled with the desired amount of the test gas, the valves leading to the test section are closed. The driver section is then filled gradually with helium until the pressure difference between the two tube sections becomes greater than the yield strength of the diaphragm material, which leads to rupturing the diaphragm. A shock wave forms and travels along the driven section, increasing the pressure and the temperature of the test gas. For example, for an experiment at a reflected shock pressure of 12 atm, the driven section is filled with the test gas (e.g. 2.7% fuel, 20.4% O_2, and 76.9% Ar) to about 40 kPa, then the driver gas is filled with helium. The diaphragm ruptures when the pressure in the driver section is nearly 9.5 atm, leading to the desired test pressure of 12 atm. For subsequent runs, the tube is evacuated, returned to atmospheric pressure and cleaned out, as need arises. The diaphragm is then replaced; the thickness is chosen in accordance with the desired nominal pressure. The effect of temperature is studied by varying the fill pressure, while the pressure effect is investigated by varying the diaphragm thickness. The instrumentation used for data acquisition in the shock tube facility is discussed in the next section.

2.3   Data acquisition and processing

The shock tube is equipped with four fast-response PCB transducers (3 units of PCB 113A24 and one PCB 113A26) mounted 40 cm apart along the end of the driven section, with one transducer mounted at the endwall, as shown in Figure 2.3. Pressure signals from the transducers are used to capture the arrival times of the shock wave at the locations of the transducers. Post-reflected shock temperatures are determined from the one-dimensional shock equations. The pressure transducers are powered using a signal conditioner (PCB 482C).

Sidewall and endwall ignition delay time measurements in the new facility can be simultaneously performed by means of mounted optical fibers, connected to photodiodes. The photodiodes are equipped with 430 ± 10 nm narrow band filters to obtain CH chemiluminescence signals for ignition delay time determination.

All voltage signals output from the pressure transducers and the photodiodes are acquired by a National Instruments 100 MHz data acquisition card (NI PCI-5105). A LabVIEW program is written to interface the data acquisition card to a desktop computer. Data acquisition is triggered by a positive gradient of the pressure registered by a designated sensor near the endwall. Figure 2.4 illustrates the data obtained from a typical experimental realization.

The pressure transducer and photodiode signals are further processed to obtain the ignition delay time, the shock velocity, and the post-reflected shock pressures. For this purpose, a MATLAB code is developed. The code identifies the arrival times by capturing the intersection of the maximum gradient line with the initial baseline pressure signal. Figure 2.5a illustrates the identification of the arrival time at a pressure transducer location.

From the shock arrival times, the shock velocity is determined as the ratio of transducer separation to arrival time differences between the sensors. The shock velocity is observed to
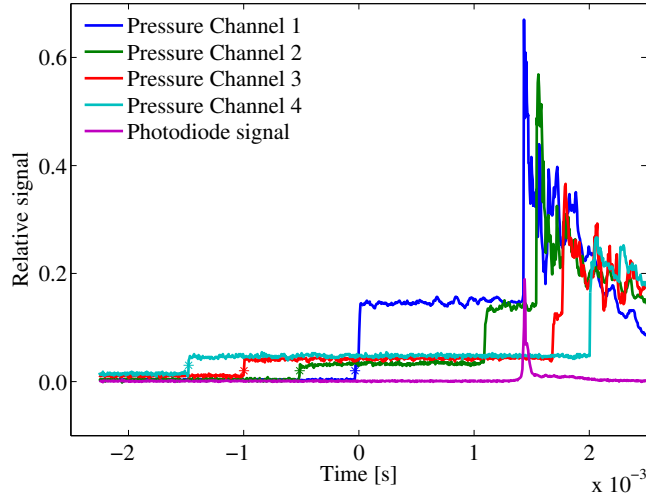
Figure 2.4: Representative signals from an experiment. Shown are pressure and photodiode recording of CH chemiluminescence signals for a DMF/O_2/Ar mixture with $\phi = 1.0$, $D = 3.76$, $p = 1.9$ atm and $T = 1258$ K.
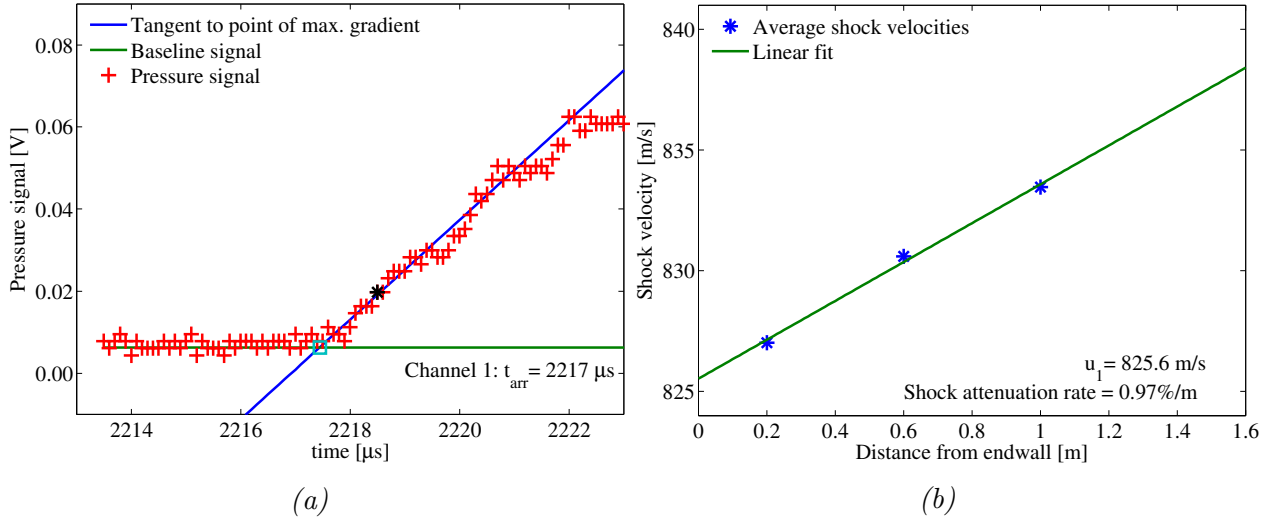
Figure 2.5: (a) Representative shock wave arrival time measurement. Shown is pressure signal near the endwall with corresponding arrival time for a DMF/O_2/Ar mixture with $\phi = 1.0$, argon/oxygen ratio, $D = 3.76$, $p = 1.9$ atm and $T = 1258$ K. (b) Representative shock velocity profile. Shown are shock velocities at intermediate locations between pressure transducers with a linear fit, for a DMF/O_2/Ar mixture with $\phi = 1.0$, argon/oxygen ratio, $D = 3.76$, $p = 4.2$ atm and $T = 1253$ K.

decrease as the wave travels down the tube. This shock attenuation is caused by boundary layer and other non-ideal effects. The calculated velocities are then extrapolated to the endwall location using linear regression to estimate the shock velocity at the test section, as

shown in Figure 2.5b. The shock attenuation rate is also calculated and illustrated in the figure.

The ignition delay time is the time between the pressure rise due to the arrival of the shock wave at the pressure sensor at the endwall and the maximum gradient of the photodiode signal. Figure 2.6 is an example of the pressure and CH chemiluminescence signal used to determine the ignition delay times.
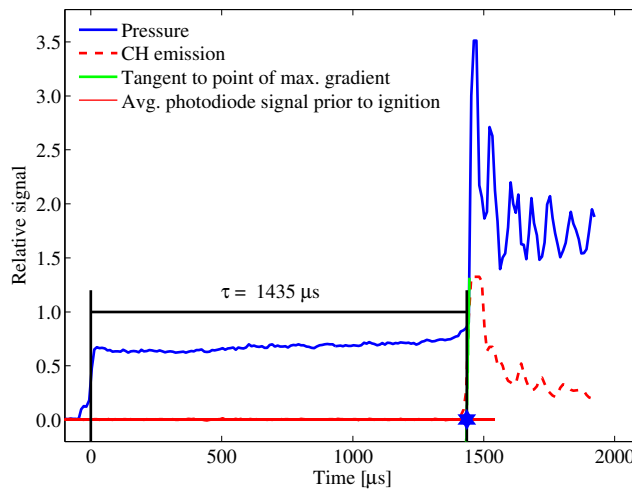
Figure 2.6: Representative ignition delay time measurement. Shown are the sidewall pressure and CH emission signals, for a 2-EF/O_2/Ar mixture with $\phi = 1.0$, $D = 3.76$, $p = 4.6$ atm, and $T = 1065$ K.

Post-reflected shock pressures are compared to measurements and they generally show excellent agreement, as will be demonstrated later on. The post-reflected temperature is calculated using the CANTERA software package [100] along with the Caltech shock and detonation toolbox [114], which utilize the shock equations along with temperature dependent thermodynamic properties of the test gases; to determine T_5 from the initial conditions and the measured shock velocity as previously discussed. Together with the initial conditions and the shock velocity, accurate thermodynamic data and concentration of species are necessary for the determination of the post-reflected temperature. Thermodynamic properties used in this work are determined using group additivity methods which have been proven to be sufficiently accurate. The agreement between the calculated and measured p_5 attest to the

validity of the estimated temperature.

It is known that endwall and sidewall ignition delay times are such that the sidewall delay times generally tend to be shorter than those measured at the endwall [115–117]. For highly diluted mixtures, Petersen [117] recommends using sidewall emission signals to define ignition delay times. The author recommends endwall emission signals for less diluted mixtures with the reasoning that the associated strong ignition can affect the ignition process downstream. If the distance of the sidewall from the endwall is minimized, the differences can also be minimized. It is observed that for long ignition delay times, both definitions yield approximately the same delay time while for the shorter delay times that are observed at higher temperatures, the differences are more pronounced, as shown in Figure 2.7b.
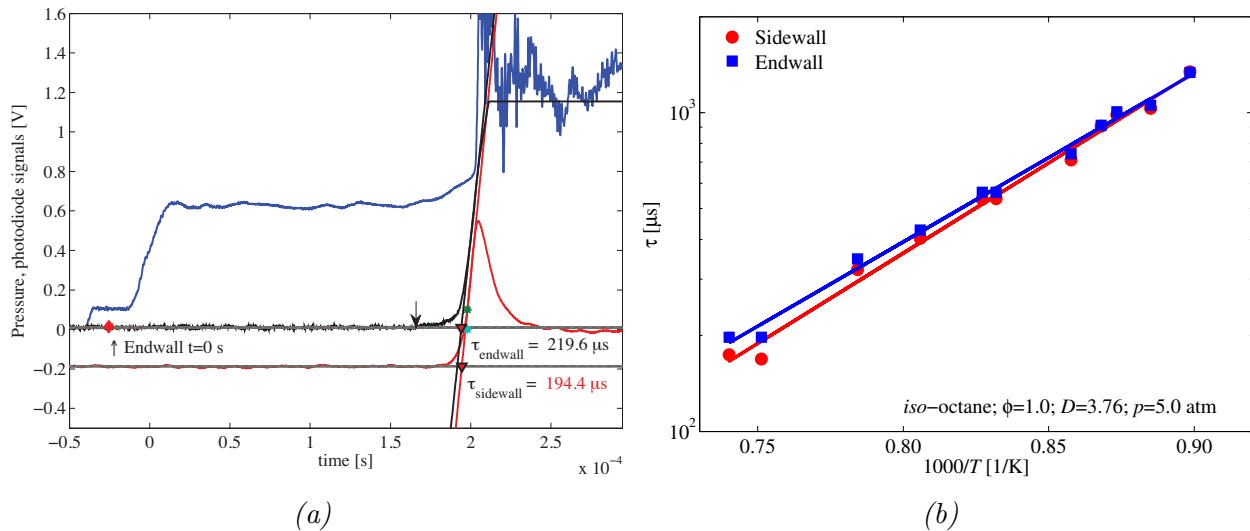
Figure 2.7: (a) Sidewall and endwall CH emission signals for stoichiometric iso-octane/O_2/Ar mixture at pressure of 5.0 atm, temperature of 1351 K, and D of 3.76. (b) Sidewall and endwall ignition delay time measurements for stoichiometric iso-octane/O_2/Ar mixture at pressure of 5.0 atm, and D of 3.76.

This is thought to be related to the fact that the endwall signal results from cumulative ignition of layers of mixture that have been processed by the reflected shock wave at different times. These cases are exemplified in Figure 2.7a. This time difference is negligible for long delay times but significant for shorter delay times. In the results presented later, sidewall measurements are used.

2.4   Experimental validation

As this facility is newly built and first employed for the studies in this work, it is necessary to validate the experimental facility against theoretical gas dynamic predictions and literature data on ignition. For validation of the gas dynamics embodied in the shock equations; the measured post-reflected shock pressures are compared with calculated pressures at various conditions. Figure 2.8 shows a representative comparison of measured and calculated post-reflected shock pressures for two series of shock tube experiments, one is for a non-reactive mixture, and the other is for stoichiometric DMF/O_2/Ar mixtures with $D = 16.6$. The figure shows good agreement between the measured and calculated pressures, which attests to the accurate measurement of the shock velocity and confirms that the one-dimensional model captures the shock behavior after accounting for attenuation. Hence, it can be inferred that the calculated temperatures are reflective of the actual temperatures behind the reflected shock.
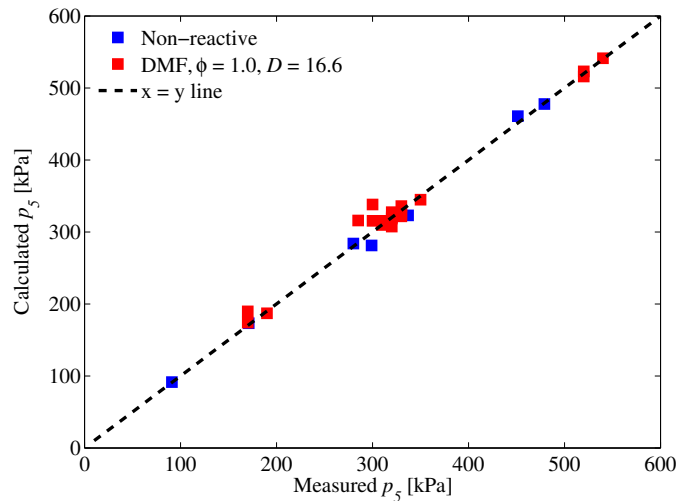
Figure 2.8: Comparison of calculated and measured p_5 for non-reactive mixtures of Ar, and reactive stoichiometric DMF/O_2/Ar mixtures with $D = 16.6$.

The shock tube has also been validated against ignition delay time measurements from the literature. Figure 2.9 shows comparison of DMF ignition delay times from this work against

data by Somers et al. [12], while Figure 2.10 compares ignition delay times of 2-MF against previous results by Wei et al. [43]. Good agreement with literature data is observed in both cases. This implies that the facility reproduced reasonably well measurements of other labs.
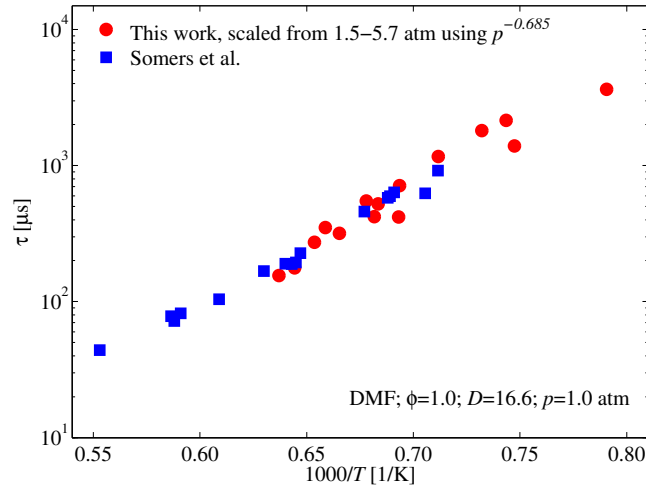
Figure 2.9: Comparison of ignition delay times for stoichiometric DMF/O$_2$/Ar at a pressure of 1.0 atm and D = 16.6 with data by Somers et al. [12].
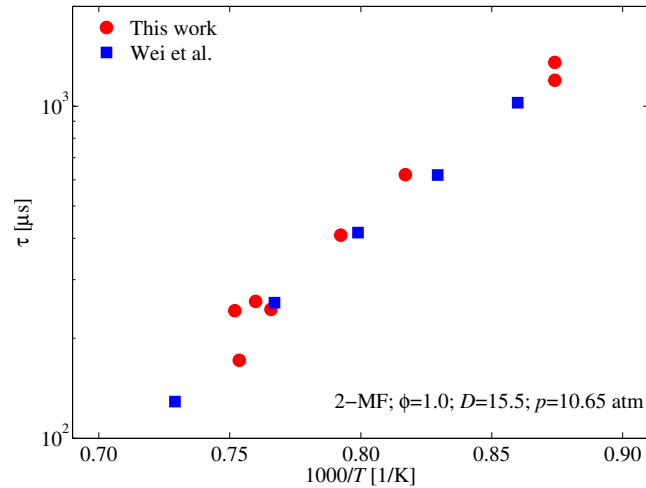
Figure 2.10: Comparison of ignition delay times for stoichiometric 2-MF/O$_2$/Ar mixture at a pressure of 10.65 atm and D = 15.5 with data by Wei et al. [43].

For gas dynamic reasons, such as relaxation timescales, it is preferable to use argon as a diluent, instead of the standard nitrogen in technical oxidizers, such as air. In this case, we need to know how the results relate to those of fuel/air experiments. To this end, the ignition delay times of *iso*-octane/O$_2$/Ar and *iso*-octane/O$_2$/N$_2$ mixtures are compared. Ignition

delay times are obtained for stoichiometric *iso*-octane/O_2/Ar and *iso*-octane/O_2/N_2 mixtures with $D = 3.76$ at 8.0 atm. Figure 2.11 shows that both data sets are in good agreement with each other, implying that the type of diluent has a limited effect on the ignition behavior of *iso*-octane mixtures. However, it has been noted, and can also be seen here at lower temperatures; that argon diluted mixtures tend to have lower ignition delay times which are not markedly outside the uncertainty band of the data for nitrogen diluted mixtures. Because of the negligible differences between Ar-diluted and N_2-diluted mixtures, more extensive comparisons can be made with other data sets under similar ϕ, D, and p conditions. For the rest of this work, mixtures consist of fuel, O_2, and Ar.
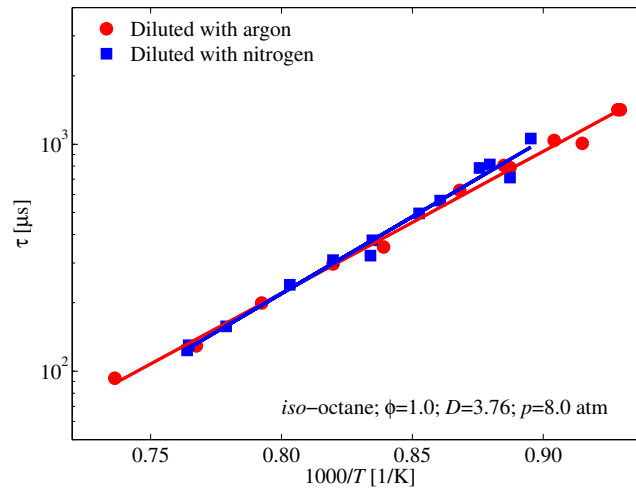
Figure 2.11: Diluent effect on ignition of stoichiometric iso-octane/O_2/diluent mixtures at a pressure of 8.0 atm and D = 3.76. The lines represent Arrhenius fits to the data points for improved legibility.

2.5 Experimental uncertainties

In this section, uncertainty analysis is presented for ignition delay time measurements, assuming a known dependence of ignition delay time on pressure, equivalence ratio, and temperature in the form:

$$\tau \propto p^a \phi^n \exp\left(\frac{E_a}{RT}\right) \tag{2.11}$$

Uncertainties in the results are linked to the ignition delay time determination from CH emission signals and the initial conditions of the ignition reactor. The post-reflected shock temperature constitutes the greatest source of uncertainty, due to the high temperature sensitivity of chemical reaction rates. The major source of temperature uncertainty is the shock velocity uncertainty. This in turn arises from uncertainties in sensor separation, the time intervals between sensors, and shock attenuation.

A typical shock attenuation rate is usually below 1% per meter [118]; this rate, combined with short test times, render the post-reflected temperature rise due to boundary layer fairly negligible. For the following temperature uncertainty analysis, it is therefore assumed that the incident shock velocity, V_s, is constant in the region of test observation.

The total uncertainty in shock velocity and post reflected shock temperature are often calculated using the maximum-error method, in which the error is calculated in a given function by assuming the maximum possible error in each of the variables in the function. Another method for uncertainty calculation, the statistical method, is commonly used. This method can be used for error estimation for functions that contain several variables whose uncertainties are independent [119–121]. According to a study by Peterson et al. [121], the uncertainty estimates from the maximum-error method are generally more conservative than those from the statistical method. However, the study shows that the statistical method

produces more realistic uncertainty estimates. The statistical method is therefore used in the following uncertainty analysis.

The reflected shock temperature is calculated from the 1D shock equations. For the purpose of these analysis we shall use the simplified equation, assuming constant specific heats and ideal gas behavior. Thus the temperature is calculated as a function of the unshocked gas temperature, T_1, the driven gas specific heat ratio, γ, and the shock Mach number, M, as follows [109]:

$$T_5 = \frac{T_1 \left[2\left(\gamma - 1\right)M^2 + \left(3 - \gamma\right)\right]\left[\left(3\gamma - 1\right)M^2 - 2\left(\gamma - 1\right)\right]}{\left(\gamma + 1\right)^2 M^2} \tag{2.12}$$

In this thesis, the driven gas used is argon, which has a specific heat ratio, γ, of 1.67. Adding fuel and O_2 reduces the γ of the mixture. But generally the most abundant gas is argon. To better suit the statistical method of uncertainty calculations, equation (2.12) can be approximated at an initial temperature of 300 K to [121]:

$$T_5 = 225.1M^2 + 149.85 - 74.99M^{-2} \tag{2.13}$$

The Mach number, M, is a function of the shock velocity, V_s, and the speed of sound in the driven gas, as follows:

$$M = \frac{V_s}{\sqrt{\gamma R T_1}} \tag{2.14}$$

where R is the specific gas constant for the driven gas, which can be calculated by dividing the universal gas constant, $\bar{R}$, by the molecular weight of argon. The shock velocity, V_s, can be calculated from the pressure transducer separation, Δx, and the time between the transducers, Δt, as follows:

$$V_s = \frac{\Delta x}{\Delta t} \tag{2.15}$$

If the maximum-error method is used, the worst-case values of Δx and Δt are used to calculate V_s from (2.15), which is used to calculate the worst-case Mach number and T_5 from equations (2.12) and (2.14). In the statistical method used in this thesis, the uncertainty in each variable is considered in the calculation of T_5 through the root-sum-squares (RSS) method [120], which is used first to obtain the uncertainty in shock velocity, δ_{V_s}, as a function of Δx, Δt, and their uncertainties, $\delta_{\Delta x}$ and $\delta_{\Delta t}$. The sensor separations can be measured to 1 mm while the temporal resolution of the fast-response PCB pressure transducers is 1 μs. These values are therefore used herein as conservative estimates of spatial and temporal uncertainties in sensor separation. The uncertainty in shock velocity is calculated as follows [121]:

$$\delta_{V_s} = \sqrt{\left(\frac{\partial V_s}{\partial (\Delta x)}\delta_{\Delta x}\right)^2 + \left(\frac{\partial V_s}{\partial (\Delta t)}\delta_{\Delta t}\right)^2}$$
$$= \sqrt{\left(\frac{1}{\Delta t}\delta_{\Delta x}\right)^2 + \left(\frac{-\Delta x}{(\Delta t)^2}\delta_{\Delta t}\right)^2} \tag{2.16}$$

T_5 is a function of Mach number of the driven gas. The post reflected shock temperature uncertainty can therefore be calculated from equations (2.12) and (2.14) as follows:

$$\delta_{T_5} = \frac{\partial T_5}{\partial M}\delta_M = \left(450.19M + 149.98M^{-3}\right)\frac{\delta_{V_s}}{\sqrt{\gamma R T_1}} \tag{2.17}$$

For most dilute mixtures, a shock velocity uncertainty of 1 m/s, equivalent to 0.12% uncertainty in Mach number, can lead to a temperature difference of 3-4 K.

The next step is to derive the ignition delay time uncertainty from the uncertainty in temperature and other sources. Based on equation (2.11), ignition delay time can be written as a function of pressure, temperature, and equivalence ratio in the form:

$$\tau = A p^a \phi^n \exp\left(\frac{b}{T}\right) \tag{2.18}$$

For a mixture with a constant equivalence ratio, the equivalence ratio is no longer a factor in the ignition delay time calculation. The ignition delay time uncertainty is therefore calculated using the root-sum-squares (RSS) method from pressure and temperature uncertainties as follows [122]:

$$\delta_\tau = \sqrt{\left(A e^{\frac{b}{T}} a p^{a-1} \delta_p\right)^2 + \left(A e^{\frac{b}{T}} p^a \frac{b}{T^2} \delta_T\right)^2} \tag{2.19}$$

Prior to ignition, the postreflected pressure can rise as a result of non-ideal effects of mild exothermicity of the reactor. For simulations of ignition using constant volume reactors, the rise due to non-ideal effects needs to be accounted for. It has been observed that for ignition delay times of the order of 1 ms, simulated ignition delay times are insensitive to moderate pressure rise of a few percents per millisecond [123–125]. The majority of the delay times in this work are shorter than 2 ms and, therefore, the experimental delay time is not significantly affected by the pressure rise during the induction period. The latter has been determined to range from near zero to 6%/ms. Otherwise, the effect of pressure rise would have to be accounted for in simulations. An example of shock attenuation rate for this study has been shown in Figure 2.5b. The ignition delay time uncertainty from equation (2.19) can therefore be expressed as follows:

$$\delta_\tau = A e^{\frac{b}{T}} p^a \frac{b}{T^2} \delta_T \tag{2.20}$$
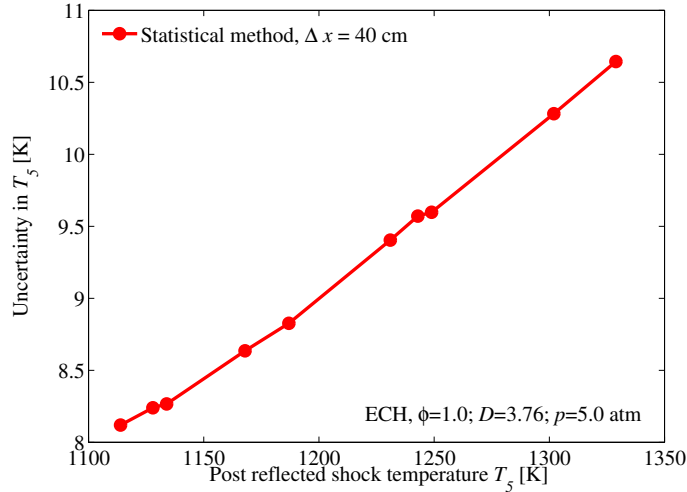
Figure 2.12: Post reflected shock temperature uncertainties for a stoichiometric ECH mixture at a nominal pressure of 5.0 atm and an Ar/O_2 ratio of 3.76.

An example uncertainty analysis is performed for ignition delay time measurement for stoichiometric mixtures of ethylcyclohexane (ECH) at a nominal pressure of 5.0 atm and an Ar/O_2 ratio of 3.76. The uncertainty analysis starts with the calculation of the shock velocity uncertainty from equation (2.16) for a sensor separation of 40 cm, a spatial separation uncertainty of 1 mm, and a temporal separation uncertainty of 1 μs, as discussed earlier, followed by the calculation of temperature uncertainty. The post reflected shock temperature uncertainties for test temperatures between 1114 and 1329 K are shown in Figure 2.12. The figure shows that the temperature uncertainties range from $\pm 8.1 - \pm 10.6$ K. It is also observed that the uncertainty increases with increasing temperature and shock velocity. These results correspond to shock velocity uncertainty between $\pm 2.4 - \pm 2.8$ m/s, which means that a shock velocity uncertainty of 1 m/s translates into a temperature uncertainty between $\pm 3.3 - \pm 3.7$ K.

To study the effect of temperature uncertainty on ignition delay times, the ignition delay time uncertainty is calculated from equation (2.20). A logarithmic multiple linear regression is performed for this data set to identify the values of A, a, and b in equation (2.21). The resulting correlation is:
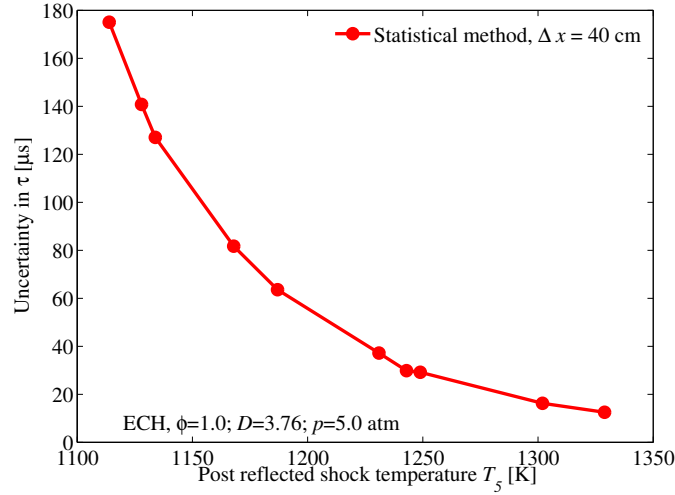
Figure 2.13: Ignition delay time uncertainties for a stoichiometric ECH mixture at a nominal pressure of 5.0 atm and an Ar/O_2 ratio of 3.76.

$$\tau = 9.00343 \times 10^{-5} p^{0.5704} \exp\left(\frac{17571.27}{T}\right) \tag{2.21}$$

The uncertainty in ignition delay time resulting from temperature uncertainty is then calculated, and the results are presented in Figure 2.13. This figure shows that the ignition delay time uncertainties range from $\pm 12 - \pm 175 \ \mu$s. Ignition delay time uncertainties increase with decreasing temperature as the ignition delay time increases. Therefore, the ignition delay time uncertainty due to temperature uncertainty is observed to be up to $\pm 13\%$ at the lowest temperature, 1114 K.

It has been established that the actual ignition delay times determined from CH chemiluminescence signals are relatively more accurate with errors in slope fit and extrapolation within 3%. Taking this source of uncertainty into consideration, the overall ignition delay uncertainty is up to $\pm 13.34\%$. Generally, it is assumed that the estimated uncertainties are fairly systematic and do not compromise the result of comparative studies, as undertaken here.

A more conservative estimate of uncertainties has been reported by the author in a number of

studies [104, 105], where the temperature corresponding to this measurement is uncertain to about 20-30 K, according to a shock velocity uncertainty of 5-10 m/s at a typical shock velocity of 800 m/s. An Arrhenius-type ignition delay dependence on temperature was assumed, where an uncertainty of 25 K would translate into an ignition delay time uncertainty of up to 30% at 1000 K. However, the results presented in this section are based on more detailed uncertainty analysis and therefore they can be considered a more realistic representation of the experimental uncertainties in the shock tube facility.

Chemical kinetic model analysis

3.1 Analysis of homogeneous constant volume reactor

The transformation of fuel and oxidizer to combustion products is generally described by detailed chemical kinetic mechanisms. For example, the oxidation of an alkane of general formula, RH, proceeds through a number of elementary reactions that involve a number of intermediate species, as shown in Figure 3.1. Thus, a detailed chemical kinetic model usually contains elementary reactions among a number of species. The main objective of mathematical modeling of combustion kinetics is to predict the temporal evolution of the species compositions and the other thermodynamic properties.

Three different model systems are often used in chemical kinetic for combustion: the kinetics of a homogeneous reactor, that of a perfectly stirred reactor, and the one-dimensional propagation of a laminar premixed flame [126]. Of interest in this work is the homogeneous reactor model, in which the time evolution of a chemical system, consisting of I elementary steps among K species, is represented by an initial-value problem that is governed by a set of first-order ordinary differential equations (ODEs). The reactor is considered under adiabatic, constant-volume conditions [126]. These equations include: temporal evolution of species

RH

OH

Smaller radical (R₁) + Alkene (A₁)

R

- **A₁ further reacts as RH.**
- **R₁ further reacts as R.**
- **Smaller compounds are formed.**

O₂

O₂   HO₂ + Alkene (A₂)

RO₂

QOOH ⟶ Products + OH

O₂

O₂QOOH

OH + R'OOH ⟶ R'O + OH
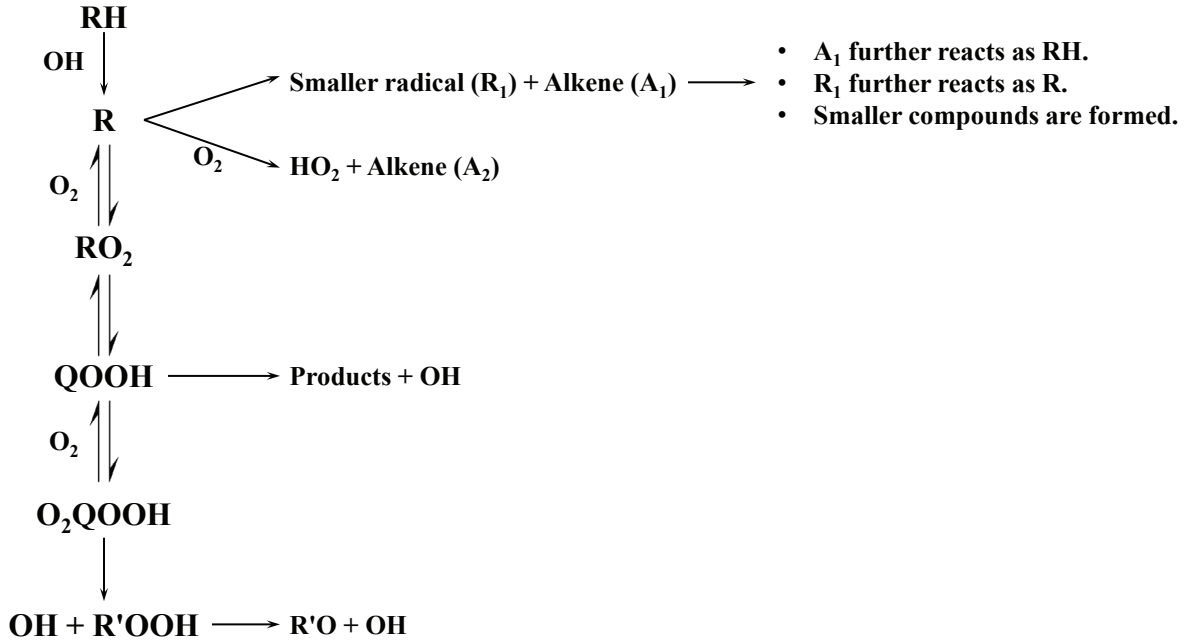
Figure 3.1: Mechanistic description of the oxidation of a generic fuel, RH. QOOH is an alkyl hydroperoxide radical, produced from RO_2 by intramolecular H atom transfer.

concentration:

$$\rho \frac{\mathrm{d}Y_k}{\mathrm{d}t} = \dot{\omega}_k W_k \tag{3.1}$$

conservation of energy:

$$\rho c_v \frac{\mathrm{d}T}{\mathrm{d}t} + \sum_{k=1}^{K} e_k \dot{\omega}_k W_k = 0 \tag{3.2}$$

and equation of state:

$$p = \rho \frac{R}{\overline{W}} T. \tag{3.3}$$

where Y_k is the mass fraction of the kth species, W_k is the molar mass of the kth species, e_k is the specific internal energy of the kth species, c_v is the averaged constant volume specific heat, $\overline{W}$ is the mean molecular weight of the mixture, and $\dot{\omega}_k$ is the molar rate of production of the kth species by chemical reaction, mathematically defined as:

$$\dot{\omega}_k = k_f \prod_{i=1}^{N} Y_i^{v_i'} - k_r \prod_{i=1}^{N} Y_i^{v_i''} \tag{3.4}$$

where k_f and k_r are the forward and reverse reaction rate of the ith elementary chemical reaction, and v_i' and v_i'' are the reactant and product stoichiometric coefficients of the ith elementary chemical reaction, respectively.

For a mechanism with hundreds of species and thousands of elementary reactions, it can be challenging to solve the ODEs for each of the species at small time steps. As a result, chemical kinetic software packages have been developed and widely implemented to solve these ODEs. These software modules are generally systems of subroutines that make use of chemical kinetic and thermodynamic data bases to compute the terms in the governing ODEs, and hence solve them for each of the species [126]. Among these chemical kinetic softwares, the CHEMKIN [127] and the CANTERA [100] software packages are the most widely used software in combustion chemical kinetic analyses.

In this thesis, the main objective of chemical kinetic analyses is to simulate ignition delay times at conditions similar to the experimental conditions, in order to compare model predictions with experimental results. Moreover, reaction pathway analyses are carried out to gain better understanding of the fuel reaction pathways. Such analyses enable us to properly rationalize the experimentally established reactivity trends, and clarify the reactivity differences among various fuels.

For more general use of chemical kinetic models, mechanism reduction is required. Here, different approaches of mechanism reduction are compared and one is used in this work. First, a new reduction method which is aimed at reducing computational requirements of the ASE method is developed and evaluated. The new method is referred to as the Stochastic Species Elimination (SSE) method. Finally, the SSE and the ASE approaches are compared with respect to the reduction of the *iso*-octane model version 3 by Mehl et al. [102], the *n*-heptane model version 3.1 by Mehl et al. [10], and the *n*-octanol model by Cai et al. [103].

3.2 Chemical kinetic model reduction

Chemical kinetic model reduction has become an important aspect in combustion research, as discussed in chapter 1. In this section, the chemical kinetic model reduction methods used in this work are explained. Firstly, the existing Alternate Species Elimination (ASE) method [96] is demonstrated, highlighting the challenges to the application of this method in mechanism reduction. A stochastic species sampling approach, referred to as the Stochastic Species Elimination (SSE) method, is then proposed based on the existing ASE method. The chapter ends with a discussion of the proposed SSE method. Reduced versions of detailed chemical kinetic models that are obtained without modifying model parameters are referred to as skeletal mechanisms.

3.2.1 Alternate species elimination (ASE)

For the purpose of skeletal mechanism extraction from detailed chemical kinetic models, it is essential to identify the chemical species that are crucial for the prediction of key combustion properties. The alternate species elimination (ASE) [96], previously discussed in the literature review, can be considered as a simple and yet effective model reduction approach. A brief explanation of the standard ASE approach [96] is provided in this section. In essence, the method seeks to identify the most important chemical species in a chemical kinetic model by the evaluating of the effect of eliminating given chemical species on the prediction of combustion properties during the process of combustion simulation. Typically, the homogeneous gas-phase chemical system consists of elementary reactions among chemical species, that can be considered as the degrees of freedom of the system. In such systems, the evolution from an unburnt state to a burned equilibrium state can be described by a system

of ordinary differential equations:

$$\frac{dX}{dt} = f(x_1, x_2, ..., x_n) \tag{3.5}$$

In equation 3.5, X is a column state vector with n variables, consisting of temperature and concentrations of all the $(n-1)$ chemical species involved in the system. The thermodynamic state of the chemical system can be fully defined at each instance of time through the temperature and species concentrations included in the column vector as well as an adequate equation of state. The RHS represents a nonlinear function that includes Arrhenius type reaction rate constant and related species concentrations.

In the case of combustion, the special features of the chemically reacting systems can be exploited for a better understanding of the geometry of their evolution in composition space. One of these systems is the homogeneous reactor, where the chemical system evolves from an unburnt state to a quasi-equilibrium state through a rapid ignition process. Therefore, the initial solution of the system can be formulated in the form of m nonzero components of the initial state vector, X_0:

$$X(t_0) = X_0(x_{10}, x_{20}, ..., x_{m0}) \tag{3.6}$$

with $m \ll n$.

Following the ignition event, the system moves gradually towards an equilibrium burned state, X_∞, which consists of q components of the state vector, X_∞, with equilibrium concentrations above a certain threshold; a few parts per billion for instance.

$$X(t_\infty) = X_\infty(x_{1\infty}, x_{2\infty}, ..., x_{q\infty}) \tag{3.7}$$

with $m < q < n$, since a number of species is formed after ignition, including major combustion products such as CO_2 and H_2O, pollutants, such as CO, soot, unburned hydrocarbons (UHCs),

and other volatile organic compounds (VOCs). Between the initial and equilibrium states, a large number of intermediate species is formed, such that the number of nonzero components of the system approaches n, especially near the ignition event.

The complete chemical system consisting of $n - 1$ species can be replaced with a system of a smaller size with $r - 1$ species, while preserving the predictive performance of key combustion properties similar to that of the detailed model. These key properties include global combustion properties, such as ignition delay times and burning velocities, as well as concentration profile of various species, including fuel and pollutants. The removal of species which have no effect on the prediction of such properties would result in a reduction of the number of species in the chemical system.

The effect of eliminating each species on the prediction of a characteristic combustion property can be assessed using a normalized change in the property. In this work, the ignition delay time, τ, is used as the combustion property of interest. In this case, the normalized change, NC, is defined as:

$$NC_i = \frac{\tau_i - \tau_0}{\tau_0} \tag{3.8}$$

where τ_0 and τ_i are the ignition delay times observed before and after suppressing the sub chemistry of the ith species under consideration.

All chemical species in the system are then ranked based on the absolute magnitude of their normalized changes, NC. The number of chemical species crucial for the prediction of desired combustion properties can be determined at a specific accuracy level compared to the predictions of the detailed model.

The main goal of the ASE method is to obtain a skeletal model from the detailed mechanism. This can be achieved by imposing a user-defined threshold, NC_{thresh}, followed by the elimination of all species whose NCs are below this threshold. The value can be determined by testing the new skeletal mechanism against the detailed model in terms of predicting

different combustion properties. To accurately predict flame propagation, a lower threshold is often necessary, compared to the relatively simpler prediction of ignition delay time. It has been observed that a threshold less than or equal to 1×10^{-4} ensures relatively good agreement with detailed models for both flame propagation and ignition delay. A threshold of 5×10^{-4} can provide good prediction of ignition behavior with acceptable deviations in flame propagation predictions [96].

3.2.2 Stochastic species elimination (SSE)

While the ASE method is a simple and effective model reduction approach, some challenges to the full exploitation of its capabilities need to be addressed. Firstly, the ASE method is applied by alternately considering all the species in the detailed mechanism using the CANTERA [100] software package. Model developers tend to list the species in a random manner or such that certain radicals and intermediate species appear close to each other in the species list. Some of these radicals may be identified as dispensable and can be removed. However, they may be placed at the end of the list so that they are only considered for elimination towards the end of the ASE reduction process. Therefore, the number of iterations needed to reach a certain level of reduction is not fixed; it depends on the order in which the chemical species are listed in the detailed model. The statistical dependence of the ASE method on the species arrangement need to be eliminated for a better control over the desired level of reduction. Secondly, the computational requirements of the ASE method are relatively high for various reasons. In ASE method, the normalized changes (NCs) in a given combustion property from stoichiometric, rich, and lean conditions are calculated, averaged, and ranked for model reduction purposes. Therefore, the ASE process needs to be performed at least three times to capture the chemistry of a wide range of conditions. Moreover, for each eliminated species, an ignition delay time simulation needs to be performed for a nearly full sized mechanism, since only one species is eliminated at a time.

In this work, the alternate species elimination (ASE) [96] method is modified to a stochastic sampling model reduction approach, with the possibility of multi-species sampling. The modified approach is referred to in this work as the Stochastic Species Elimination (SSE) method. The main feature of the SSE method is that the species under consideration are randomly sampled, regardless of their original position in the species list. This species randomization eliminates the statistical dependence of the reduction process on the order of species in the detailed model. This allows for a real-time observation of the level of reduction attained in terms of the number of retained species. The users have the freedom to stop the reduction process when a certain user-defined reduction level is reached, thus leading to a less computationally expensive reduction process.

Another feature of the SSE method is the dynamic mechanism sizing. As mentioned previously, each iteration in the ASE method uses a full sized mechanism less are the reactions involving the species under examination, which increases the computational requirements of the process. In SSE, the mechanism size used in ignition delay simulation decreases dynamically as species are eliminated. As more species are eliminated, zeros are entered in the solution matrix for the eliminated species, and thus the matrix becomes more sparse. For example, for an iteration with m species already eliminated, the mechanism used in ignition delay simulation contains $n - m - 2$ species, with all the species already eliminated as well as the species under consideration entered as zeros in the solution matrix. For the same iteration in the ASE method, the mechanism size would be typically $n - 2$ species. This feature leads to a relatively faster reduction process compared to the standard ASE method. The dynamic mechanism sizing calls for dynamic threshold determination, as the NC from eliminating a certain species in SSE would differ from that in ASE due to mechanism size differences. As unimportant species are continuously removed in SSE, important species become more important, leading to greater NC value for important species in SSE compared to ASE. Therefore, a larger threshold value (NC_{thresh}) can be used safely as the mechanism size decreases in the SSE method. The threshold is set to dynamically increase with each eliminated species until it

reaches an error value of 0.1% by the end of the reduction process.

Moreover, the SSE method eliminates the need for multiple NC calculations for different equivalence ratios. Species are automatically retained in SSE if the NC for a species under consideration exceeds the set threshold for elimination at stoichiometric condition. Rich and lean conditions are only investigated if the NC at stoichiometric condition is not sufficient for species retention. This contributes to the reduction of the computational requirements of the reduction method. In ASE, the species elimination is based on an average NC value from three different equivalence ratios. Because elimination of a species in SSE is based on a simple simulation, and not an average as in ASE, the NC_{thresh} is set a bit higher, up to 3 times the value that would be used in a corresponding ASE.

Ignition investigations of various fuels

In this chapter, the ignition behavior of various fuels is investigated through shock tube ignition delay time measurements. These fuels have been presented in Figure 1.3 and will be recalled at the beginning of each section. Firstly, a comparative study of the ignition behavior of the furans, DMF, 2-MF, and furan is performed. This is followed by a comparison between experimental results and model predictions of recently published chemical models of these fuels by Sirjean et al. [13] and Somers et al. [12]. Secondly, the ignition behavior of DMF, a representative furan, is compared to that of *iso*-octane, a representative gasoline surrogate. The ignition behavior of their blends is also studied. A combined *iso*-octane/DMF model is then assembled from recently published models of the pure fuels by Somers et al. [12] and Mehl et al. [10], to enable the simulation of blend combustion. Further, a comparative ignition study of the saturated furans, THF and MTHF, is then presented. The results of MTHF are used to highlight kinetic differences between 2-MF and 2-MTHF. Finally, the ignition behavior of dimethyl and ethyl isomers of cyclohexane, DMCH and ECH is compared. The ignition delay times of DMCH and ECH are further compared to ignition data of dimethyl and ethyl isomers of furan, DMF and 2-EF.

4.1   Comparison of dimethyl furan, 2-methyl furan, and furan

In this section, the comparative ignition behavior of different furans is investigated. The three furans, DMF, 2-MF, and furan, shown in Figure 4.1, are studied at equivalence ratios, ϕ, of 0.5, 1.0, and 2.0 over a range of pressures, up to 12.0 atm, and various diluent/O_2 ratios. The mixtures investigated are shown in Table 4.1.

2,5-dimethyl furan   2-methyl furan   furan
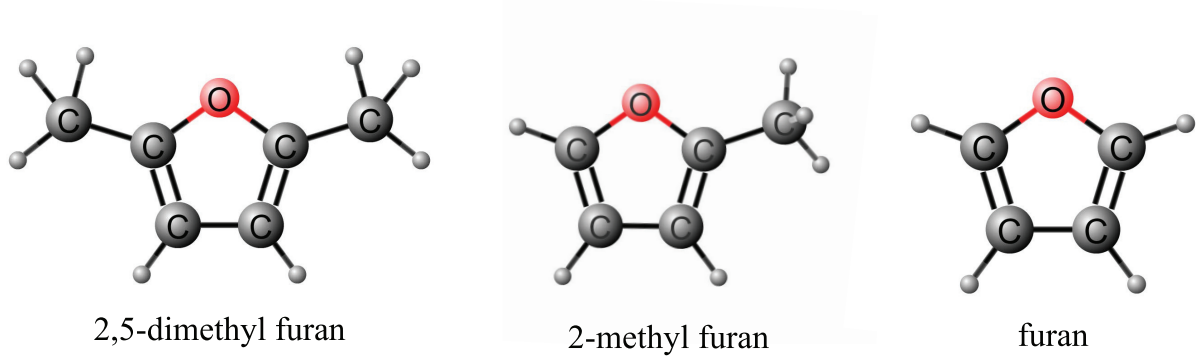
Figure 4.1: Chemical structure of the investigated furans.

Table 4.1: DMF, 2-MF, and furan mixtures investigated using constraints of ϕ and D

Fuel	ϕ	D	Fuel %	O_2 %	Ar %
DMF	1.0	3.76	2.56	20.47	76.97
	2.0	3.76	5.32	19.90	74.78
	0.5	3.76	1.38	20.72	77.90
	*1.0	12.2	1.00	7.49	91.51
	*1.0	16.6	0.76	5.63	93.62
2-MF	1.0	3.76	3.38	20.28	76.34
	2.0	3.76	6.54	19.63	73.83
	0.5	3.76	1.72	20.65	77.63
	1.0	12.2	1.22	7.48	91.30
	*1.0	15.5	1.00	6.00	93.00
Furan	1.0	3.76	4.46	20.07	75.47
	2.0	3.76	8.54	19.21	72.25
	0.5	3.76	2.28	20.53	77.19

* Mixtures used for validation experiments.

Variations in the post-reflected shock pressures of individual experimental realizations from the nominal pressure are accounted for in the figures using a power law of the form $\tau \propto p^n$.

The exponent n is determined from linear regression of stoichiometric data with the same argon/oxygen ratios. The exponents are found to be -0.59 for DMF, -0.83 for 2-MF, and -0.69 for furan. The individual powers for each fuel are obtained using a separate ignition delay correlation for each of fuels, in the format:

$$\tau = C p^{\alpha} \exp\left(\frac{E_a}{RT}\right) \tag{4.1}$$

where τ is the ignition delay time in microseconds, C is a constant, p is the pressure in atmospheres. E_a is the global activation energy in kcal/mole, and $R = 1.986 \times 10^{-3}$ kcal/(mol K) is the universal gas constant. The powers are calculated by linear regression of the correlation using its logarithmic form:

$$\ln(\tau) = \ln(C) + \alpha \ln(p) + \frac{E_a}{RT} \tag{4.2}$$

4.1.1 Experimental results

The ignition behavior of the three furans is investigated at stoichiometric conditions and nominal pressures of 2.0, 5.0, and 10 atm with Ar/O_2 ratio maintained at 3.76, in line with engine combustion, whereby air is used as an oxidizer with a N_2/O_2 ratio, D, of 3.76. The ignition delay times are presented together with an Arrhenius fit for better delineation of trends.

Figure 4.2 shows that at a nominal pressure of 2.0 atm, DMF has the longest ignition delay times, while 2-MF ignites most readily. Furan ignition delay times lie between DMF and 2-MF, with a possible cross-over between DMF and furan at temperatures above 1410 K. This trend is a key finding in this work, which is eluded by previously reported studies of the individual fuels. The relative ignition behavior of DMF and 2-MF also differs from the observation by Uygun et al. [44], where the authors assume that DMF and 2-MF have similar
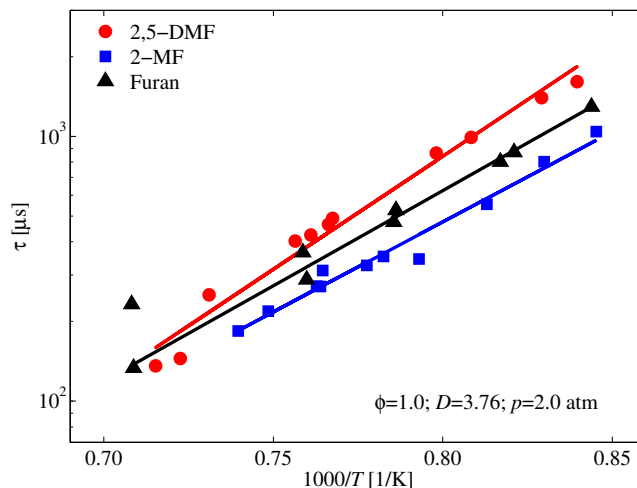
Figure 4.2: Relative ignition behavior of furan, 2-methyl furan (2-MF), and 2,5-dimethyl furan (DMF) at nominal pressure of 2.0 atm. The fuel/O_2/Ar mixture is stoichiometric and the Ar/O_2 ratio, D, is maintained at 3.76.

ignition delay times. They use this as a basis to scale and re-plot DMF data together with 2-MF.

The relative ignition behavior of DMF and 2-MF observed in Figure 4.2 implies that DMF could be well suited for combustion systems where ignition is least desired and that while 2-MF has hitherto only been considered for gasoline applications, its high reactivity could find application in compression-ignition engines as well. From a chemical perspective, it means that double alkylation of furan confers greater chemical stability while the mono alkylated 2-MF introduces higher reactivity. The observed trend is in line with the findings of a number of ignition [128, 129] and flame studies [130–132] of various linear dimethyl and mono-methyl alkanes. These studies reveal that dimethylated alkanes tend to exhibit less chemical reactivity than similar mono-methylated alkanes. However, the differences in reactivity are generally observed to decrease at higher temperatures.

Although a number of quantum mechanical calculations have been carried out for each of these furans [12, 13, 48, 133], it is difficult to comment on the reactivity trends observed among these furans only based on these calculations. A recent study by Sudholt et al. [48] has
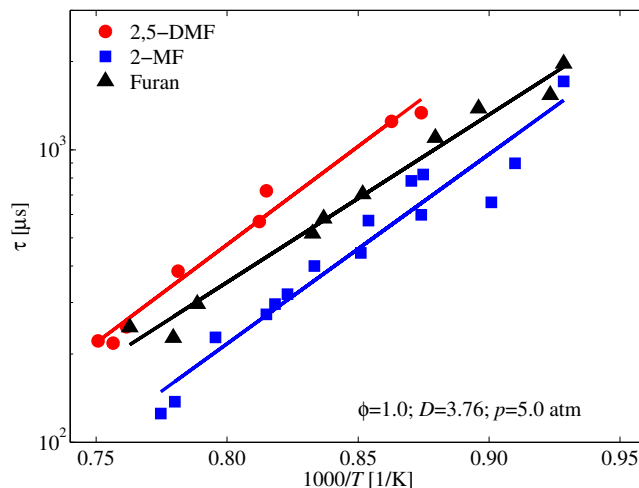
Figure 4.3: Relative ignition behavior of furan, 2-methyl furan (2-MF), and 2,5-dimethyl furan (DMF) at nominal pressure of 5.0 atm. The fuel/O_2/Ar mixture is stoichiometric and the Ar/O_2 ratio, D, is maintained at 3.76.

performed quantum chemistry calculations to determine bond dissociation energies (BDEs) for furan and 2-MF, which are therefore compared to BDEs of DMF reported by Simmie and Curran [134]. The study has shown minimal differences in the BDEs of C–H bonds of the three furans for H-abstraction from side chain carbon, H-abstraction from ring carbon, and methyl group abstraction. However, abnormally high reactivity has been observed for
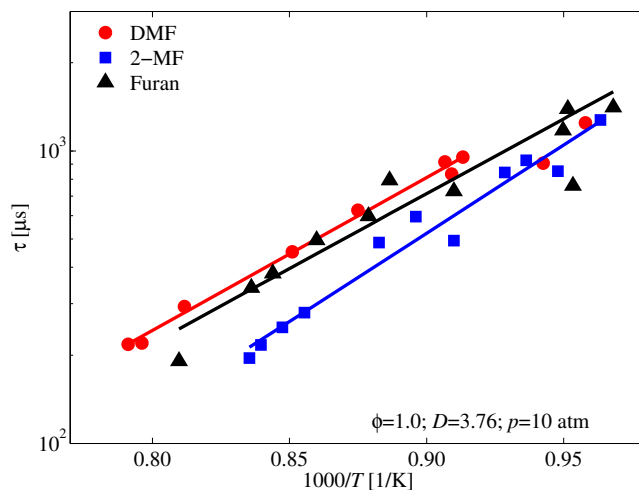
Figure 4.4: Relative ignition behavior of furan, 2-methyl furan (2-MF), and 2,5-dimethyl furan (DMF) at nominal pressure of 10.0 atm. The fuel/O_2/Ar mixture is stoichiometric and the Ar/O_2 ratio, D, is maintained at 3.76.
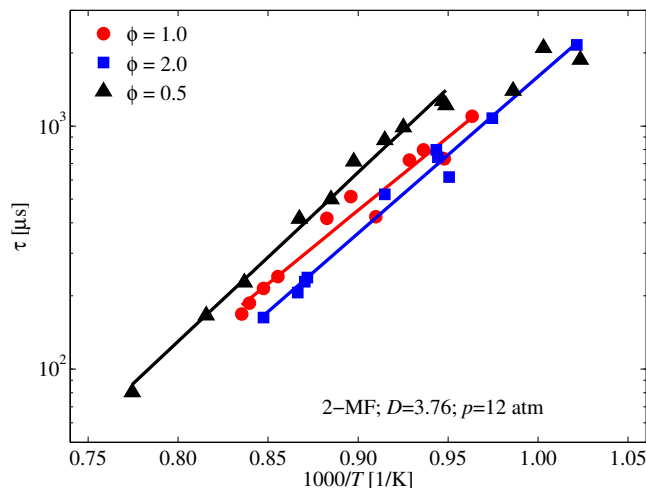
Figure 4.5: Equivalence ratio effect on 2-MF ignition delay times for 2-MF/O₂/Ar mixtures at nominal pressures of 12.0 atm.

methoxyfuran, which Simmie et al. [135] attribute to the very weak methoxy (C–O) bond. It is possible that the high reactivity of 2-MF observed here could also be linked to the C–C bond being much weaker than C–C bonds in DMF.

The trend shown in Figure 4.2 is also observed at a higher pressure of 5.0 atm as shown in Figure 4.3. Increasing the pressure to 10 atm as in Figure 4.4 preserves the established reactivity trend. However, Figure 4.4 shows that the reactivity difference between DMF and furan is not as significant as at the other two conditions, while 2-MF is consistently the most reactive.

The effect of equivalence ratio on ignition behavior of the three furans is then explored. Experiments for the lean and rich mixtures are conducted at nominal pressures of 12.0 atm, and the stoichiometric data at 10.0 atm are scaled to 12.0 atm using a pressure scaling with exponents as discussed previously. Figure 4.5 shows the equivalence ratio effect on 2-MF ignition; it is observed that ignition delay times decrease with increasing equivalence ratios over the investigated temperature range. This means that constraining the ratio of the number of inert molecules to oxygen molecules and increasing fuel concentration results in higher reactivity.
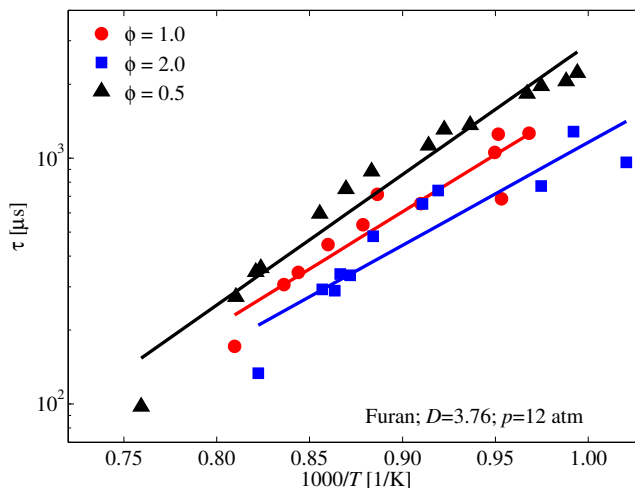
Figure 4.6: Equivalence ratio effect on furan ignition delay times for furan/O_2/Ar mixtures at nominal pressures of 12.0 atm.

It should be noted that in other studies, for instances, Somers et al. [12], equivalence ratio effects are investigated by keeping the fuel concentration constant. This leads to the opposite observation that lean mixtures are more reactive. In this scenario the oxygen concentration (lower dilution) is higher for the lean mixtures, and controls ignition more strongly. Further, although differences are observed in the approach used in this work, they are usually within 80% of the stoichiometric delay time, making the stoichiometric ignition delay times at given pressure, dilution, and temperature, a very useful reference to estimate ignition delay times at other equivalence ratios. These equivalence ratio effects are in line with studies where fuel/air mixtures are used; since N_2/O_2 ratio is then constant. In most hydrocarbon/air ignition at high temperatures, the ignition delay times decrease with increasing equivalence ratio, as in Ciezki and Adomeit [136], due to increased oxygen-linked reactivity through peroxy chemistry.

The same equivalence ratio effect for 2-MF is observed for furan, as shown in Figure 4.6. Ignition delay times reduce with increasing equivalence ratio. In Figure 4.7 the equivalence ratio effect on DMF ignition is less distinct for stoichiometric and rich mixtures. Rich mixtures ignite more readily than stoichiometric at high temperatures while at temperatures less than
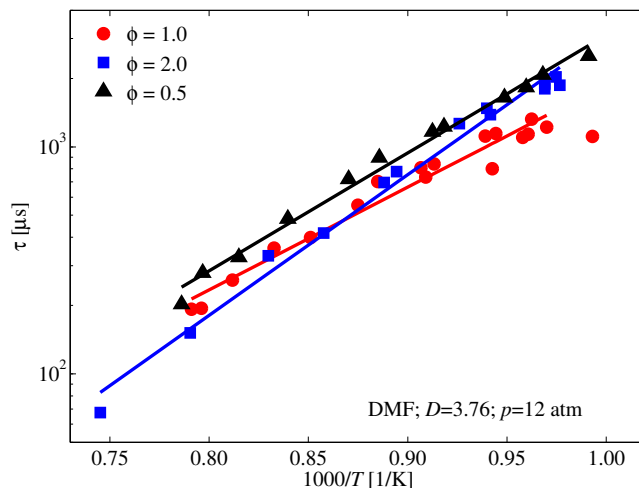
Figure 4.7: Equivalence ratio effect on DMF ignition delay times for DMF/O₂/Ar mixtures at nominal pressures of 12.0 atm.

1130 K the rich mixtures become less reactive.

4.1.2   Comparison with model predictions

The experimental results on the ignition of the three furans are compared to predictions of recently published chemical kinetic models by Sirjean et al. [13] and Somers et al. [12]. These models focus on DMF but also have 2-MF and furan as sub models. The furan sub models have not been tested against experiments and their predictions are not included in this discussion.

In Figure 4.8, ignition delay times of the three furans at stoichiometric conditions and nominal pressure of 2.0 atm are compared with model predictions. The figure reveals that Model 2 [12] captures the ignition behavior of DMF with reasonable accuracy, while Model 1 [13] over-predicts the ignition delay times. With regard to 2-MF, both models predict shorter ignition delay times than the actual measurements.

The ignition delay times at 10 atm in Figure 4.9 represents a shift in the direction of lower temperatures with respect to Figure 4.8. Predictions of Model 1 [13] and Model 2 [12] are
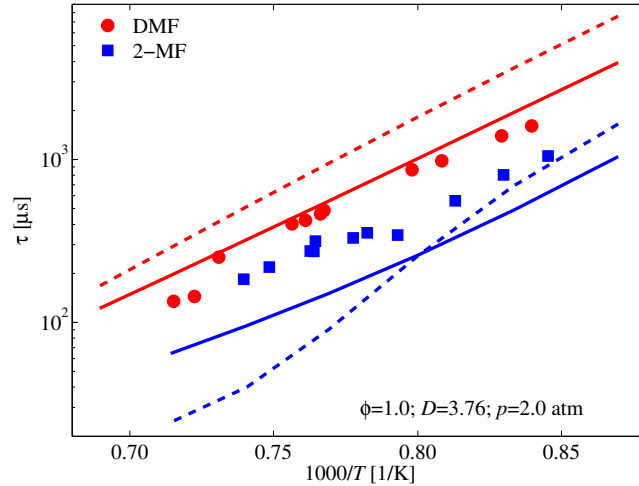
Figure 4.8: Experimental and model predictions of ignition delay times for stoichiometric mixtures of DMF, 2-MF and furan at nominal pressures of 2.0 atm. Dashed lines: Model 1 by Sirjean et al. [13], solid lines: Model 2 by Somers et al. [12].

longer than measured delay times. Because of the lower temperatures and the temperature-sensitivity displayed by the 2-MF predictions in Figure 4.8, the models predict longer delay times in Figure 4.9, with the Model 2 in closer agreement at the higher temperature end.

Rich mixtures ($\phi = 2.0$) of DMF and 2-MF are compared at a pressure of 12.0 atm with model predictions in Figure 4.10. Model 2 [12] is in better agreement with the experimental
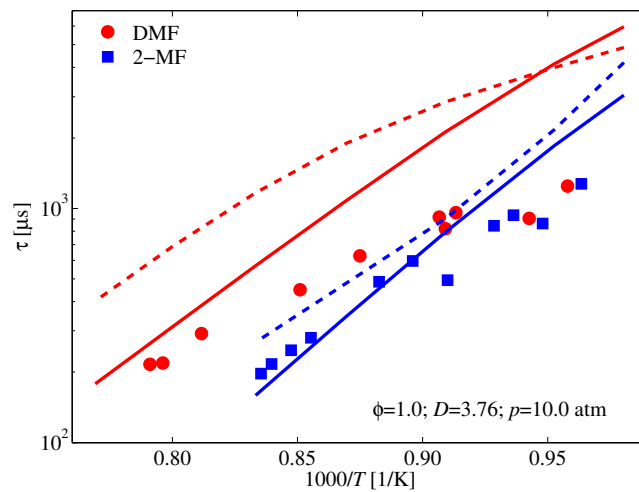
Figure 4.9: Experimental and model predictions of ignition delay times for stoichiometric mixtures of DMF, 2-MF and furan at nominal pressures of 10.0 atm. Dashed lines: Model 1 by Sirjean et al. [13], solid lines: Model 2 by Somers et al. [12].
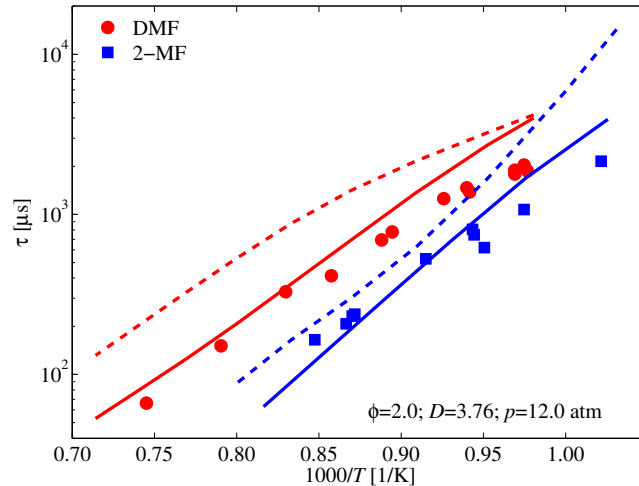
Figure 4.10: Experimental and model predictions of ignition delay times for rich mixtures of DMF, 2-MF and furan at nominal pressures of 12.0 atm. Dashed lines: Model 1 by Sirjean et al. [13], solid lines: Model 2 by Somers et al. [12].

data, while Model 1 [13] predicts longer ignition delay times for both DMF and 2-MF. Both models accurately predict the trend, such that DMF has longer ignition delay times than 2-MF. However, when the furan sub models in the comprehensive models are used, the ignition predictions are much longer than those measured. Compared to the other predictions, both models predict a reactivity trend, such that furan is the least reactive and 2-MF the most reactive. This is at variance with the experiment, where DMF is consistently the least reactive under all investigated conditions. For models to capture the trends observed in this study, further improvement of the furan sub models and the temperature sensitivity of their ignition delay times over a wider temperature range is needed.

From the comparison above, it is observed that the models predict ignition delay times to a varying degree of success. The current data set is obtained at high-temperature conditions. Further experiments at lower temperatures are needed to verify if these conclusions hold consistently over a wider temperature range. A key question that needs to be addressed is whether these fuels exhibit strong Negative Temperature Coefficient (NTC) at lower temperatures. The presence of NTC behavior would explain the non-Arrhenius behavior observed at lower temperatures as indicated in lean mixtures in Figure 4.5. For these studies
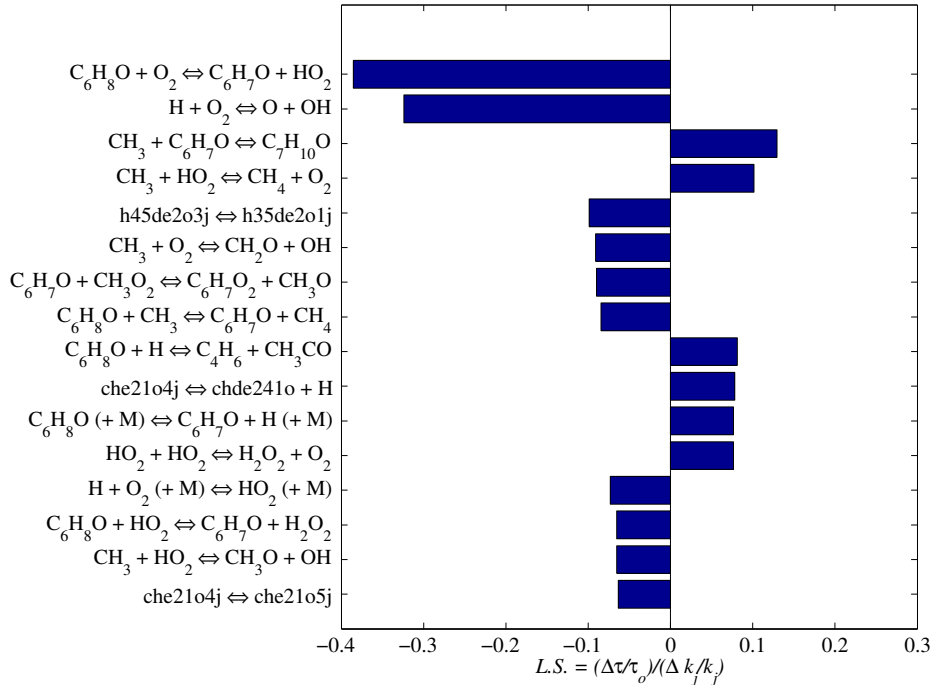
Figure 4.11: The 16 most important reactions from the sensitivity analysis of the DMF model by Somers [12] for a stoichiometric DMF/O$_2$/Ar mixture at 10.0 atm with a dilution, D, of 3.76 at a temperature of 1150 K. The unperturbed ignition delay time is 1089 μs.

longer test times than those achievable with current setup are needed.

Although good agreement between model predictions and experimental data is not observed at all conditions, the models capture the reactivity trend between 2-MF and DMF. This motivated further sensitivity and reaction pathway analyses in order to understand differences in the DMF and 2-MF models. Sensitivity analyses of the two models are based on ignition of stoichiometric fuel/O$_2$/Ar mixtures with $D = 3.76$ at 1150 K and 10.0 atm. A-factors of the reaction rate constants are multiplied by 10 to establish their effect on ignition delay times. The logarithmic sensitivities of the elementary reactions are determined and sorted in order of importance. The 16 most important reactions are plotted below. As is usually the case in hydrocarbon oxidation, most of the reactions are C0–C1 oxidation reactions, with a few reactions specific to the fuel. The fuel specific-reactions include decomposition, H-abstraction reactions from the fuel, and further reaction of primary fuel radicals.
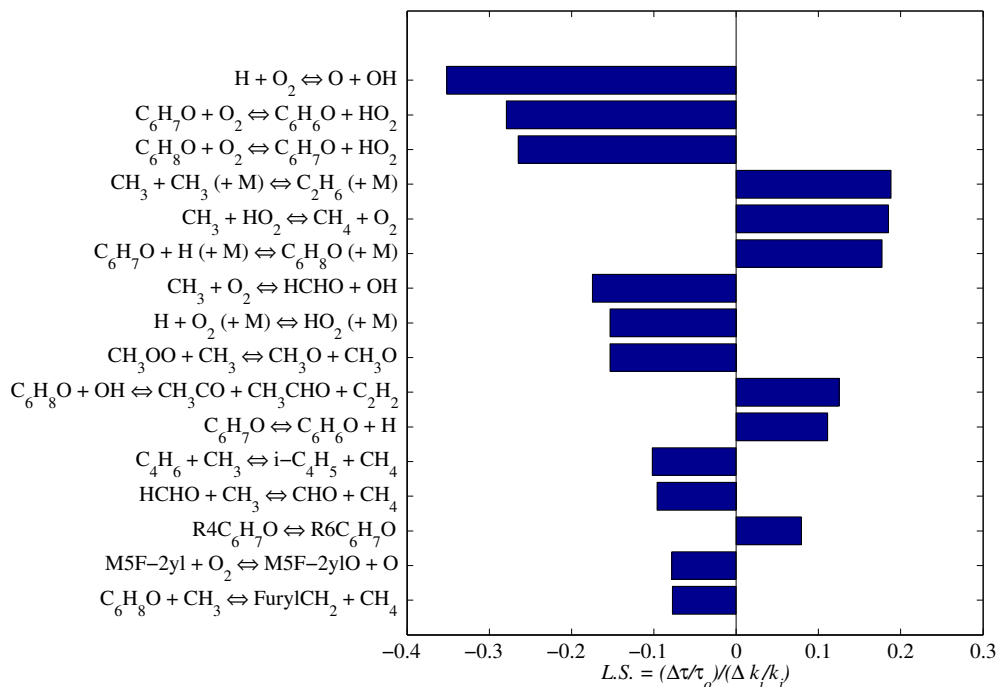
Figure 4.12: The 16 most important reactions from the sensitivity analysis of the DMF model by Sirjean [13] for a stoichiometric DMF/O$_2$/Ar mixture at 10.0 atm with a dilution, D, of 3.76 at a temperature of 1150 K. The unperturbed ignition delay time is 1519 μs.

4.1.3   Chemical kinetic model analyses

The sensitivity analyses for DMF (appears as C_6H_8O) are shown in Figure 4.11 for the Somers et al. model (Model 2) [12] and in Figure 4.12 for Sirjean et al. model (Model 1) [13]. It is observed that in both models, $H + O_2 \rightleftharpoons O + OH$, is highly sensitive as expected. It is less sensitive in Model 1 [13]. The reaction, $C_6H_8O + O_2 \rightleftharpoons C_6H_7O + HO_2$, is more sensitive in Model 2 than in Model 1. These factors contribute to the observed reduced global reactivity of Model 1. The reaction, $C_6H_7O + O_2 \rightleftharpoons C_6H_6O + HO_2$, has a very high sensitivity in Model 1 while it does not appear among the 16 most sensitive reactions in Model 2.

The sensitivity analyses for 2-MF are shown in Figure 4.13 for Model 2 and in Figure 4.14 for Model 1. It is observed that the main branching reaction, $H + O_2 \rightleftharpoons O + OH$, is very sensitive in Model 2, while its sensitivity is reduced in Model 1. Also, the propagation
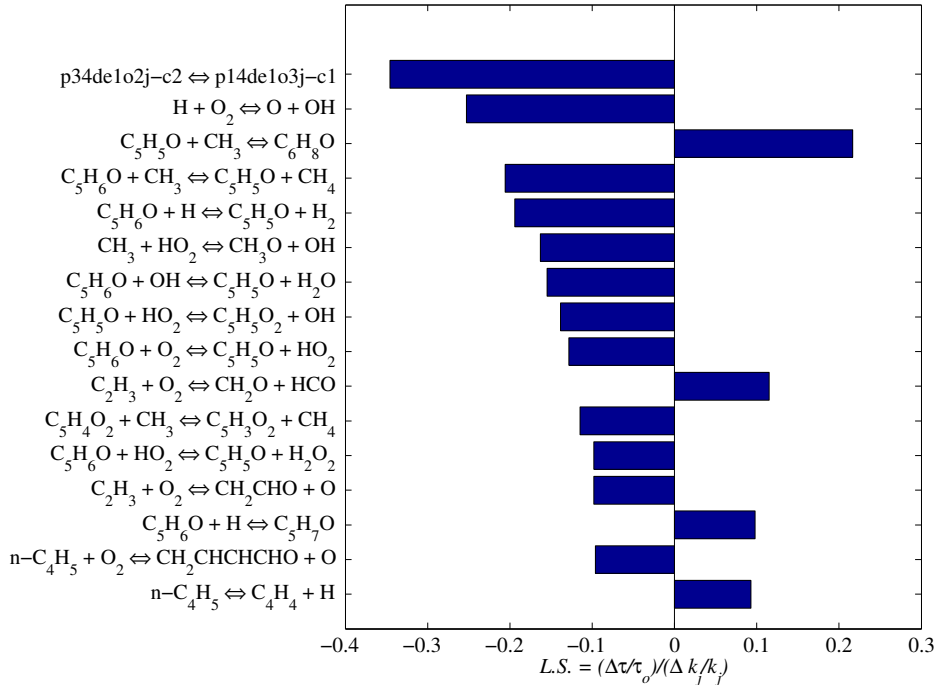
Figure 4.13: The 16 most important reactions from the sensitivity analysis of the 2-MF model by Somers [12] for a stoichiometric 2-MF/O_2/Ar mixture at 10.0 atm with a dilution, D, of 3.76 at a temperature of 1150 K. The unperturbed ignition delay time is 1089 μs.

reaction, $CH_2CCHCHCHO \rightleftharpoons CH_2CHCHCHCO$, is the most sensitive reaction in Model 2, while it is not included in Model 1. On the other hand, the H-abstraction reaction, $C_5H_6O + HO_2 \rightleftharpoons C_5H_5O + H_2O_2$, is the most sensitive in Model 1 while its shows reduced sensitivity in Model 2. The isomerization reaction, $C_5H_6O \rightleftharpoons CH_3COCHCCH_2$, is very sensitive in Model 1 while it is not among the 16 most sensitive reactions in Model 2. As would be expected, reactions which favor the formation of stable molecules tend to reduce reactivity and increase the ignition delay times in all cases.

Reaction pathway analysis are performed for an ignition process of stoichiometric fuel/O_2/Ar mixtures with $D = 3.76$ at a temperature of 1150 K and pressure of 10.0 atm. For DMF, the system is analyzed at 10, 500 μs, and close to ignition. Fuel consumption is found to initially proceed mainly through H-abstraction reactions by O_2, with contributions from CH_3 and H radicals. In contrast to the model by Somers et al. [12] in Figure 4.15, analysis of the model
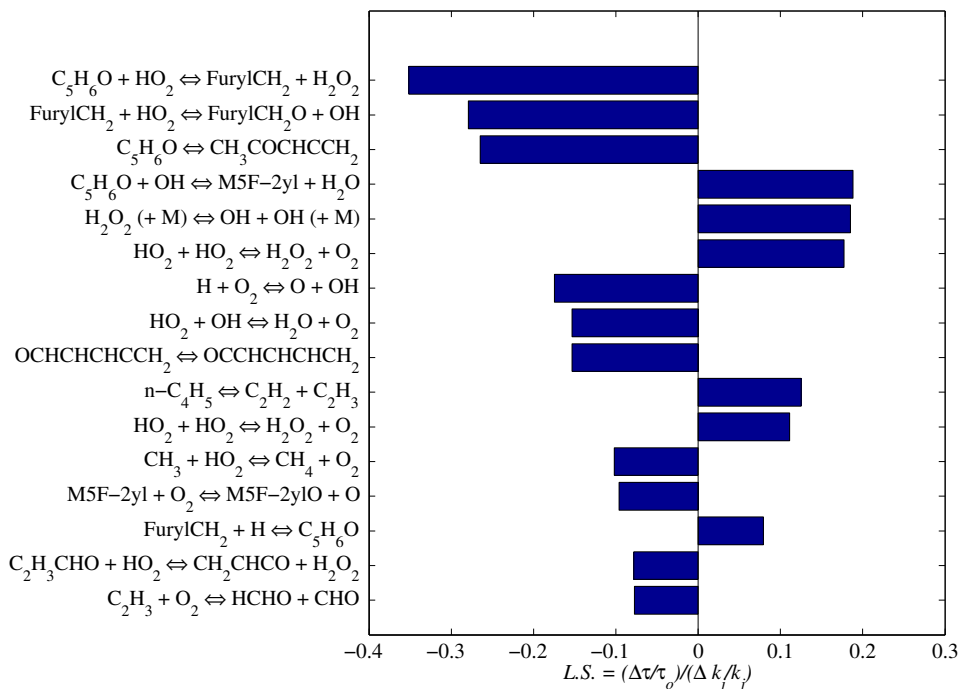
Figure 4.14: The 16 most important reactions from the sensitivity analysis of the DMF model by Sirjean [13] for a stoichiometric 2-MF/O$_2$/Ar mixture at 10.0 atm with a dilution, D, of 3.76 at a temperature of 1150 K. The unperturbed ignition delay time is 481 µs.

by Sirjean et al. [13] shows that 27.5% of DMF consumption at 10 µs proceeded through isomerization to 2,4-DMF, as shown in Figure 4.16. This partly explains the reduced reactivity of the model, since this stable fuel molecule still needs to be attacked by radicals before ignition. Further, fuel-derived radicals are produced more slowly as compared to Model 2. At later times, fuel consumption proceeds by H-abstraction by OH, CH$_3$, and H. Whereas in Model 2, the abstraction is mostly by OH and H radicals, in Model 1 the abstracting partner is mostly CH$_3$. This suggests that Model 1 focuses more on a pyrolytic fuel consumption pathway, with oxygen-containing radicals becoming more important only close to ignition. Fuel radicals are consumed subsequently by beta-scission and radical abstraction reactions.

In the case of 2-MF, ignition delay times are 481 µs for Model 1 and pathways are analyzed at 10, 200, and 450 µs while the delay time is 347 µs for Model 2 with reaction pathways examined at 10, 150, and 300 µs. Similar to DMF, in both models fuel is initially consumed
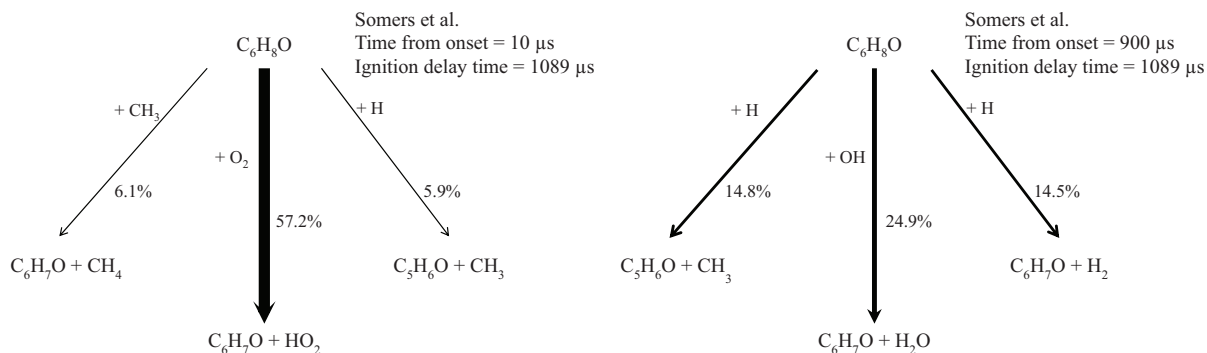
Figure 4.15: Reaction pathways for DMF at two different time intervals prior to ignition using the mechanism by Somers [12] for a stoichiometric $DMF/O_2/Ar$ mixture at 10.0 atm with a dilution, D, of 3.76 at 1150 K.
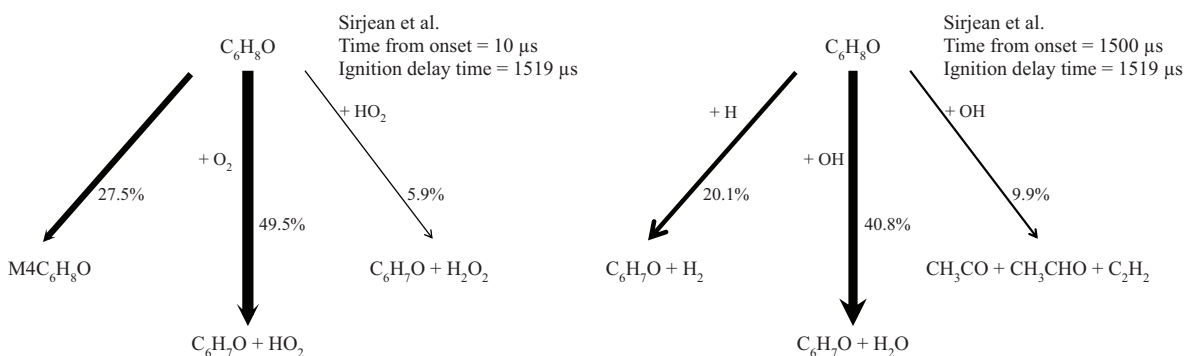
Figure 4.16: Reaction pathways for DMF at two different time intervals prior to ignition using the mechanism by Sirjean [13] for a stoichiometric $DMF/O_2/Ar$ mixture at 10.0 atm with a dilution, D, of 3.76 at 1150 K.

through reactions with O_2 to yield HO_2 and primary fuel radicals. For Model 1, shown in Figure 4.18, this occurs through direct ring-opening of MF to $CH_3COCHCCH_2$ radical. $CH_3COCHCCH_2$ decomposes to release CH_3 which is a major abstraction partner unlike in Model 2, where abstraction is mostly by OH radicals, as shown in Figure 4.17. In summary, reaction pathway analyses suggest that Model 1 is more focused on pyrolytic reactions, which yield other stable molecules, thereby retarding reactivity. In addition to these reaction pathway and sensitivity analyses, thermodynamic properties could also partially account for observed differences. Model 2 is an improved version of Model 1 but further work is needed to improve its prediction of the experimental data reported here as well as other flame and flow reactor data sets in the literature.
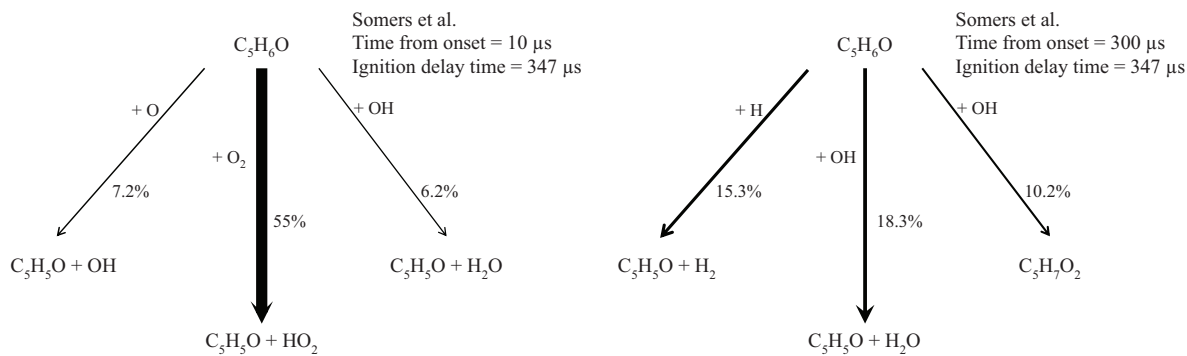
Figure 4.17: Reaction pathways for 2-MF at two different time intervals prior to ignition using the mechanism by Somers [12] for a stoichiometric 2-MF/O_2/Ar mixture at 10.0 atm with a dilution, D, of 3.76 at 1150 K.
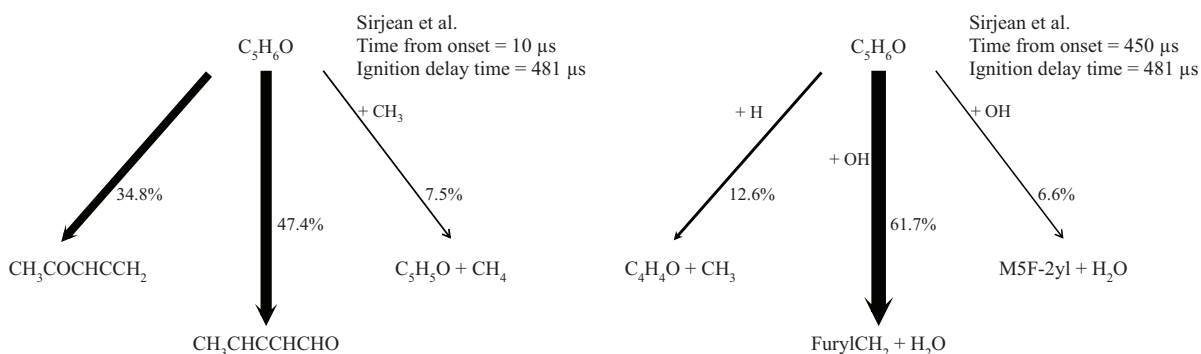
Figure 4.18: Reaction pathways for 2-MF at two different time intervals prior to ignition using the mechanism by Sirjean [13] for a stoichiometric 2-MF/O_2/Ar mixture at 10.0 atm with a dilution, D, of 3.76 at 1150 K.

In summary, this part of the thesis systematically investigates the ignition of a class of oxygenated cyclic hydrocarbons, furans, which are of interest as alternative transportation fuels or fuel additives. Important trends are revealed and the results are compared with model predictions, revealing some weaknesses in model performance. Ignition delay times obtained at conditions of previous studies agree with those data sets and model predictions at conditions where the models have been tested.

With regards to structure-reactivity trends, the results show a non-monotonic trend with respect to chemical structure, whereby DMF is the least reactive while 2-MF is the most readily ignitable. Two chemical models also predict 2-MF to be more reactive than DMF, although quantitative agreement varies over the range of conditions investigated. Equivalence

ratio effects for each furan are also investigated. Generally, ignition delay times decrease with increasing equivalence ratios, except for DMF whose rich mixtures show reduced reactivity at lower temperatures. Although individual studies of these fuels have been reported in the literature, the main contribution of this part of this work is to reveal trends which cannot be gleaned from individual experimental, modeling, and quantum chemical calculations.

4.2   Ignition study of dimethylfuran, *iso*-octane, and blends

In this section, the ignition behavior of DMF, *iso*-octane, and their blends is investigated. To confirm that DMF is the least reactive furan, its ignition behavior is compared with that of the isomer, 2-ethyl furan (2-EF). For the DMF/*iso*-octane comparative study, ignition delay times are measured over a temperature range from 1009 to 1392 K and pressures up to 12.0 atm for lean, stoichiometric, and rich mixtures of fuel, oxygen, and argon. Further, ignition delay times of a blend of DMF and *iso*-octane of equal proportions by liquid volume are measured. They are also compared to those of the pure fuels at stoichiometric and rich conditions and pressure of 12.0 atm.

A combined model for DMF and *iso*-octane combustion is developed, drawing from recent literature models for the pure components. Further modifications are carried out to improve agreement with the current and previous ignition data. Reaction pathway analysis and species sensitivity analysis are performed for more insight on the governing chemical kinetics. The molecular structures of the fuels investigated in this section are shown in Figure 4.19.

2,5-dimethyl furan   2-ethyl furan   *iso*-octane
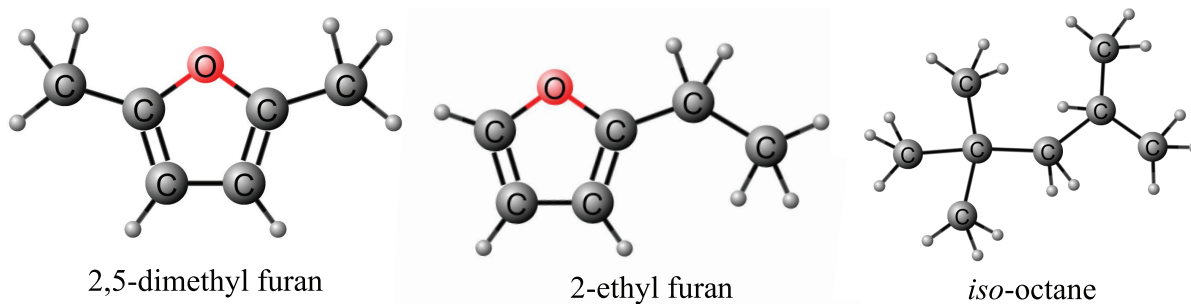
Figure 4.19: Chemical structure of DMF, 2-EF, and iso-octane.

4.2.1   Experimental studies

In this part, experimental results are presented. First, 2-EF ignition measurements are compared to DMF at stoichiometric conditions and pressures of 5.0 and 12.0 atm. Further, the ignition delay times of DMF and *iso*-octane are measured at equivalence ratios, ϕ, of 0.5, 1.0, and 2.0 over a range of pressures up to 12.0 atm. Furthermore, blends of equal proportions of both fuels (by volume) are studied at equivalence ratios, ϕ, of 1.0, and 2.0 at 12.0 atm. Table 4.2 shows the mixtures investigated in this study.

Table 4.2: DMF, iso-octane, blend, and 2-EF mixtures investigated using ϕ and D constraints

Fuel	Diluent	ϕ	D	Fuel %	O_2 %	Diluent %
DMF	Ar	1.0^a	3.76	2.73	20.43	76.84
	N_2	1.0^a	3.76	2.73	20.43	76.84
	Ar	2.0	3.76	5.32	19.90	74.78
	Ar	0.5	3.76	1.38	20.72	77.90
iso-octane	Ar	1.0^a	3.76	1.65	20.66	77.69
	N_2	1.0^a	3.76	1.65	20.66	77.69
	Ar	2.0	3.76	3.25	20.33	76.42
	Ar	0.5	3.76	0.83	20.83	78.34
50/50 blend	Ar	0.97	3.76	2.10	20.57	77.33
	Ar	1.94	3.76	4.13	20.14	75.73
2-EF	Ar	1.0	3.76	2.72	20.43	76.85

^{a} Mixtures used for validation experiments.

In the figures shown later, as mentioned earlier, a power law of the form, $\tau \propto p^n$, is used to account for small variations from the nominal pressure over a range of temperatures. The exponents are found to be -0.95 for DMF, -1.18 for 2-EF and -0.85 for *iso*-octane. Pressure dependence exponent for the blends of DMF and *iso*-octane are assumed to have the same exponent as DMF. Arrhenius fits are added to the figures to clarify the trends

Relative ignition behavior of DMF and 2-EF

DMF and 2-EF are isomers that differ in the structure of their furan substitution. The relative ignition behavior of DMF and its isomer, 2-EF, is studied at stoichiometric conditions and
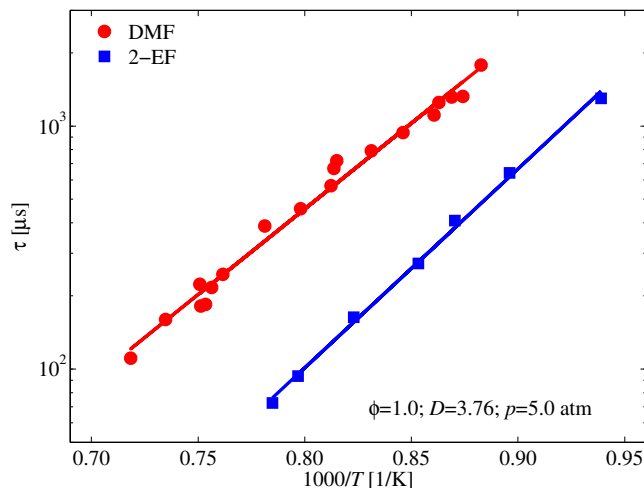
*Figure 4.20: Relative ignition behavior of DMF and 2-EF at a nominal pressure of 5.0 atm.
The fuel/O_2/Ar mixture is stoichiometric, and the Ar/O_2 ratio, D, is 3.76.*

nominal pressures of 5.0 and 12.0 atm at Ar/O_2 ratio of 3.76. This dilution level reflects the situation in engine combustion where air, as oxidizer, has a nitrogen/oxygen ratio, D, of 3.76. The results are shown in Figures 4.20 and 4.22, with Arrhenius fits added for clarity.

Figure 4.20 shows ignition delay times of DMF and 2-EF at a nominal pressure of 5.0 atm. It is observed that the ignition delay times of DMF are about 4.7 times longer than those of 2-EF at 1280 K, and 4 times longer at 1205 K. This substantial difference has not been reported before, partly because of lack of 2-EF ignition data and limited focus on comparative studies. These data combine with the results shown in the previous section, to establish that DMF is the least reactive substituted furan.

The differences in the ignition propensity of DMF and 2-EF are similar to these observed for xylene and ethyl benzene, as shown in Figure 4.21. A shock tube ignition study by Shen and Oehlschlaeger [137] showed that ethyl benzene is much more reactive than dimethyl benzene (xylene) at pressures of 9–45 atm, and temperatures of 941–1408 K; the ignition delay times of xylene reported there are up to 5 times longer than those of ethyl benzene. The observed differences can be rationalized in two ways.

Firstly, the alkyl radicals resulting from direct bond cleavage reactions are methyl radicals
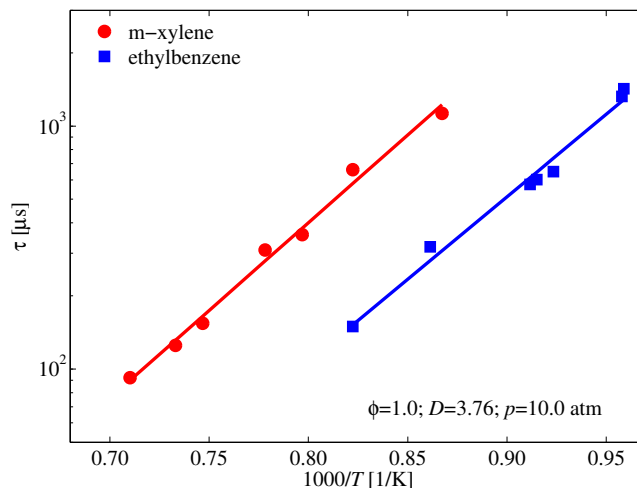
Figure 4.21: Relative ignition behavior of xylene and ethyl benzene reported by Shen and Oehlschlaeger [137], at a nominal pressure of 10.0 atm. The fuel/O_2/Ar mixture is stoichiometric, and the Ar/O_2 ratio, D, is 3.76.

in the case of dimethyl furan and ethyl radicals in the case of ethyl isomer. Whereas the ethyl radical can undergo beta-scission to yield ethylene and an H atom, methyl radicals can recombine to form stable ethane molecules or undergo a slower beta-scission reaction to yield H atoms and methylene radicals. Secondly, whereas the dimethyl isomer presents terminal C–H bonds for radical attack, weaker C–H bonds in the ethyl radical present a more favorable site for H-abstraction by radicals. As an analogy, one considers H-abstraction from ethylbenzene by the HO_2 radical, using rate parameters recommended by Baulch et al. [138]; it is observed that H-abstraction from the secondary site can be up to 300 times faster than abstraction from the primary site at 1000 K and up to 20 times faster at 1450 K. Thirdly, it is also feasible that ring-opening of the primary fuel radicals (those obtained after first H-abstraction) is easier for the radicals of ethyl furan compared to those of the 2,5-dimethyl furan.

With respect to other combustion properties, Mehl et al. [139] showed that ethyl benzene flames propagate fastest among investigated alkyl benzenes from methyl to butyl benzene. The structural appearance can be compared to 2-EF and DMF behavior, although no xylenes flames were considered, which are generally slower or comparable with toluene. Returning to
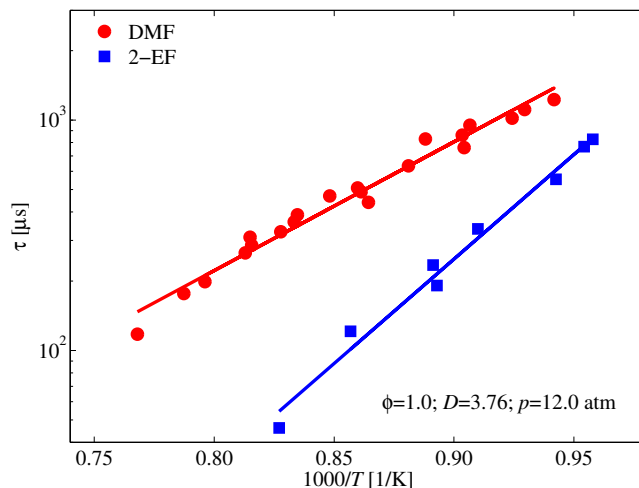
Figure 4.22: Relative ignition behavior of DMF and 2-EF at a nominal pressure of 12.0 atm. The fuel/O_2/Ar mixture is stoichiometric, and D is 3.76. Lines represent Arrhenius fits to the respective data.

the subject of DMF and 2-EF, quantum chemical calculations of bond dissociation energies were presented in the study by Sudholt et al. [49], which shows that 2-EF has a slightly lower bond dissociation energy for the C–H bond at side chain carbon compared to that of DMF, which can lead to higher reactivity through more rapid H-abstraction from this location. On the other hand, the BDEs of the C–H bonds of the ring carbon are observed to be similar for the two isomers. The BDE information is therefore insufficient to draw conclusions on the huge reactivity differences of these fuels, but can be informative when coupled with reaction rate calculations.

The same trend is observed at the pressure of 12.0 atm, as shown in Figure 4.22. It is observed that the ignition delay times of DMF are 6 times longer than those of 2-EF at 1210 K, and 2.3 times longer at 1065 K. It is also observed that the ignition delay times of DMF are less sensitive to temperature than those of 2-EF. The established reactivity trends reveal that DMF is more suitable for use in spark-ignition engines than its isomer, since its reduced reactivity is desirable for knock resistance. Therefore, the relative reactivity trends between DMF and a conventional gasoline surrogate, *iso*-octane, are investigated for further evaluation of furan and gasoline combustion.
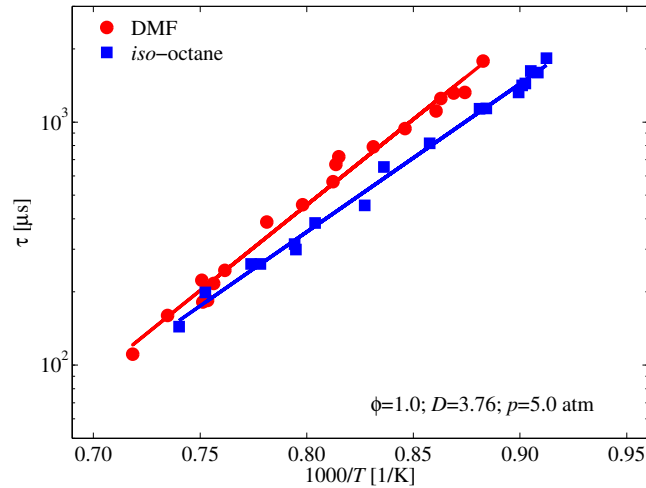
Figure 4.23: Relative ignition behavior of stoichiometric fuel/O_2/Ar mixtures of DMF and iso-octane at a pressure of 5.0 atm.

Comparative ignition study of DMF and *iso*-octane

Ignition delay time measurements for DMF and *iso*-octane, a representative of conventional gasoline, are carried out at equivalence ratios of 0.5, 1.0, and 2.0, and nominal pressures of 5.0, and 12.0 atm, under a fixed Ar/O_2 ratio of 3.76. The ignition delay times are shown in Figures 4.23–4.26.

Figure 4.23 shows ignition delay times of stoichiometric mixtures at a pressure of 5.0 atm. It shows that DMF has longer ignition delay times than *iso*-octane, indicating reduced reactivity. At this pressure, it is observed that the ignition delay times of DMF are 1.5 times longer than those of *iso*-octane at 1136 K, and 1.13 times longer at 1351 K.

Figure 4.24 shows the ignition behavior of stoichiometric DMF and *iso*-octane mixtures at a higher pressure of 12.0 atm. The trend shown in Figure 4.23 is also observed in Figure 4.24, with a possible cross-over effect at temperatures below 1080 K.

The established reactivity trend is preserved for lean mixtures of DMF and *iso*-octane. DMF has longer ignition delay times than *iso*-octane at an equivalence ratio of 0.5 and a nominal pressure of 5.0 atm, with reduced differences at temperatures above 1360 K. The same trend
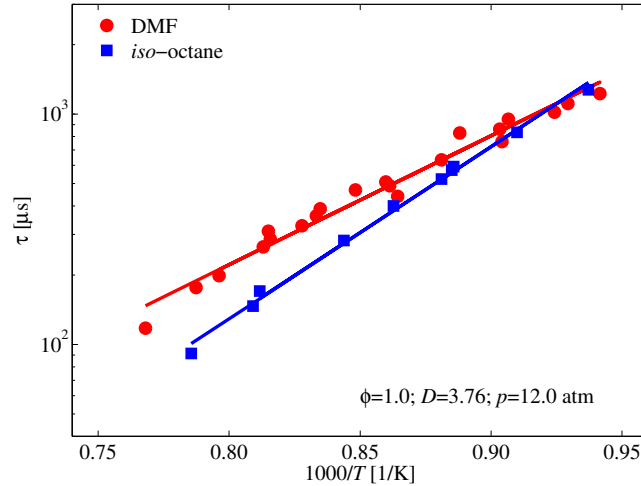
Figure 4.24: Relative ignition behavior of stoichiometric fuel/O$_2$/Ar mixtures of DMF and iso-octane at a pressure of 12.0 atm.

is observed for lean mixtures of $\phi = 0.5$ at the higher pressure of 12.0 atm with a cross-over at temperatures lower than 1100 K, as shown in Figure 4.25.

At rich conditions of $\phi = 2.0$ and a pressure of 5.0 atm, there is no significant difference in the reactivities of DMF and *iso*-octane under rich conditions and low pressures, unlike the trend consistently observed in the previous conditions. However, the previously established reactivity trend is restored at a higher pressure of 12.0 atm, where *iso*-octane is consistently
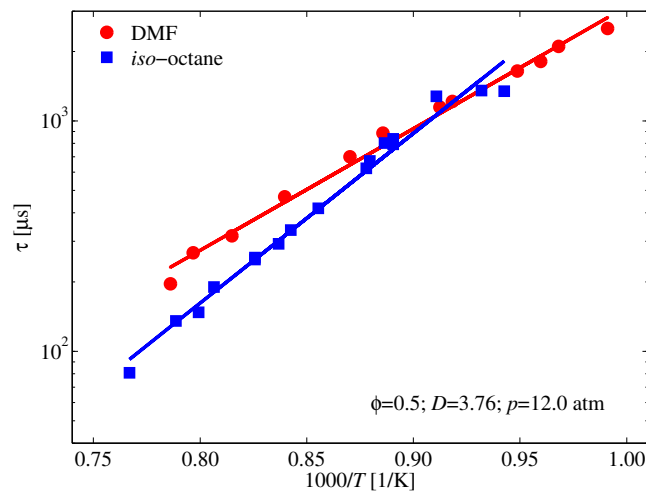
Figure 4.25: Relative ignition behavior of lean fuel/O$_2$/Ar mixtures of DMF and iso-octane at a pressure of 12.0 atm.
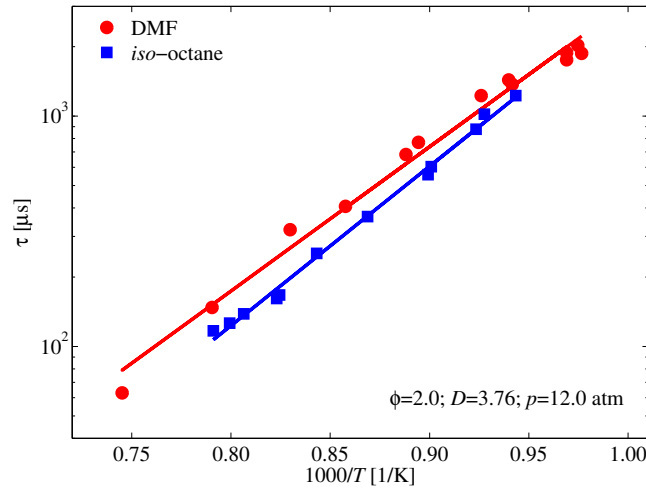
Figure 4.26: Relative ignition behavior of DMF, and iso-octane at a nominal pressure of 12.0 atm. The fuel/O_2/Ar mixture is rich, and the Ar/O_2 ratio D is maintained at 3.76.

more reactive, as shown in Figure 4.26.

These reactivity trends indicate that DMF has better resistance to auto ignition than the conventional gasoline surrogate *iso*-octane. Reactivity trends are strictly for situations where the pressure and Ar/O_2 ratio are kept constant. The comparison is more closely related to conditions encountered in combustion engines, and differs from other approaches in the literature where reactivity trends are assessed based on constraints on fuel concentrations. Moreover, the approach used in this study also enables one to relate reactivity trends observed in ignition to those observed in flame propagation of fuel/air mixtures. Since the data sets presented in the work fall in the high temperature zone, further ignition data at lower temperatures are needed to clarify the behavior over an extended temperature range, including the negative temperature coefficient (NTC) behavior at lower temperatures.

Equivalence ratio effect on DMF and *iso*-octane ignition

The effect of equivalence ratio on ignition behavior is investigated for DMF and *iso*-octane. The equivalence ratio effect on DMF ignition at 12.0 atm is shown in Figure 4.27. The figure demonstrates a decrease in ignition delay times with increasing equivalence ratios over the investigated temperature range, with a possible cross-over at temperatures below 1010 K.
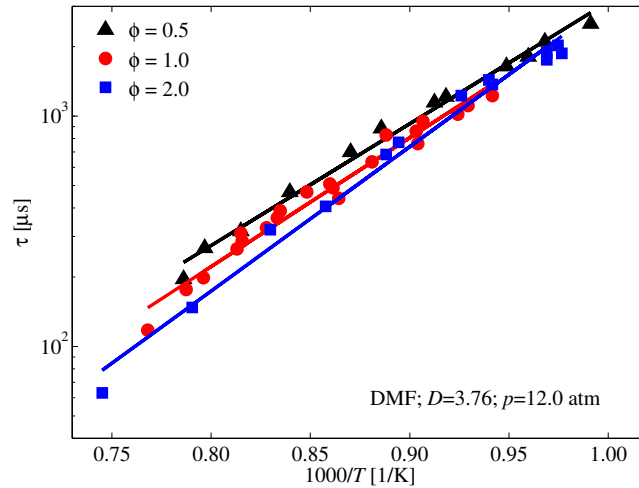
Figure 4.27: Equivalence ratio effect on ignition delay times for DMF/O$_2$/Ar mixtures at a pressure of 12.0 atm.

This shows the effect of constraining the Ar/O$_2$ ratio and varying the fuel concentrations, which reveals that increasing the fuel concentration leads to increased reactivity. Fixing the fuel concentration and exploring equivalence ratio effect would lead to opposite observations, as discussed in the previous section. The equivalence ratio effect presented in this work is in line with the results in the previous section and in the literature [136].

Figure 4.28 shows the equivalence ratio effect on *iso*-octane ignition at 12.0 atm. The same
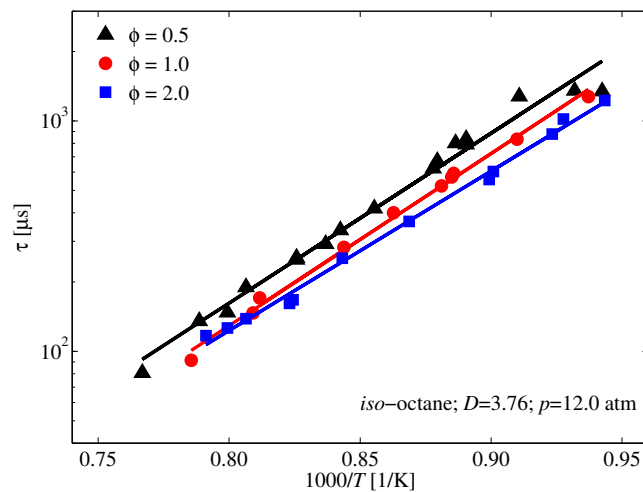
Figure 4.28: Equivalence ratio effect on ignition delay times for iso-octane/O$_2$/Ar mixtures at a pressure of 12.0 atm. Lines represent Arrhenius fits to the respective data.
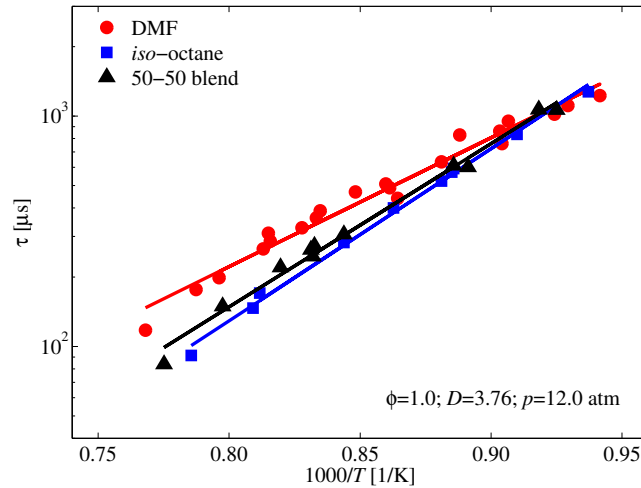
Figure 4.29: Relative ignition behavior of DMF, iso-octane, and a blend of both (50/50 % by liquid volume) at a pressure of 12.0 atm. Then fuel/O_2/Ar mixture is stoichiometric, and D is 3.76. Solid lines: DMF, dashed: iso-octane, and dash-dot: 50/50 blend.

equivalence ratio effect is observed over the entire temperature range, where ignition delay times decrease with increasing equivalence ratio, with a possible cross-over between the stoichiometric and the rich mixtures at temperatures above 1280 K, where the equivalence ratio effect can be reversed.

DMF and *iso*-octane blend ignition behavior

The effect of blending DMF with *iso*-octane on ignition behavior is investigated by measuring ignition delay time of blends of equal proportion by liquid volume of both fuels at equivalence ratios of 1.0 and 2.0 and a nominal pressure of 12.0 atm. The ignition data of the blends are compared to ignition delay times of the pure fuels at the same conditions to establish relative reactivity trends.

Figure 4.29 is a comparison between the ignition delay times of the DMF/*iso*-octane blend and of the pure fuels at stoichiometric conditions and a pressure of 12.0 atm, under a constrained Ar/O_2 ratio, D, of 3.76. The figure shows that the blend has observably longer ignition delay times than *iso*-octane, while it is more reactive than DMF. However, the ignition propensity of the blend is generally close to that of *iso*-octane, with less distinct differences from the
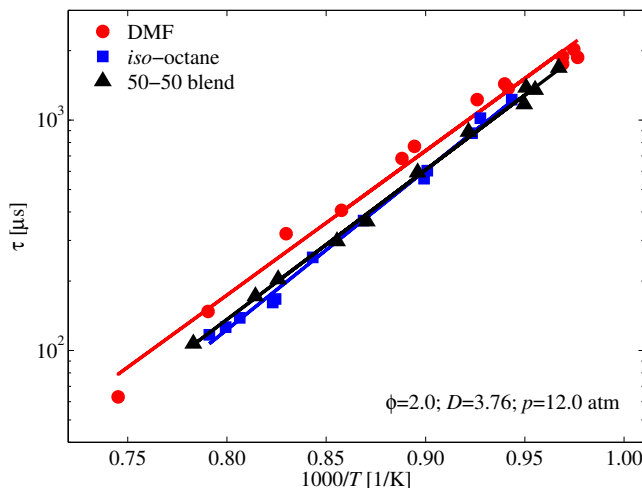
Figure 4.30: Relative ignition behavior of DMF, iso-octane, and a blend of both (50/50 % by liquid volume) at a pressure of 12.0 atm. Then fuel/O_2/Ar mixture is rich, and D is 3.76. Solid lines: DMF, dashed: iso-octane, and dash-dot: 50/50 blend.

two fuels at lower temperatures. This suggests that in blends of DMF and *iso*-octane, the *iso*-octane acts as a source of more reactive intermediates for the oxidation of DMF.

The same trend is observed at conditions of $\phi = 2.0$ and a pressure of 12.0 atm as shown in Figure 4.30, where the blend reactivity lies between the two pure fuels, albeit in closer agreement with *iso*-octane here than the previous stoichiometric case, especially at lower temperatures.

These results compliment the ignition data previously presented. They show the blending effect on chemical reactivity and provides a set of experimental ignition data, which is of interest to fuel technology as well as chemical kinetic model development.

Comparison of pure DMF and *iso*-octane data with model predictions

The ignition delay times of DMF and *iso*-octane are compared to the predictions of recent chemical kinetic models for DMF by Somers et al. [12], and for *iso*-octane by Mehl et al. [10]. In Figure 4.31, ignition delay times of DMF are compared with model predictions for mixtures at equivalence ratios of 0.5, 1.0, and 2.0 at a pressure of 12.0 atm. It is observed
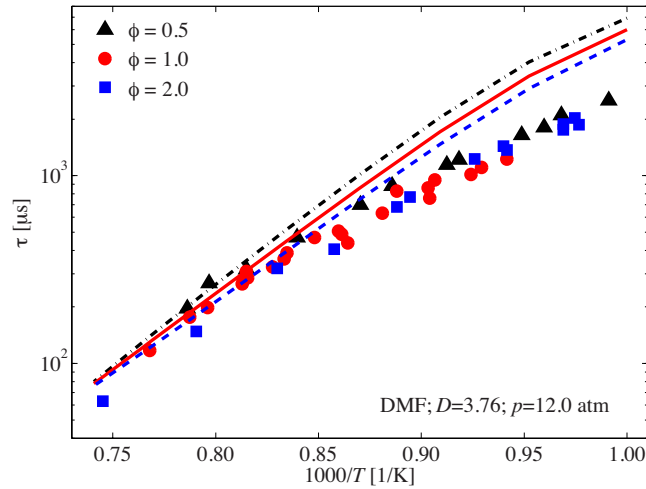
Figure 4.31: Experimental and model predictions of ignition delay times for stoichiometric, lean, and rich mixtures of DMF at a pressure of 12.0 atm. Lines indicate predictions using the model by Somers et al. [12], where solid lines: stoichiometric, dashed: rich, and dash-dot: lean.

that the model predictions capture the equivalence ratio effect seen in experimental data. Moreover, quantitative ignition delay times are captured with reasonable agreement at high temperatures. However, the agreement between the experimental data and the model is reduced as the temperature decreases, with the model over-predicting ignition delay times, suggesting reduced reactivity of DMF in the model.

Predictions using the model by Mehl et al. [10] are compared with ignition delay times of *iso*-octane at equivalence ratios of 0.5, 1.0, and 2.0 at a pressure of 12.0 atm in Figure 4.32. The model captures the equivalence ratio effect for temperatures below 1155 K, but the equivalence ratio trends are inverted at higher temperatures. The model accurately predicts the ignition behavior of the lean condition. However, there are discrepancies between the model and the experimental data as the equivalence ratio increases. The model over-predicts ignition delay times, especially at rich conditions.

These results and associated discussions show that models predict ignition delay times for DMF and *iso*-octane to a varying degree of success. The much reduced reactivity observed for the DMF model by Somers et al. [12] at lower temperature needs to be addressed in
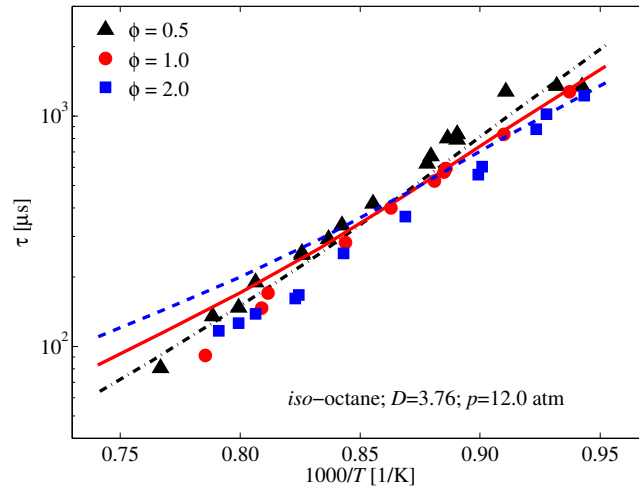
Figure 4.32: Experimental and model predictions of ignition delay times for stoichiometric, lean, and rich mixtures of iso-octane at nominal pressure of 12.0 atm. Lines indicates predictions using the model by Mehl et al. [10], where solid lines: stoichiometric, dashed: rich, and dash-dot: lean.

order to improve the predictive performance. Reaction rate constants need to be reviewed, together with exploration of key reaction pathways that can explain the deviations between experiments and model.

4.2.2   Combined *iso*-octane/DMF model

There is no chemical kinetic model of both DMF and *iso*-octane that can be used to better analyze kinetic interactions. It is of interest to develop a chemical kinetic model which enables the detailed investigation of fuel blends. Further, the performance of the DMF model could be improved toward increased reactivity. Here, a combined model is assembled starting with the recently published *iso*-octane model by Mehl et al. [10] which contains 7522 reactions among 874 species. Due to the large size of the chosen model, it is necessary to reduce the size of the model while preserving the kinetic performance. Here, the Alternate Species Elimination (ASE) method [96] discussed in the previous chapter is used to identify species that are indispensable to the prediction of ignition delay times.
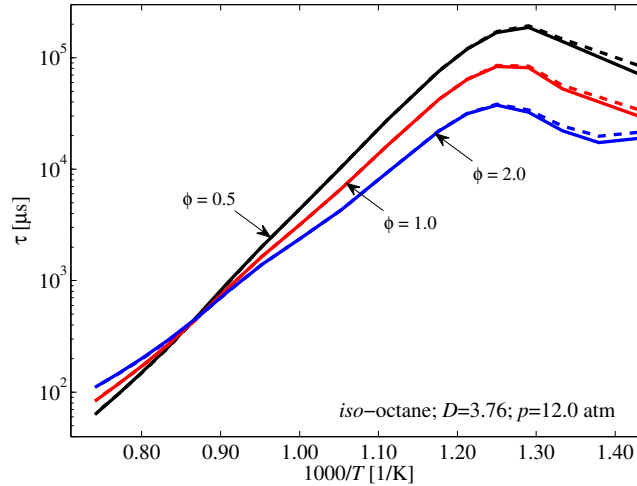
Figure 4.33: Experimental and model predictions of ignition delay times for stoichiometric, lean, and rich mixtures of iso-octane at nominal pressure of 12.0 atm. Solid line: Model by Mehl et al. [10], Dashed line: Skeletal iso-octane model.

The initial temperature is set to 950 K to capture both the low and high temperature ignition chemistry. Three equivalence ratios are used to cover the peculiarities of lean ($\phi = 0.5$), stoichiometric, and rich ($\phi = 2.0$) ignition. The pressure is set to 30 atm. The normalized change (NC) arising from alternate suppression of each of the 874 species is calculated. Three reactor conditions are used. The average NCs from the three conditions are ranked and the skeletal model consisting of 2441 reactions among 269 species is obtained by imposing an NC threshold of 1×10^{-4}. Figure 4.33 shows the relative performance of the skeletal model with respect to ignition prediction at equivalence ratios of 0.5, 1.0, and 2.0, at a pressure of 12.0 atm, conditions that are different from those used in the reduction process. It is observed that the skeletal model performance accurately reproduces predictions of the original model.

Before incorporating the skeletal mechanism of *iso*-octane into the detailed DMF model by Somers et al. [12], the two models are compared to identify and exclude from the skeletal model the common species, only focusing on the fuel-specific species in the *iso*-octane model. This process results in 141 *iso*-octane specific species, which are involved in 923 reactions. These additional species and reactions are then integrated into the DMF model of Somers et al. [12], to form the first version of the combined DMF/*iso*-octane model.

In order to improve the performance of the DMF model, the DMF model is reviewed for possible deficiencies. Two types of changes are carried out for this purpose. Some reaction rate parameters are updated as shown in Table 4.3 with other kinetic database entries. These are identified by reviewing reaction rates and adopting recommendations as referenced.

Table 4.3: Updated reaction rate parameters applied to the DMF model (Unit system: cm^3, mol, s, cal)

Reaction	$[A$	n	$Ea]_{new}$	$[A$	n	$Ea]_{old}$
ic3h7 + o2 ⇒ c3h6 + ho2 [a]	1.0e12	0.0	2981	4.5e-19	0.0	5020
nc3h7 + o2 ⇒ c3h6 + ho2 [a]	1.0e12	0.0	5028	3.0e-19	0.0	3000
bc5h11 + o2 ⇒ ac5h10 + ho2 [a, f]	1.0e12	0.0	2981	2.0e-18	0.0	5000
bc5h11 + o2 ⇒ bc5h10 + ho2 [a, f]	1.0e12	0.0	2981	2.0e-18	0.0	5000
xc7h15 + o2 ⇒ xc7h14 + ho2 [b, g]	4.7e12	0.0	6359	1.5e-29	0.0	2000
yc7h15 + o2 ⇒ xc7h14 + ho2 [b, g]	4.7e12	0.0	6359	6.0e-29	0.0	5020
yc7h15 + o2 ⇒ yc7h14 + ho2 [b, g]	4.7e12	0.0	6359	3.0e-29	0.0	3000
pc7h15 + o2 ⇒ oc7h14 + ho2 [b, g]	4.7e12	0.0	6359	3.0e-29	0.0	3000
pc7h15 + o2 ⇒ pc7h14 + ho2 [b, g]	4.7e12	0.0	6359	4.5e-29	0.0	5020
cc8h17 + o2 ⇒ ic8h16 + ho2 [b, g]	4.7e12	0.0	6359	3.0e-19	0.0	5000
cc8h17 + o2 ⇒ jc8h16 + ho2 [b, g]	4.7e12	0.0	6359	1.5e-19	0.0	4000
dc8h17 + o2 ⇒ jc8h16 + ho2 [b, g]	4.7e12	0.0	6359	2.0e-18	0.0	5000
h + o2 ⇒ o + oh [c]	9.8e13	0.0	14800	1.0e14	0.0	15286
ch3 + dmf252j ⇒ m2e5f [d, h]	3.8e12	0.0	0	1.3e13	0.0	0
ch4 + o2 ⇒ ch3 + ho2 [e]	8.5e06	2.0	52100	1.2e05	2.2	-3022 [k]
h35de2o1j ⇒ c4h5-n + ch2co [a, i, j]	3.0e14	0.0	33200	-	-	-
h35de2o1j ⇒ p134te1o + ch3 [a, i, j]	3.0e14	0.0	33200	-	-	-

[a] Warnatz [140]. [b] Baker et al. [141]. [c] Baulch et al. [138].
[d] Müller-Markgraf and Troe [142]. [e] Shaw [143].
[f] Analogous to ic3h7 + o2 ⇒ c3h6 + ho2.
[g] Analogous to ic4h9 + o2 ⇒ ic4h8 + ho2.
[h] Analogous to c7h7 + ch3 ⇒ c8h10.
[i] Analogous to nc3h7 ⇒ c2h4 + ch3.
[j] Reactions added to the model. [k] Reverse reaction rate.

The first 12 reactions are H-abstraction from radicals by O_2 to yield a stable species and HO_2. Reaction rates evaluated using original model entries at 1000 K are compared to chemical kinetic database entries for similar reactions and found to be markedly different. New values are assigned as referenced, with rate parameters for other reactions assigned based on analogous reactions, i-$C_3H_7 + O_2 \rightleftharpoons C_3H_6 + HO_2$, and n-$C_3H_7 + O_2 \rightleftharpoons C_3H_6 + HO_2$,

with recommended values by Warnatz [140] and Baker et al. [141], respectively.

For the reaction, $H + O_2 \leftrightharpoons OH + O$, the rate parameters proposed by Baulch et al. [138] are adopted, which lead to an effective increase of the reaction rate over the high temperature range by approximately 20%. The increased reactivity of this channel is deemed necessary to accord with shorter ignition delay times observed in the experiments and it aligns with the comprehensive review and recommendation by Baulch et al. [138]. For the reaction, $CH_4 + O_2 \leftrightharpoons CH_3 + HO_2$, the forward rate of Shaw [143] is adopted, in place of the values for the reverse reaction.

For reactions with species closely related to the DMF, two changes are implemented involving three reactions. Firstly, reaction rate parameters are adopted which effectively slow down by a factor of 10 the recombination of dmf252j (5-methyl-2-furanyl-methyl) radical with a methyl radical to form the higher carbon species, m2e5f (5-methyl-2-ethylfuran). The rate parameters used are those of the recombination of benzyl and methyl radicals to form ethyl benzene. Increasing the rate of this channel corresponds to a reduction in the reactivity of the system. Secondly, an analysis of the fate of dmf252j shows that in the original model ring opening yields the species, h35de2o1j (3,5-hexadiene-2-one-1-yl). Further reactions of this resultant species do not include possible beta-scissions. Two possible beta-scission reactions are included: the decomposition to methyl radical and p134te1o (penta1,3,4trien1one) as well as the decomposition to n-c_4h_5 and a ketene molecule, ch_2co. Reaction rate parameters for the beta-scission of propyl radical to ethylene and methyl radical are employed.

The aforementioned modifications are first applied to the detailed versions of both DMF and *iso*-octane models to verify that they lead to the intended increase in reactivity. In Figure 4.34, predictions of two versions of the DMF model by Somers et al. [12], with and without the modifications, are compared to the ignition delay times for DMF at stoichiometric conditions, a pressure of 12.0 atm, and D of 3.76. It is observed that the modified version predicts shorter ignition delay times than the original version as intended, and shows better agreement with
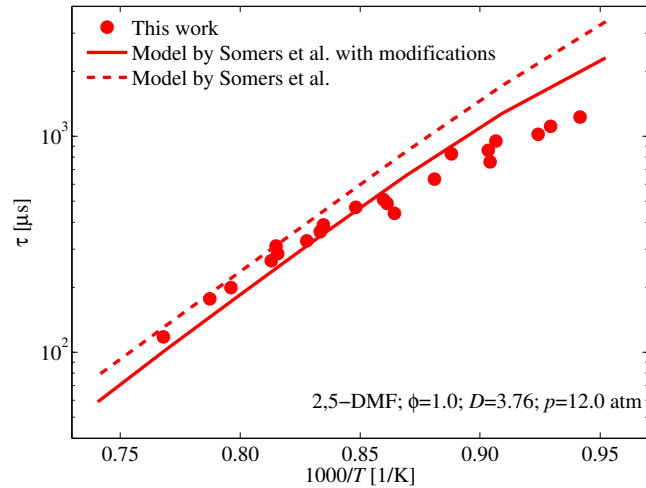
Figure 4.34: Experimental and model predictions of ignition delay times for stoichiometric DMF mixture at nominal pressure of 12.0 atm. Solid lines: DMF model by Somers et al. [12] with modifications. Dashed lines: DMF model by Somers et al. [12].

experimental data. Similarly, the original and modified versions of the detailed *iso*-octane model by Mehl et al. [10] are compared to ignition delay times for *iso*-octane at stoichiometric conditions, a pressure of 12.0 atm, and D of 3.76, in Figure 4.35. Similar to the DMF model, the predictions of modified *iso*-octane model exhibit higher reactivity than the original model.
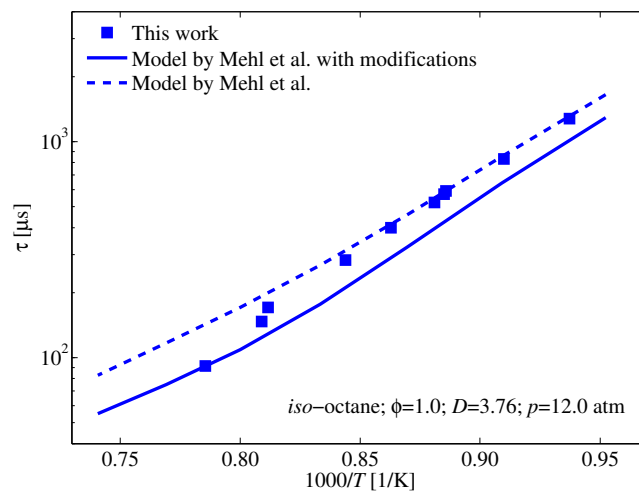
Figure 4.35: Experimental and model predictions of ignition delay times for stoichiometric iso-octane mixture at nominal pressure of 12.0 atm. Solid lines: iso-octane model by Mehl et al. [10] with modifications. Dashed lines: iso-octane model by Mehl et al. [10].
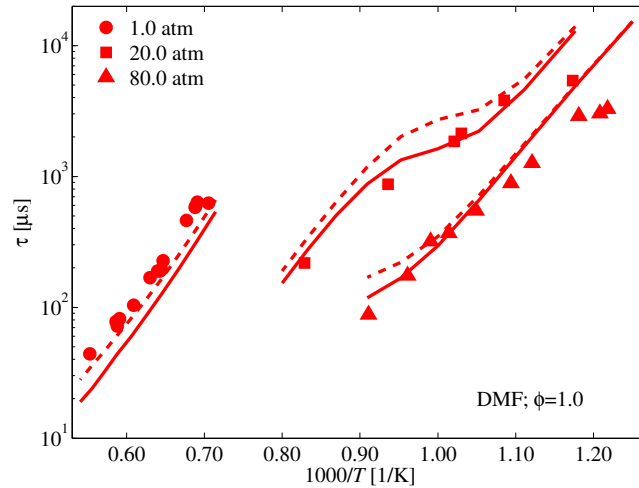
Figure 4.36: Comparison of model predictions with ignition delay times for stoichiometric DMF mixtures at pressures of 1.0, 20, and 80 atm from the work by Somers et al. [12]. The Ar/O_2 ratio is 16.6 for the 1.0 atm data, and N_2/O_2 ratio is 4.01 for the 20 and 80 atm data. Solid lines: DMF/iso-octane blend model. Dashed lines: Original DMF model by Somers et al. [12].

4.2.3   Comparison with simulation results

The present version of the DMF/*iso*-octane model contains 3691 reactions among 686 species. The performance of the combined model is validated against ignition data from literature, as well as the current data set. Although the experiments show that the ignition behavior of the fuel blends are closer to those of *iso*-octane, the blend model is more sensitive to DMF. The blend model is compared to previous DMF ignition data by Somers et al. [12] at stoichiometric conditions and pressures of 1.0, 20, and 80 atm, with an Ar/O_2 ratio of 16.6 for the 1.0 atm data, and an N_2/O_2 ratio of 4.01 for the other two pressures as shown in Figure 4.36. The figure shows improved performance of the blend model compared to the original model, especially at 20 atm and 80 atm. As shown in previous work [12] and in the previous section, the ignition delay times of Sirjean et al. [13] are longer than those predicted by the model of Somers et al. [12]. At the lower pressure of 1.0 atm the updated model predicts increased reactivity.
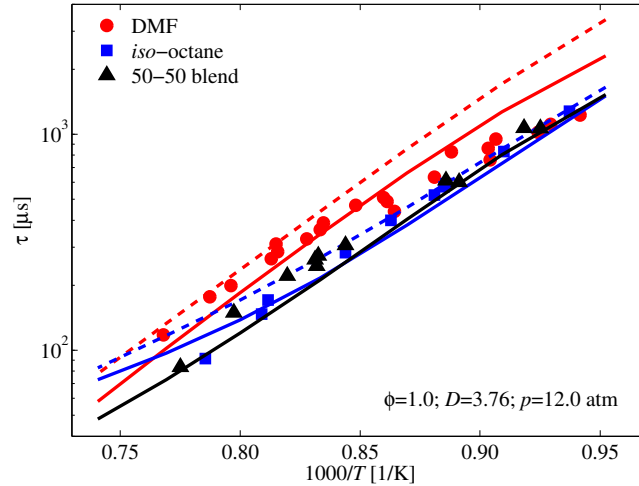
Figure 4.37: Experimental and model predictions of ignition delay times for stoichiometric mixtures of DMF, iso-octane, and 50-50 blends at nominal pressure of 12.0 atm. Solid lines: DMF/iso-octane blend model. Dashed lines: Original model of DMF by Somers et al. [12], and model of iso-octane by Mehl et al. [10].

In Figure 4.37, the blend model is compared with the ignition delay times for DMF, *iso*-octane, and the fuel blends at stoichiometric conditions, a pressure of 12.0 atm, and D of 3.76. The blend model is also compared with the predictions of the original models for both DMF [12] and *iso*-octane [10]. It is observed that the blend model predictions are in better agreement with the experimental data than the original models [10, 12] for both DMF and *iso*-octane. Moreover, the relative ignition behavior of the blend is captured by the model, with reasonable agreement. The comparative reactivity trend between the three fuels is captured by the model; DMF has the longest ignition delay times, while *iso*-octane ignites more readily. The blend reactivity falls between the two pure fuels, closer to delay times of *iso*-octane. This is in line with the experimental observations. There is a cross-over between *iso*-octane and the blend at temperatures above 1190 K, where the model starts to over-predict ignition delay times for *iso*-octane.

The blend model is also compared to the experimental data and the original models of DMF and *iso*-octane at rich conditions of $\phi = 2.0$, at a pressure of 12.0 atm and D of 3.76, as shown in Figure 4.38. The model consistently performs better than the original models. Also,
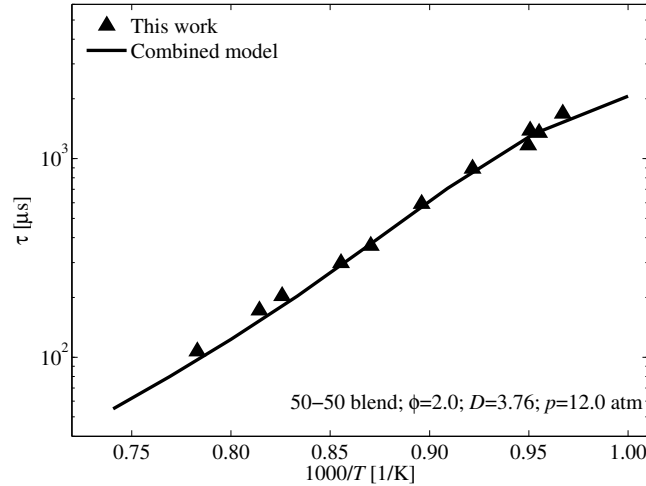
Figure 4.38: Experimental and model predictions of ignition delay times for a rich mixture of DMF/iso-octane 50-50 blend at nominal pressure of 12.0 atm. Solid line: DMF/iso-octane blend model.

the blend model predictions of the blend ignition are in good agreement with the experiment. As in the stoichiometric case, the relative reactivity trend established by the experimental data is captured by the blend model; DMF is still the least reactive, and *iso*-octane ignites fastest. The blend reactivity falls between those of the pure fuels, closer to delay times of *iso*-octane. The focus in this current combined model is ignition prediction with attention to pressures above 10.0 atm. As seen previously the model predicts higher reactivity at lower pressure.

The rather poor performance is also seen in the simulations of atmospheric laminar flame speeds of pure fuels and a DMF/*iso*-octane blend at the conditions investigated by Wu et al. [144]. Additionally, it is observed that the simulated trend differs from that of measured flame speed by Wu et al. [144] as shown in Figure 4.39. Further flame data are needed to determine the correct trend. Although there are still deviations between the newly developed blend model and the experimental data, the performance of the model is generally considered as an improvement on the initial models of DMF and *iso*-octane. Further improvement with more experimental constraints is needed.

Blend model analyses

To understand fuel interactions in the new model, reaction pathway analyses are carried out using the CHEMKIN software package [127] for an ignition process of stoichiometric fuel/O_2/Ar mixtures with D of 3.76 at a temperature of 1150 K and a pressure of 12.0 atm, for the fuels DMF, *iso*-octane, and a blend of equal liquid volume proportions.

The reaction pathway analysis for DMF is performed at the times 10, 300, and 625 μs close to the ignition delay time of 663 μs. At 10 μs, very little fuel is consumed, however, this is included because of observed differences in reaction pathways. At 10 μs, DMF is mainly consumed through H-abstraction reactions by O_2, with 62.5% of DMF consumption proceeding through this channel. Other H-abstraction reactions by HO_2 and CH_3 radicals contribute but less significantly. This partly explains the improved DMF reactivity in the new model, since the fuel molecule is mostly attacked by molecular oxygen, in addition to the radicals formed at later times. At later times, H-abstraction by OH and H radicals become more significant, as shown in Figure 4.40. The results of the reaction pathway analysis for pure DMF are in line with the results in the previous section, with a higher significance in
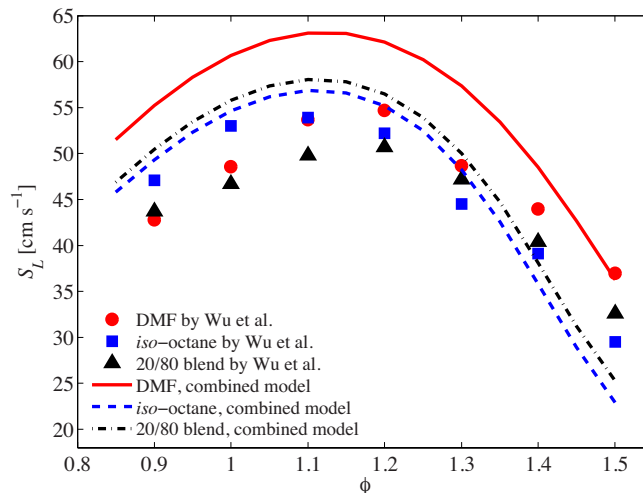
Figure 4.39: A comparison of laminar burning velocity measurements by Wu et al. [144] and combined model predictions for DMF, iso-octane, and 20/80 volumetric blends, at atmospheric pressure and initial temperature of 393 K.

2,5-DMF
Time from onset = 300 μs
Ignition delay time = 663 μs
18.5% consumed

C_6H_8O

+ CH_3 +OH   + H

16.7%   18.7%   15.7%

$C_6H_7O + CH_4$ $C_5H_6O + CH_3$

$C_6H_7O + H_2O$

iso-octane
Time from onset = 150 μs
Ignition delay time = 381 μs
39.8% consumed

C_8H_{18}

+ OH   + OH

12.6%   16.5%   8.5%

$aC_8H_{17} + H_2O$ $dC_8H_{17} + H_2O$

$C_7H_{15} + CH_3$

2,5-DMF/iso-octane blend
Time from onset = 200 μs
Ignition delay time = 406 μs
2,5-DMF: 35.4% consumed
iso-octane: 40.5% consumed

C_6H_8O

+ CH_3 + OH   + OH

17.2%   27%   16.6%

$C_6H_7O + CH_4$ dmf252oh3j

$C_6H_7O + H_2O$

C_8H_{18}

+ H   + OH

9.9%   25.1%   6.9%

$C_8H_{17} + H_2$ $C_8H_{17} + H_2O$

$C_7H_{15} + CH_3$

Figure 4.40: A representative reaction pathway analysis scheme for stoichiometric fuel/O_2/Ar mixtures of DMF, iso-octane, and equal liquid volume proportion blend, at a pressure of 12.0 atm, a temperature of 1150 K, and D of 3.76.

the initial H-abstraction by O_2, due to the improved DMF reactivity.

In the case of *iso*-octane, the ignition delay time is 381 μs, and the pathway analysis is performed at the times 10, 150, and 350 μs. Unlike DMF, in the *iso*-octane system the main reaction pathway is unimolecular decomposition of the original fuel molecule to heptyl and methyl radicals, which accounts for 17.8% of the *iso*-octane consumption at 10 μs. H-abstraction through CH_3, H, and OH radicals are the other important pathways at 10 μs. This early radical generation through decomposition contributes to the rapid ignition of *iso*-octane compared with DMF, where decomposition is less important. Later on, unimolecular decomposition increases to 55% as the system approaches ignition. The significance of H-abstraction reactions declines as ignition is approached. This suggests a more pyrolytic

consumption pathway for *iso*-octane compared to DMF.

For the fuel blend, the ignition delay time is 404 μs, and the pathway analysis is also performed at 10, 200, and 375 μs. Initially, *iso*-octane preserves the main reaction pathway observed in the case of pure fuel, where 37.6% of the *iso*-octane is consumed through unimolecular decomposition to heptyl and methyl radicals. However, the main initial pathway of DMF consumption becomes H-abstraction through CH_3, which accounts for 34.8% of the DMF consumption. This is in contrast to the most important H-abstraction by O_2 in the case of pure DMF. Later on, H-abstraction reactions by OH and H radicals become more significant in DMF consumption, while the H-abstraction by CH_3 channel remains an active pathway. The main consumption pathway of *iso*-octane is similar to the pure fuel. The main result of these analyses is the difference in initial reaction pathway difference for DMF in the pure fuel and blend cases. DMF favors H-abstraction by molecular oxygen in the case of the pure fuel, while it prefers H-abstraction by radicals in the case of blends. At play in this scenario is the CH_3 radical formation by *iso*-octane decomposition, which attacks DMF molecules. This results in faster consumption of DMF compared to the pure DMF case, with approximately 87% of the DMF consumed close to ignition in the blend case, compared to 71% consumption of DMF close to ignition in the pure fuel case. Sensitivity analysis has also shown that the addition of the new reaction channels of the 3,5-hexadiene-2-one-1-yl (h35de2o1j) radical, such as h35de2o1j $\rightleftharpoons$ *n*-C_4H_5 + CH_2CO, and h35de2o1j $\rightleftharpoons$ p134te1o + CH_3, (shown in Table 4.3) has an accelerating effect on the ignition behavior of the blend, revealed by sensitivity analysis.

In summary, this part of the thesis establishes the following with respect to the ignition of furans, *iso*-octane, and their blends:

- ■ 2-Ethyl furan (2-EF) ignites up to 6 times faster than DMF, indicating much higher chemical reactivity. For combustion systems with the need to avoid ignition, DMF is better suited, while 2-EF could be a better fuel for diesel engines.

■ *iso*-Octane ignites faster than DMF, in line with their reactivity trends revealed through the Research Octane Numbers (RON). Reactivity trends established by ignition delay times show that *iso*-octane is more reactive than DMF under all conditions. This confirms that DMF is well-suited for use in spark-ignition engines where auto ignition is best avoided.

■ DMF and *iso*-octane become more reactive as the equivalence ratio increases, based on a constrained diluent/O_2 ratio approach, with possible changes in this trend over the temperature range.

■ Blends of DMF and *iso*-octane show reduced impact of the DMF fraction in mixture. Blend reactivity falls between the two pure fuels, with more tendency towards *iso*-octane. A chemical kinetic model for the fuel blend is presented with improved performance with respect to DMF ignition prediction and reasonable prediction of the blend ignition.

The combined model and its analysis contribute to improved understanding of fuel blend combustion involving *iso*-octane and furans. The experimental data set presented in this work can be useful for further understanding and modeling of the combustion of DMF and *iso*-octane blends.

4.3   Ignition investigation of tetrahydrofurans

The furans considered earlier in this chapter are unsaturated cyclic ethers. Saturated furans, also known as tetrahydrofurans, are equally attractive as fuel additives or pure fuels. The structural differences between unsaturated furans and tetrahydrofurans suggest that their fundamental combustion properties may differ in a manner that can be used to further refine chemical kinetic models or develop generalized correlation for key combustion properties.

This section addresses the need for structure-activity studies of saturated and unsaturated furans. Ignition delay times of THF/O_2/Ar mixtures are measured at a nominal pressure of 12.0 atm and compared with ignition delay times of other furans presented. The ignition behavior of MTHF/O_2/Ar mixtures is also investigated at temperatures above 1000 K and pressures of about 3.0 atm and 12.0 atm, comparing the results with 2-MF data from this work. MTHF and 2-MF are compared to the predictions of recently published models of the respective fuels. The molecular structures of the fuels investigated in this section are shown in Figure 4.41.

tetrahydrofuran   2-methyltetrahydrofuran   2-methyl furan
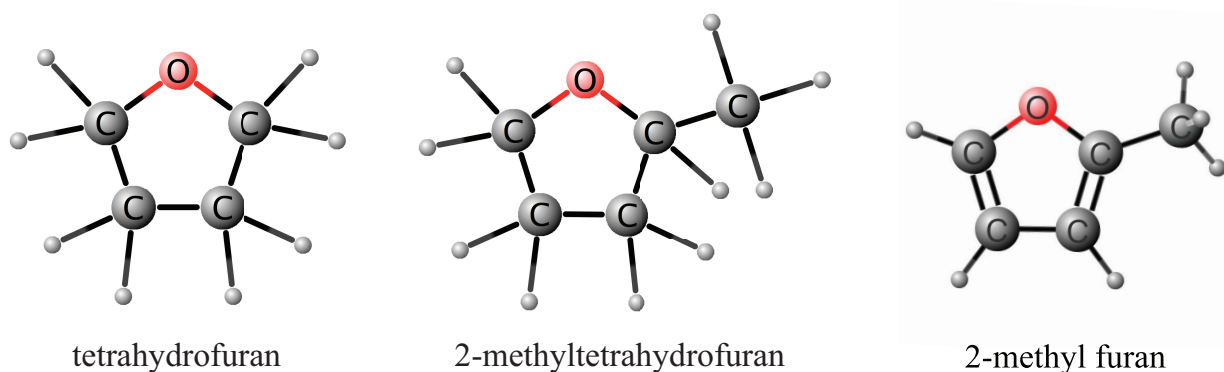
Figure 4.41: Chemical structure of THF, MTHF, and 2-MF.

4.3.1   Ignition study of tetrahydrofuran and 2-methyl tetrahydrofuran

In this part, results of the relative ignition behavior of the saturated furans, THF and MTHF are presented. Table 4.4 shows the mixtures investigated in this study.

Table 4.4: THF and MTHF mixtures investigated using ϕ and D constraints

Fuel	Diluent	ϕ	D	Fuel %	O_2 %	Diluent %
THF	Ar	1.0	3.76	3.68	20.23	76.09
	Ar	2.0	3.76	7.03	19.53	73.44
	Ar	0.5	3.76	1.87	20.61	77.52
MTHF	Ar	1.0	3.76	2.82	20.42	76.76
	Ar	2.0	3.76	5.66	19.82	74.52
	Ar	0.5	3.76	1.48	20.70	77.82

Ignition delay times of THF and MTHF at stoichiometric conditions, a pressure of 12.0 atm, and an Ar/O_2 ratio of 3.76 are compared in Figure 4.42. It is observed that MTHF has longer ignition delay times than THF up to a factor of 1.5 for temperatures below 1125 K, where a cross-over effect occurs, and THF becomes less reactive than MTHF at higher temperatures. This is in contrast to the trend observed for the structurally similar unsaturated furans, furan
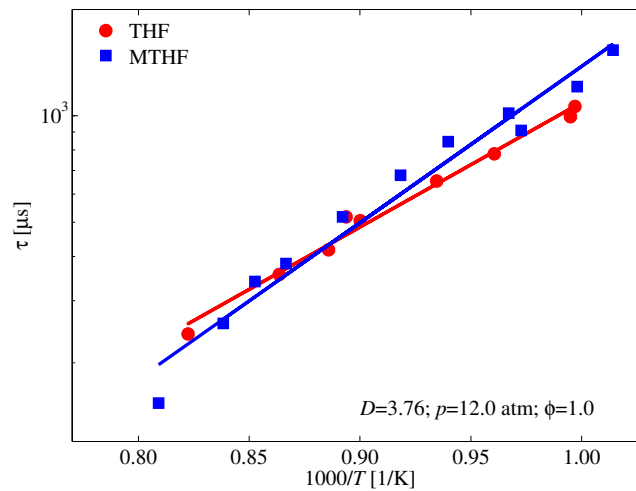
Figure 4.42: Relative ignition behavior of stoichiometric fuel/O_2/Ar mixtures of THF and MTHF at a pressure of 12.0 atm and an Ar/O_2 ratio of 3.76. Lines represent Arrhenius fits to the respective data.

and 2-MF, where 2-MF is consistently more reactive than furan, as shown in Figures 4.2, 4.3, and 4.4.

The ignition behavior of THF and MTHF at lean ($\phi = 0.5$) and rich ($\phi = 2.0$) conditions at a pressure of 12.0 atm and an Ar/O_2 ratio of 3.76 is also compared in Figure 4.43. At lean conditions, the reactivity trend is similar to that at stoichiometric conditions. MTHF has longer ignition delay times at temperatures below 1175 K where a cross-over effect is observed. For the rich condition, MTHF remains less reactive than THF all over the investigated temperature range. Again, this observed trend is the opposite of that established for furan and 2-MF at similar conditions, where 2-MF is consistently more reactive than furan at both lean and rich conditions. A recent study by Sudholt et al. [48] Quantum chemical calculations of bond dissociation energies of THF and MTHF reported show that the highest BDEs are observed for C–H bond for H-abstraction from side chain carbon of MTHF, compared to the C–H bonds for H-abstraction from ring chain carbon, which are generally similar for both fuels. The observed BDEs can rationalize the observed trend which is opposite to that of 2-MF and furan, especially that the study reports that 2-MF shows low BDE for the C–H bond at side chain carbon chain compared to furan BDEs at all locations, which can explain the high reactivity of 2-MF compared to furan.

Equivalence ratio effect

The equivalence ratio effect is studied for THF and MTHF. Ignition delay times of THF at a pressure of 12.0 atm, an Ar/O_2 ratio of 3.76, and equivalence ratios of 0.5, 1.0, and 2.0 are compared in Figure 4.44. The equivalence ratio effect is similar to that observed for all other fuels investigated in this work. It is observed that ignition delay times decrease with increasing equivalence ratios over the investigated temperature range. This means that maintaining the ratio of the number of inert molecules to oxygen molecules and increasing fuel concentration results in higher reactivity. Figure 4.44 shows a possible cross-over effect between the lean and stoichiometric mixtures for temperatures higher than the range investigated, where the
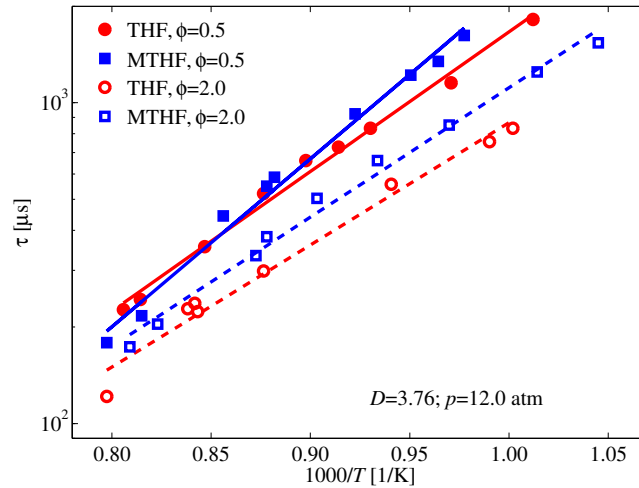
Figure 4.43: Relative ignition behavior of fuel/O_2/Ar mixtures of THF and MTHF at a pressure of 12.0 atm, an Ar/O_2 ratio of 3.76, and equivalence ratios of 0.5 and 2.0. Lines represent Arrhenius fits to the respective data.
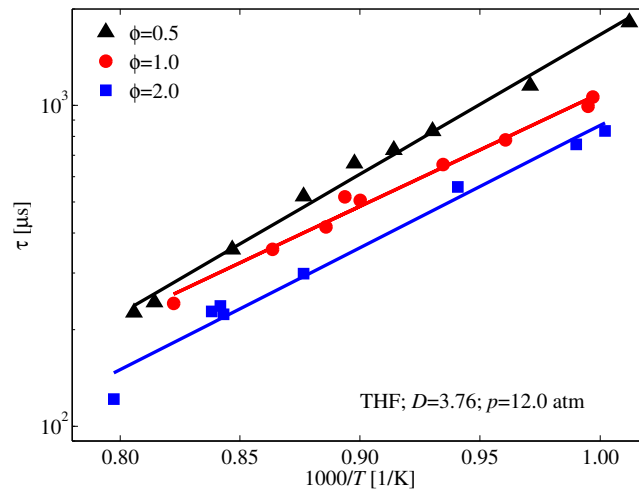
Figure 4.44: Equivalence ratio effect on THF ignition delay times for THF/O_2/Ar mixtures at nominal pressure of 12.0 atm and Ar/O_2 ratio of 3.76.

lean mixture can have shorter ignition delay times than the stoichiometric mixture.

The same equivalence ratio effect is observed for MTHF mixtures at a pressure of 12.0 atm, an Ar/O_2 ratio of 3.76, and equivalence ratios of 0.5, 1.0, and 2.0, as shown in Figure 4.45. Within the investigated temperature window, it is observed that ignition delay times decrease as the equivalence ratio increases. As suggested by the data, if the temperature is further increased, stoichiometric mixtures can ignite more readily than the richer mixtures.

The results above reveal that MTHF is the least reactive of the saturated furans investigated in this work. The next step is to compare the reactivity of MTHF with that of an unsaturated furan with a similar molecular structure.

4.3.2 2-Methyl furan (2-MF) and 2-methyl tetrahydrofuran (2-MTHF) compared

Ignition delay times of MTHF are studied at stoichiometric condition and a nominal pressure of 3.0 atm with an argon to oxygen ratio, D, of 3.76 are compared to ignition delay times of the similar unsaturated furan, 2-MF, presented earlier in subsection 4.1.1. In addition, ignition delay times of 2-MF and MTHF are measured at lean and rich conditions and D of 3.76 at 12.0 atm.

Figure 4.46 shows the results at 3.0 atm. It is observed that the ignition delay times of the saturated furan, MTHF, are longer than those of the unsaturated 2-MF up to a factor of 2 at 3.0 atm. Thus, MTHF is less reactive than 2-MF when both are subjected to the comparable initial thermodynamic conditions. The higher reactivity of methyl furan relative to furan
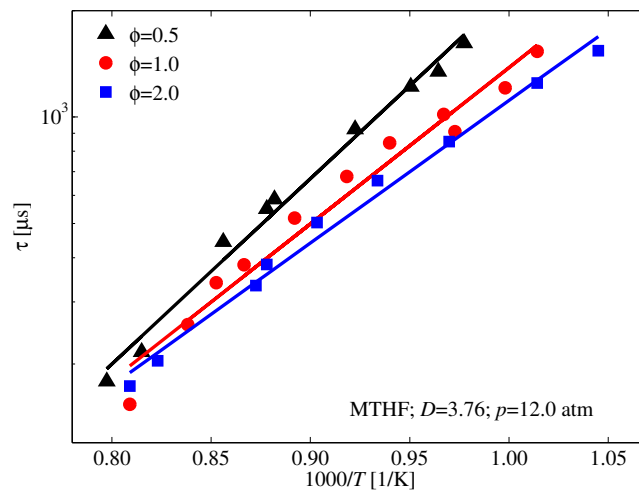
Figure 4.45: Equivalence ratio effect on MTHF ignition delay times for MTHF/O_2/Ar mixtures at nominal pressure of 12.0 atm and Ar/O_2 ratio of 3.76.
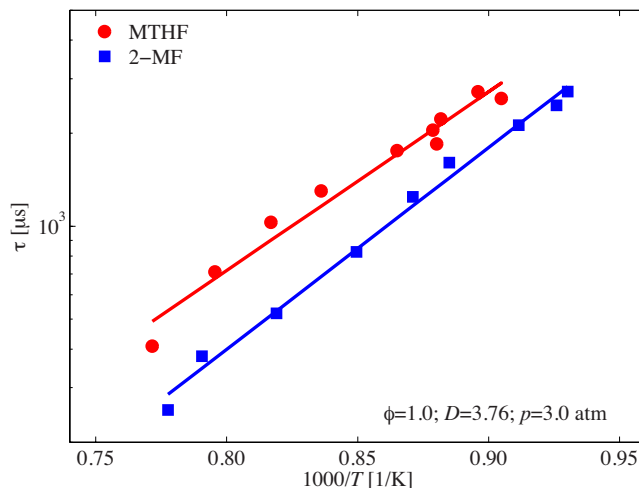
Figure 4.46: Relative ignition behavior of stoichiometric fuel/O_2/Ar mixtures of MTHF and 2-MF at a pressure of 3.0 atm. Lines represent Arrhenius fits to the respective data.
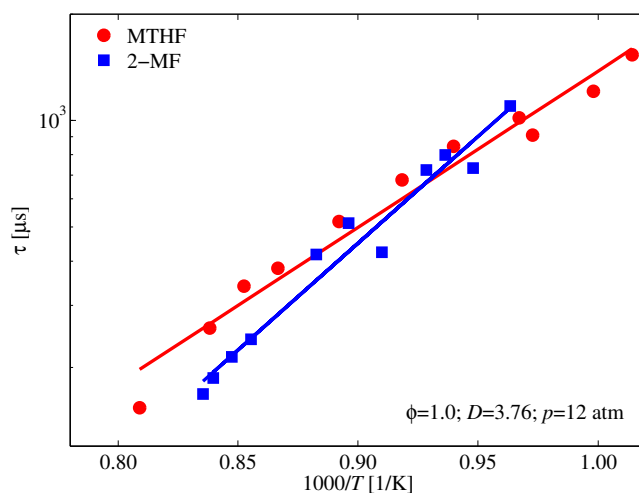
Figure 4.47: Relative ignition behavior of stoichiometric fuel/O_2/Ar mixtures of MTHF and 2-MF at a pressure of 12.0 atm. Lines represent Arrhenius fits to the respective data.

is thought to be mostly related to the weaker C–H bonds on the methyl group in 2-MF. It was shown in earlier work by Simmie and Curran [134] that ring C–H bonds in furans are exceptionally strong, so that oxidation initiation through these sites is limited. The observed difference between 2-MF and MTHF suggest that reactivity differences are localized on the methyl groups of these furans, as will later be discussed in detail. The same trend is observed at a higher pressure of 12.0 atm for temperatures above 1075 K, as shown in Figure 4.47. At lower temperatures, a cross-over effect takes place, where 2-MF has longer ignition delay
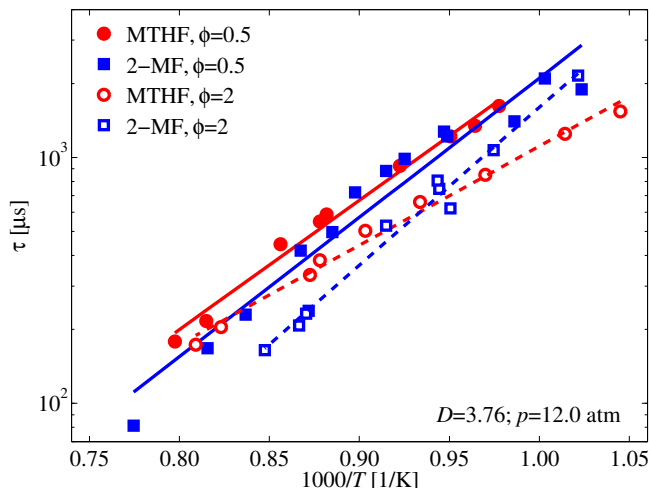
Figure 4.48: Relative ignition behavior of fuel/O$_2$/Ar mixtures of MTHF and 2-MF at a pressure of 12.0 atm and equivalence ratios of 0.5 and 2.0. Lines represent Arrhenius fits to the respective data.

times than MTHF.

In Figure 4.48, MTHF continues to have slightly longer ignition delay times than 2-MF at lean condition and a pressure of 12.0 atm. For the rich mixtures, MTHF has longer ignition delay times at higher temperatures but the trend is reversed at temperatures below 1065 K, indicating a weaker temperature sensitivity of MTHF under these conditions.

In summary, the ignition delay times of MTHF and 2-MF presented above reveal that the saturated furan MTHF exhibits lower reactivity than the unsaturated furan 2-MF with similar structure, especially at higher temperatures. Therefore, MTHF can be considered for spark ignition engine applications where auto-ignition is preferably avoided.

4.3.3   Comparison with chemical kinetic model predictions

The measured ignition delay times are now compared to model predictions using a 2-MF model by Somers et al. [12] and an MTHF model by Moshammer et al. [47]. For stoichiometric mixtures at an average pressure of 3.0 atm, the comparison is shown in Figure 4.49, where it is

observed that both models under-predict the measured ignition delay times by approximately a factor of 2. The observed reactivity trend is qualitatively reproduced at the higher temperature end. Also, the temperature sensitivity of the MTHF model is comparable with that of the experiment.

Further comparison of model predictions with measured ignition data for lean and rich mixtures at 12.0 atm are shown in Figures 4.50 and 4.51. In Figure 4.50, it is observed that model predictions are in closer agreement with the experimental data at $\phi = 0.5$ compared to the stoichiometric case at 3.0 atm. Greater deviation is observed between the measured and predicted delay times of 2-MF. Similarly, Figure 4.51 shows that model predictions and measured data agree only over a narrow temperature range at rich conditions, indicating that the modeling challenge is to accurately capture temperature dependence of the ignition delay times.

As observed in the results presented above, reactivity differences are clearly established for stoichiometric mixtures, such that MTHF is more difficult to ignite. The differences are less pronounced for lean mixtures at 12.0 atm, while rich mixtures at lower temperatures, MTHF
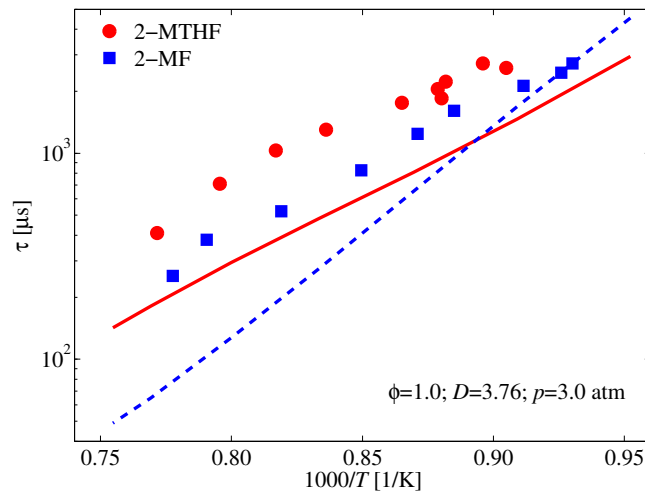
Figure 4.49: Ignition delay times of MTHF and 2-MF at stoichiometric conditions and a nominal pressure of 3.0 atm. Model predictions: solid line is MTHF model by Moshammer et al. [47] and dash line is 2-MF model by Somers et al. [12].
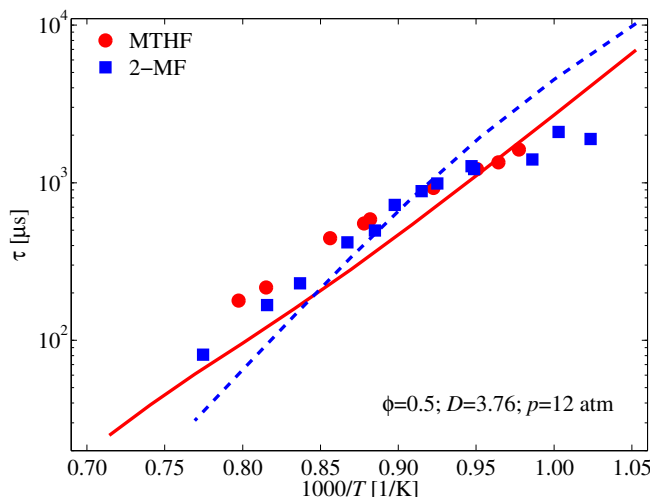
Figure 4.50: Ignition delay times of MTHF and 2-MF at an equivalence ratio of 0.5 and a nominal pressure of 12.0 atm. Model predictions: solid line is MTHF model by Moshammer et al. [47] and dash line is 2-MF model by Somers et al. [12].
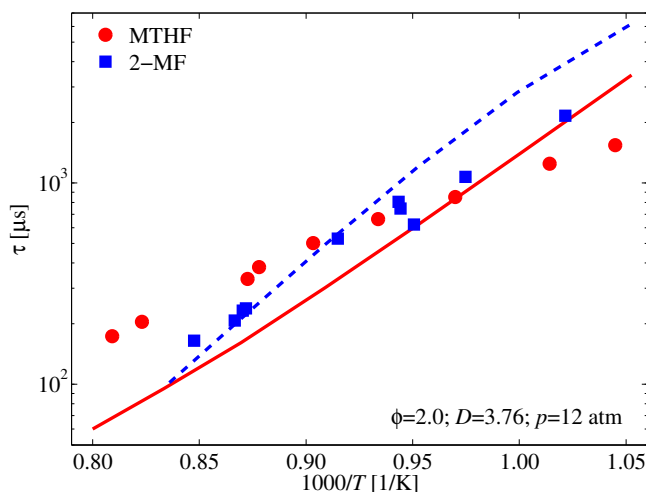
Figure 4.51: Ignition delay times of MTHF and 2-MF at an equivalence ratio of 2.0 and a nominal pressure of 12.0 atm. Model predictions: solid line is MTHF model by Moshammer et al. [47] and dash line is 2-MF model by Somers et al. [12].

can become more reactive than 2-MF. One approach to shed light on these differences is to examine the molecular structures with respect to the various bond dissociation energies (BDEs). These have been computed here by Dr. Akih-Kumgeh through direct atomization (CBS QB3 method) using the Gaussian software package [145] and the results are shown in Figure 4.52. It shows that in 2-MF the C–H bond in the methyl group (BDE of 86.3
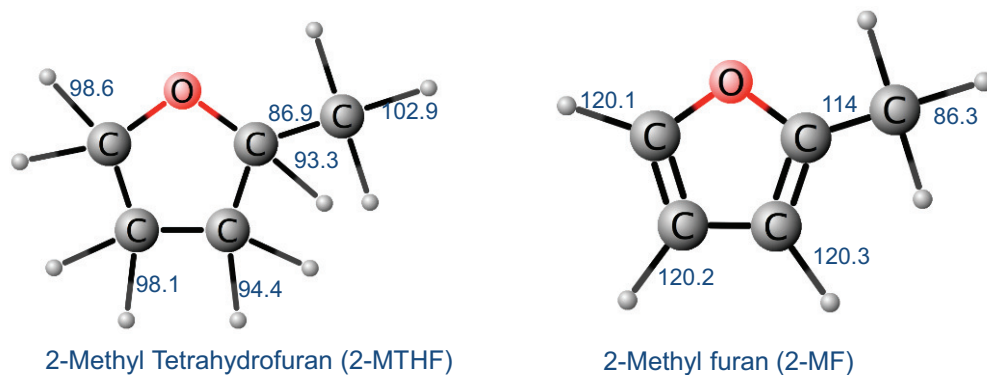
Figure 4.52: MTHF and 2-MF structures with bond dissociation energies calculated by direct atomization using the Gaussian 09 software package [145].

kcal/mol) is weaker than that the corresponding bond in MTHF (BDE of 102.9 kcal/mol). In 2-MF, as a result of the much stronger C–H bonds directly on the ring, radical or O_2 attack on the molecule is much easier at the methyl site as shown by Davis et al. [146], thus leading to the observed higher reactivity since the corresponding bond in MTHF is stronger. The calculated BDEs are in close agreement with previous 2-MF calculations by Simmie and Curran [134]. The reactivity of the various MTHF C–H sites have been investigated by Chakravarty et al. [147] focusing on H-abstraction by HO_2 radicals. The authors show that the lowest activation energy is observed for H abstraction from the C–H bond on the ring carbon to which the methyl group is attached. H abstraction from the methyl group is the most difficult, even compared to the ring C–H bonds. Kinetic differences of the resulting primary radicals and stable intermediates need further investigation and it is expected that the current experimental data will contribute toward improving the existing models.

4.4   Comparison of dimethyl cyclohexane and ethyl cyclohexane

The furans investigated in this chapter are oxygenated cyclic hydrocarbons which are considered attractive as fuel additives or pure fuels in the transportation sector. Non-oxygenated cyclic hydrocarbons, such as cycloalkanes, comprise a significant proportion in transportation fuels, such as conventional diesel ($\sim$30%), jet fuel ($\sim$20%), automotive gasoline ($\sim$10%), and aviation gasoline (20–30%) [69, 148–151]. The differences in molecular structure between oxygenated and non-oxygenated cyclic hydrocarbons can lead to disparities in their fundamental combustion properties. These differences can be utilized to develop and improve chemical kinetic models and fundamental combustion properties correlation.

This part of the thesis is aimed at generalizing the structure-activity results of isomers of oxygenated cyclic hydrocarbons, such as furans, to other non-oxygenated cyclic hydrocarbons used in transportation fuels, such as cycloalkanes. For this purpose, ignition delay times of dimethyl and ethyl isomers of cyclohexanes, DMCH and ECH, are measured at nominal pressures of 5.0 and 12.0 atm, equivalence ratios of 0.5, 1.0, and 2.0, and Ar/O_2 ratios of 3.76 and 10.0, and compared to those of similar isomers of furan, presented earlier in this chapter in subsection 4.2.1. The comparative reactivity trends are employed to test whether the observed trend is indicative of general reactivity differences between dimethyl and ethyl isomers of cyclic hydrocarbons, oxygenated or non-oxygenated. The observed trends could further be explored in chemical kinetic modeling. Ignition delay times of DMCH and ECH and compared to chemical kinetic model predictions. The molecular structure of the investigated fuels is shown in Figure 4.53, while the mixtures investigated in this section are shown in Table 4.5.

The initial hypothesis is that differences between ignition delay times of dimethyl and ethyl isomers will be factors of 2 or more, based on previous ignition studies of alkyl benzenes by Shen and Oehlschlaeger [137], discussed earlier in subsection 4.2.1. Some possible reasons for

1,3-dimethyl cyclohexane   ethyl cyclohexane
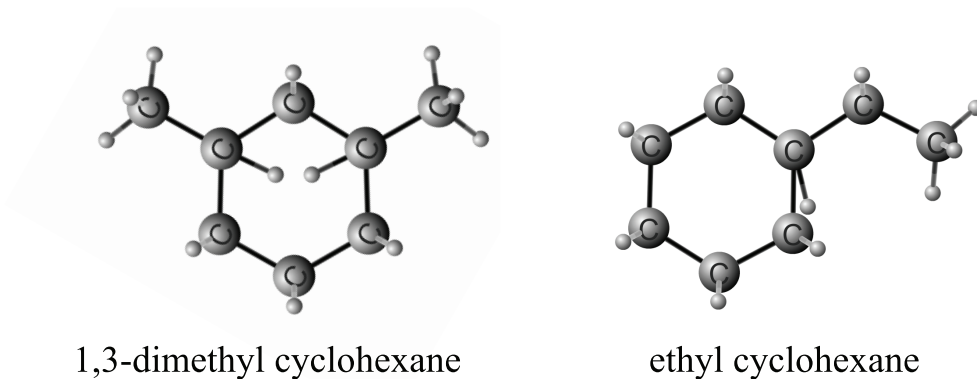
Figure 4.53: Chemical structure of DMCH and ECH.

Table 4.5: DMCH and ECH mixtures investigated using ϕ and D constraints

Fuel	Diluent	ϕ	D	Fuel %	O_2 %	Diluent %
DMCH	Ar	1.0	3.76	1.72	20.65	77.63
	Ar	1.0	10.0	0.75	9.00	90.25
	Ar	2.0	10.0	1.49	8.96	89.55
	Ar	0.5	10.0	0.38	9.06	90.56
ECH	Ar	1.0	3.76	1.72	20.65	77.63

the observed trend are discussed.

Based on the ignition delay time of DMCH obtained in this work, a new chemical kinetic model for DMCH is developed through a research collaboration between the Thermodynamics and Combustion Lab (TCL) at Syracuse University and Dr. Sarathy's group at the Clean Combustion Research Center (CCRC) at KAUST, prompted by the lack of chemical kinetic models of DMCH in the literature. Noteworthy is that the fuels investigated in this section are also studied by another PhD student at the TCL with a focus on concentration measurements.

4.4.1   Comparison of ignition delay measurements

The results of the stoichiometric cyclohexane studies are shown in Figures 4.54 and 4.55, where it can be seen that the ethyl isomer ignites more readily than the 1,3-dimethyl isomer over a
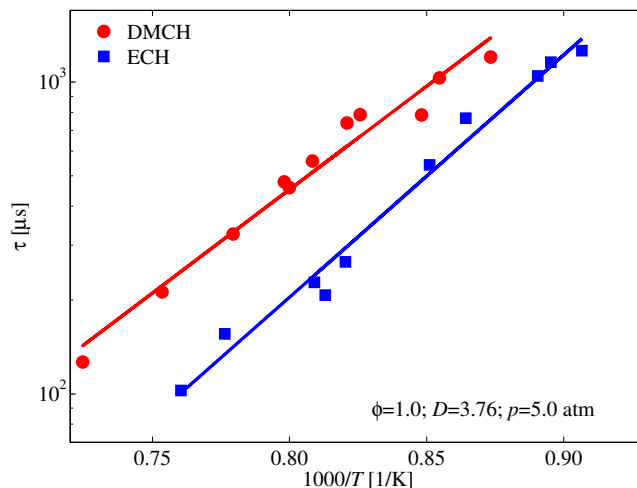
Figure 4.54: Ignition delay times of stoichiometric mixtures of fuel, oxygen, argon for DMCH and ECH with an argon/oxygen ratio of 3.76 at a pressure of 5.0 atm. Solid lines represent Arrhenius fits.

temperature range of 1057–1395 K. However, in this case it is observed that the differences are not as pronounced as those of the furan isomers shown in Figures 4.20 and 4.22, with the delay times of the dimethyl isomer being only approximately 2 times longer than those of the ethyl under similar conditions. Similar to the furans, differences are more pronounced at the lower pressure of 5 atm over the investigated temperature range. A possible explanation
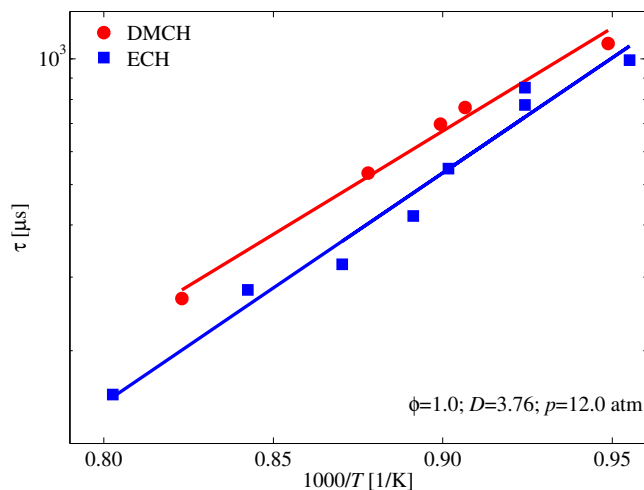
Figure 4.55: Ignition delay times of stoichiometric mixtures of fuel, oxygen, argon for DMCH and ECH with an argon/oxygen ratio of 3.76 at a pressure of 12.0 atm. Solid lines represent Arrhenius fits.
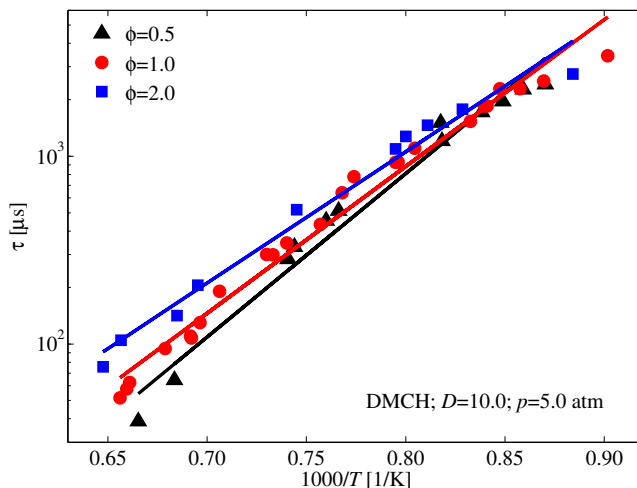
Figure 4.56: Equivalence ratio effect on ignition delay times for DMCH/O$_2$/Ar mixtures at nominal pressures of 12.0 atm and Ar/O$_2$ ratio of 3.76.

for the observed reactivity differences is that, whereas ECH has weak secondary C–H bonds, DMCH has only terminal C–H bonds that are generally more resistant to radical attack. Also, direct initiation in ECH can result from C–C bond scission, liberating more reactive C$_2$H$_5$ radicals, compared to CH$_3$ in the case of DMCH. From Figure 1.3, it is observed that one of the differences between the furan structures and the cyclohexanes is the C=C bond structure which is present in furans and absent in cyclohexanes. Radical addition reactions to these double bonds can facilitate ring opening or radical propagation. Thus if more radicals are initially produced during the oxidation of the ethyl isomers of furans and benzenes, these would tend to more effectively accelerate oxidation through attack of the C=C double bonds.

Equivalence ratio effect

Equivalence ratio effects on DMCH ignition are measured at a pressure of 5.0 atm, an Ar/O$_2$ ratio of 10.0, and equivalence ratios of 0.5, 1.0, and 2.0. Figure 4.56 shows that the equivalence ratio effect for DMCH is opposite to that observed at all other fuels in this study. Over the investigated temperature window, rich mixtures are observed to have the longest ignition delay times, lean mixtures ignite most readily, while stoichiometric mixtures continue to exhibit intermediate reactivity. The reason for the unusual behavior can be that

the temperatures investigated for this fuel are higher than the temperatures for the other fuels at same equivalence ratio. There is a competition between pyrolysis and oxidation. At higher temperatures pyrolysis contributes more than ignition and the less the fuel concentration the faster the ignition. Figure 4.56 shows that a cross-over behavior starts to occur at temperatures below 1150 K, which is typically a similar temperature range to that of other fuels investigated. Over this temperature range, the equivalence ratio effect is likely to revert to the original trend observed for the other fuels due to the cross-over effect, which supports the previous rationalization for the reversed ignition behavior.

4.4.2   Comparison with chemical kinetic model predictions

The DMCH chemical kinetic model is developed based on previous work on cyclohexane [152], methylcyclohexane [153], and ethylcyclohexane [154]. The DMCH model contains 540 species and 2929 reactions, with a DMCH submechanism that contains 102 reactions. The thermodynamic properties of DMCH and its related species are estimated using the THERM software [155]. According to the calculation by Kang et al. [156], the most stable isomer is cis-13DMCH with two equatorial methyl groups. However, the THERM software does not separate the cis- and trans- conformers. The estimated standard enthalpy at 298 K is -185.4 kJ/mol, which is close to the experimental value of -184.6 kJ/mol for cis-13DMCH reported by Cohen [157]. The estimated standard entropy and specific heat are also close to values from NIST chemistry database.

Ignition delay times of DMCH are compared to predictions of the new DMCH model, to evaluate the predictive performance of the new model at various conditions of pressure, dilution, and equivalence ratio. To study the effect of pressure on the predictions of the new model, ignition delay times of DMCH at stoichiometric conditions, an Ar/O_2 ratio of 3.76, and pressures of 3.0, 5.0, and 12.0 atm are compared to the predictions of the new DMCH model, as shown in Figure 4.57. Good agreement is observed between the model predictions and
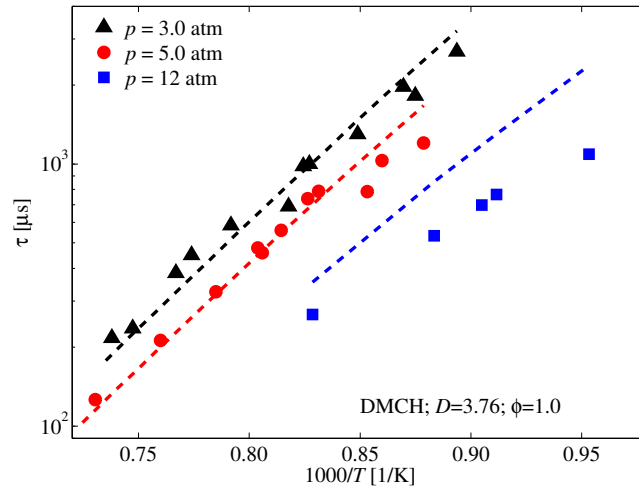
Figure 4.57: Ignition delay times of DMCH at stoichiometric conditions, an Ar/O_2 ratio of 3.76, and pressures of 3.0, 5.0, and 12.0 atm. Dashed lines: Predictions of the DMCH chemical kinetic model.

the experimental data at 3.0 and 5.0 atm, with some deviations at the low temperature end, especially at 5 atm. However, the model is observed to significantly over-predict ignition delay times of DMCH at a higher pressure of 12.0 atm, up to a factor of 2.2 at lower temperatures.

To evaluate the effect of varying equivalence ratio on the predictions of the new model, ignition delay times of DMCH at a pressure of 5.0 atm, an Ar/O_2 ratio of 10.0, and equivalence ratios
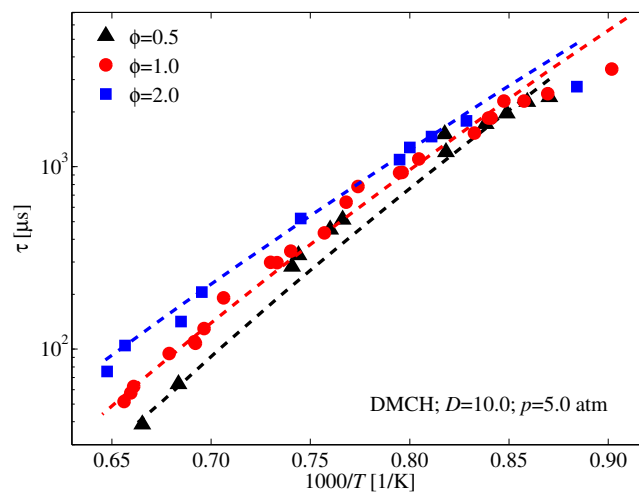
Figure 4.58: Ignition delay times of DMCH at a pressure of 5.0 atm, an Ar/O_2 ratio of 10.0, and equivalence ratios of 0.5, 1.0, and 2.0. Dashed lines: Predictions of the DMCH chemical kinetic model.
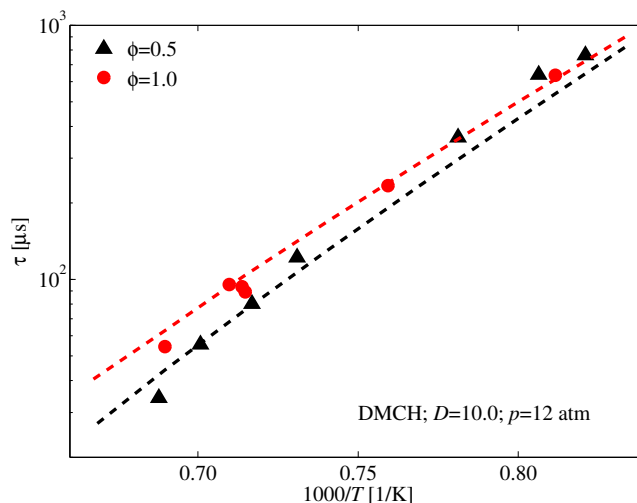
Figure 4.59: Ignition delay times of DMCH at a pressure of 12.0 atm, an Ar/O_2 ratio of 10.0, and equivalence ratios of 0.5 and 1.0. Dashed lines: Predictions of the DMCH chemical kinetic model.

of 0.5, 1.0, and 2.0 are compared to the prediction of the new DMCH model, as shown in Figure 4.58. The model also predicts the equivalence ratio trend. Varying the dilution ratio did not affect the predictive performance of the model at 5 atm. However, some deviations are observed at the low temperature end, especially at stoichiometric and rich conditions.

The equivalence ratio effect is also compared at a higher pressure of 12.0 atm, an Ar/O_2 ratio of 10.0, and equivalence ratios of 0.5 and 1.0 with results as shown in Figure 4.59. Good agreement between the experimental data and the model predictions is observed at the stoichiometric condition. At the lean condition, the model predictions reasonably agree with the experimental data in general, with deviations at the lower temperature end, where the model slightly under-predicts ignition delay times. The observed agreement at this high pressure of 12.0 atm and a dilution of 10.0 is different from that observed at the same pressure and a dilution of 3.76, shown in Figure 4.57, where the model significantly over-predicts ignition delay times. This suggests that the predictions of the new DMCH model are more accurate for highly diluted mixtures.

The newly developed DMCH model also contains the kinetic information for ECH oxidation.
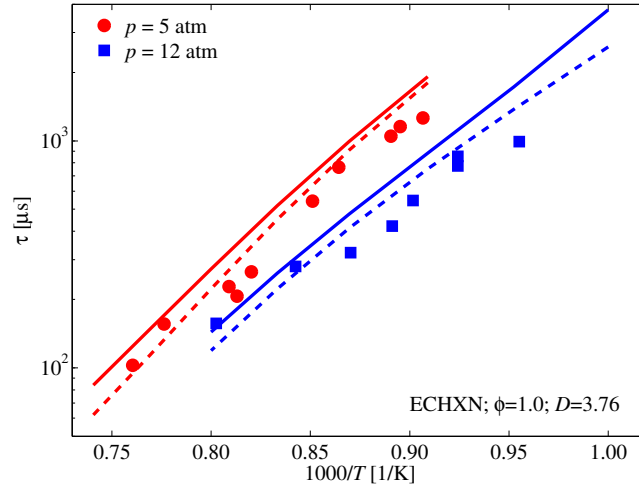
Figure 4.60: Ignition delay times of ECH at stoichiometric conditions, Ar/O_2 ratio of 3.76, and pressures of 5.0 and 12.0 atm. Solid lines: Predictions of the combined ECH and DMCH model. Dashed lines: Predictions of JetSurF 2.0 model by Wang et al. [101].

For this reason, its predictions of ECH ignition delay times are compared with measurements and to the predictions of the JetSurF2.0 model by Wang et al. [101]. For stoichiometric mixtures at pressures of $ECH/O_2/Ar$ of 5.0 and 12.0 atm and an Ar/O_2 ratio of 3.76, the comparison is shown in Figure 4.60. Generally, the JetSurF2.0 model is in better agreement with the ECH data than the combined ECH and DMCH model. Reasonable agreement is observed between the JetSurF2.0 model predictions and the ignition delay times of DMCH at both pressures, while the combined ECH and DMCH model over-predicts ignition delay times up to a factor of 1.7, especially at lower temperature. However, slight deviations between the predictions of JetSurF2.0 model and experimental data are observed at the lower temperature end for both pressures, with more pronounced deviations observed at 12.0 atm. The pressure effect is qualitatively captured by both models and the temperature sensitivity of the two models is comparable with that of the experiment.

Reaction pathway analysis are performed for DMCH ignition using the CHEMKIN software package [127] and the new DMCH model. Considered are $DMCH/O_2/Ar$ mixtures with an Ar/O_2 ratio of 3.76 at equivalence ratios of 1.0, 2.0, and 0.5, a temperature of 1150 K, and a pressure of 10 atm. Presented are the results obtained at the level of 20% fuel consumption.
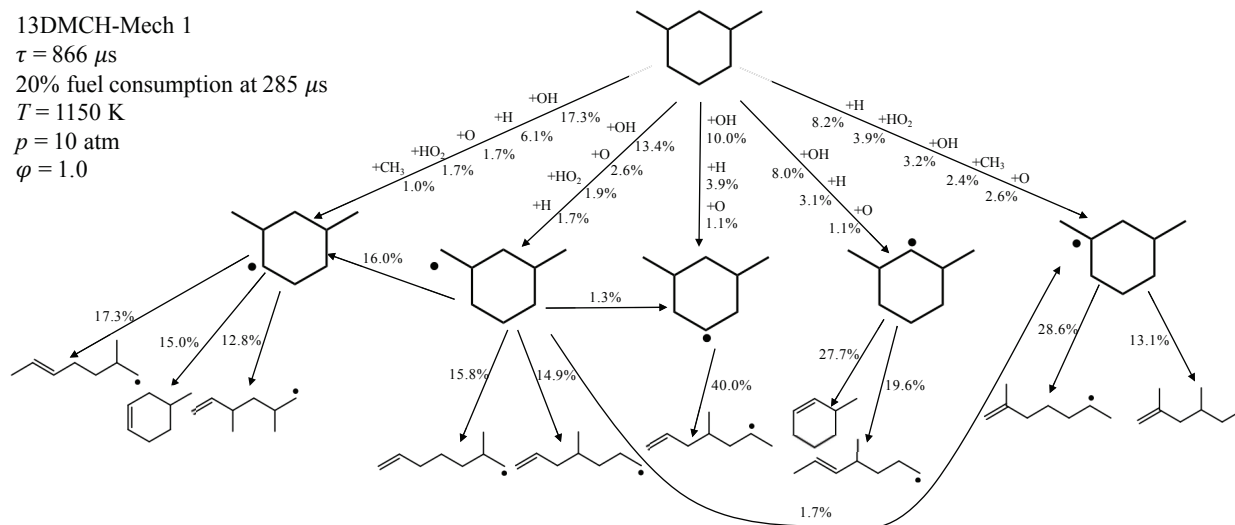
Figure 4.61: A representative reaction pathway analysis scheme for stoichiometric 13DMCH/O₂/Ar mixture at a pressure of 10 atm, a temperature of 1150 K, and D of 3.76 at 20% fuel consumption.

Figure 4.61 shows the reaction pathway analysis at stoichiometric conditions using the new DMCH model. It is observed that DMCH is mainly consumed through H-abstraction reactions by OH radical, with 51.9% of DMCH consumption proceeding through this channel. Other H-abstraction reactions by H, O, HO_2, and CH_3 also contribute but to a lesser extent. H-abstraction from carbon site 3 is favored, with 27.8% of the fuel being transformed to the radical DMCH13R3. Abstraction from carbon sites 2 and 1 are also important pathways but less significant than abstraction from site 3. The radicals resulting from H-abstraction of DMCH mainly undergo ring opening and isomerization reactions. However, some stable molecules are also formed, such as 3-methylcyclohex-1-ene and 4-methylcyclohex-1-ene. Besides the H-abstraction reactions of DMCH, a much less significant reaction channel for DMCH is observed through the cleavage of one methyl side chain to form 3-methylcyclohexyl, where only 1.1% of the fuel is consumed through this channel.

For the rich condition, the main reaction pathways observed at the stoichiometric condition are preserved using both models. Using the new DMCH model, H-abstraction reactions remain the main decomposition pathway, especially by OH radical, which is observed to be slightly less significant than the stoichiometric condition (50.6%). Moreover, the favored

abstraction site remains carbon site 3 (27.2%).

At lean conditions, H-abstraction by OH radical is more significant than the stoichiometric and rich cases (59.6%), while the abstraction by methyl radical is not significant, unlike in the other two cases. H-abstraction from carbon site 3 remains the favored abstraction site (27.5%).

In summary, the reflected shock tube technique has been employed in the investigation of the effect of molecular structure on ignition propensity for dimethyl and ethyl isomers of cyclohexanes, compared to the result for similar isomers of furan. It observed that the ignition delay times of the dimethyl isomers are generally longer than those of the ethyl isomers under similar experimental conditions. A more pronounced difference is seen between the ignition delay times of 2,5-dimethyl and ethyl furans, where a difference of up to a factor of 5 is observed compared to the difference between dimethyl and ethyl cyclohexane, which is approximately a factor of 2. The observations also align with a previous study on the ignition of alkyl benzene isomers, which established that m-xylene ignition delay times can differ from those of ethyl benzene by up to a factor of 3, or 5 under some conditions. The experimental data of DMCH support the development of an ECH/DMCH combined chemical kinetic model, which gives reasonable predictions of DMCH ignition delay times at most conditions. The ignition delay times of ECH are also compared to the predictions of the new model as well as to those by the JetSurF2.0 model [101]. Both models capture the ignition behavior of ECH with varying degrees of accuracy. The experimental results present an opportunity to further explore mechanistic pathways and rate processes controlling the oxidation of cyclic hydrocarbons of relevance to combustion systems.

Chapter 5

Skeletal chemical kinetic model development

Detailed chemical kinetic models such as those described previously are often too large for applied combustion studies. Validated models are therefore subject to reduction to obtain smaller but accurate models. Here, work is carried out to improve a robust reduction technique.

In this chapter, the reduction and simulation results of various models are presented using the SSE model reduction method, discussed in detail in Chapter 3. Firstly, the detailed, SSE, and ASE reduced versions of the *n*-heptane model by Mehl et al. [10] are compared as a means of evaluating the performance of the proposed SSE method. Secondly, the SSE approach is applied for the reduction of the relatively larger *iso*-octane model by Mehl et al. [102], then the predictions of the resulting model are compared to those of the detailed and the ASE reduced version for further performance evaluation. Finally, the standard SSE approach is extended to a multi-species sampling SSE approach to further reduce the computational cost required for the reduction of larger models. A 3-stage, multi-species sampling SSE approach is then applied for the reduction of the large *n*-octanol model by Cai et al. [103]. All reduction processes as well as ignition delay time simulations in this work are performed using the CANTERA [100] software package, while the CHEMKIN [127] software package is used to perform flame speed simulations.

Initially, the SSE method is first tested on the relatively small JetSurF2.0 model by Wang et
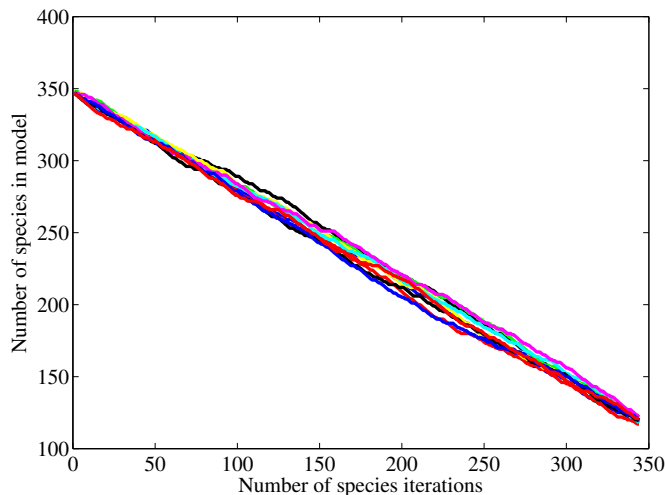
Figure 5.1: Relationship graph of number of iteration and number of retained species for 17 different SSE reduction processes of the JetSurF2.0 model by Wang et al. [101], all performed at a pressure of 12 atm, a temperature of 1050 K, and an Ar/O_2 ratio of 3.76.

al. [101] which contains 2163 reactions among 348 species, to compare the reduction efficiency and time requirement of the SSE method to those of the ASE method. In all, 17 different SSE processes are performed to test the effect of species randomizations on the reduction performance, as shown in Figure 5.1. On average, 120 species are retained in the SSE method, similar to the performance of the ASE method, where 122 species are retained. Moreover, the SSE method achieved 20% reduction in the computational time compared with the ASE method. Thus, the newly developed SSE method can effectively reduce a detailed model to a small model that is comparable to one that would be obtained using ASE. Therefore, the SSE method can be tested for the reduction of relatively larger surrogate fuel models, as will be demonstrated in the next sections.

5.1   Skeletal models of n-heptane using ASE and SSE

ASE and SSE reduction processes are applied to the recently published n-heptane model by Mehl et al. [10], which contains 654 species and 5258 reactions. The SSE reduction process leads to smaller model which contains 293 species, while the ASE reduction process results in
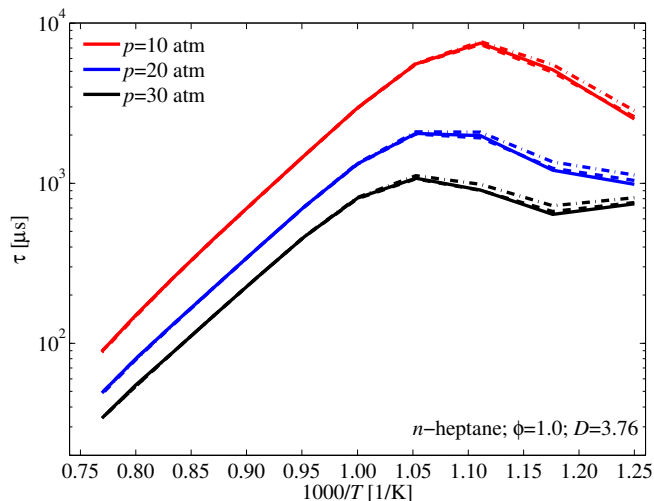
Figure 5.2: Comparison of pressure effect on the prediction of ignition delay time by the detailed, SSE and ASE reduced versions of the n-heptane model by Mehl et al. [10] at stoichiometric conditions and an Ar/O_2 ratio of 3.76. Solid lines: Detailed model. Dashed lines: SSE version. Dash dot lines: ASE version.

a model that contains 245 species. The SSE method is observed to achieve a 34% reduction in the computational time compared to the ASE reduction process. The reduction processes using both SSE and ASE methods are performed at a temperature 1050 K, a pressure of 12 atm, and an Ar/O_2 ratio of 3.76. The threshold imposed in the ASE reduction process is a fixed threshold of 3×10^{-4}, while the SSE reduction process uses a dynamic threshold which is initially equal to that used in ASE, and it increases up to approximately 1×10^{-2} as the model size decreases. The species with NC values below these threshold values are eliminated from the model, as discussed in detail in Chapter 3.

Firstly, the ignition delay time predictions of the detailed, SSE, and ASE versions of the n-heptane model are compared at stoichiometric conditions, a dilution ratio of 3.76, and pressures of 10, 20, and 30 atm, to test the capability of the SSE reduced version to capture the same pressure effect predicted by the detailed model, as shown in Figure 5.2. It is observed that the three versions capture the expected pressure effect, where the higher pressure condition exhibits shorter ignition delay times. In terms of the quantitative performance of the reduced versions, the SSE version is shown to have excellent agreement with the detailed version all
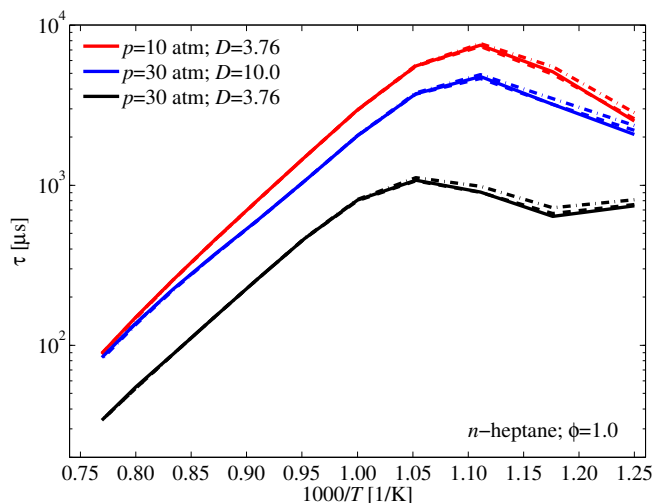
Figure 5.3: Comparison of dilution ratio effect on the prediction of ignition delay time by the detailed, SSE and ASE reduced versions of the n-heptane model by Mehl et al. [10] at stoichiometric conditions and pressures of 10 and 30 atm. Solid lines: Detailed model. Dashed lines: SSE version. Dash dot lines: ASE version.

over the tested temperature range, while a slight deviation is observed for the ASE reduced version at temperatures below 950 K, especially at the high pressure condition at 30 atm.

Ignition delay time simulations are then performed using the three versions of the n-heptane model to compare their predictions in terms of dilution factor effect. The simulations are performed at a dilution ratio of 3.76 for pressures of 10 and 30 atm, and a dilution ratio of 10.0 at a pressure of 30 atm, all at stoichiometric conditions. As shown in Figure 5.3, the three versions capture the expected reactivity trend, where the highly diluted condition at 30 atm has intermediate ignition delay times between the two conditions at a dilution ratio of 3.76 and pressures of 10 and 30 atm. Moreover, the SSE reduced version still shows good agreement with the predictions of the detailed version. The ASE version shows some deviation at temperatures below 950 K, which is more pronounced at a dilution ratio of 3.76 and a pressure of 30 atm. This deviation is similar to that observed in the previous comparison.

The predictions of the equivalence ratio effect using the three versions of the n-heptane model are also compared, as shown in Figure 5.4, which shows ignition delay times predicted by the three versions at a pressure of 30 atm, a dilution ratio of 3.76, and equivalence ratios of
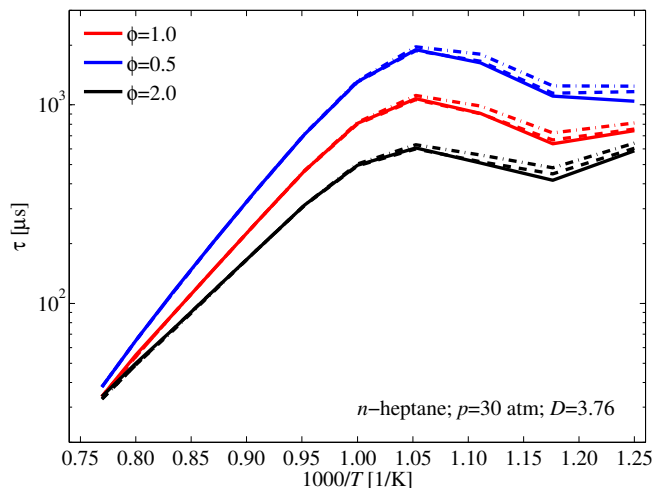
Figure 5.4: Comparison of equivalence ratio effect on the prediction of ignition delay time by the detailed, SSE and ASE reduced versions of the n-heptane model by Mehl et al. [10] at a pressure of 30 atm and an Ar/O_2 ratio of 3.76. Solid lines: Detailed model. Dashed lines: SSE version. Dash dot lines: ASE version.

0.5, 1.0, and 2.0. The expected equivalence ratio effect is qualitatively captured by the three versions, where the ignition delay times become shorter at higher equivalence ratios. For the stoichiometric condition, the SSE version shows excellent agreement with the detailed version, while the ASE version deviates slightly at temperatures below 950 K. For the lean and rich conditions, the SSE version continues to be in a better agreement with the detailed version than the ASE version, with very slight deviations observed at temperatures below 850 K for the lean condition, and below 910 K for the rich condition. The deviation of the ASE version from the detailed version is more pronounced at temperatures below 950 K, especially at the rich condition.

In addition to the previous comparisons of ignition delay time predictions, laminar burning velocity simulations are also performed to compared the predictions of the detailed, SSE, and ASE version of the n-heptane model, as shown the Figure 5.5. The simulations are performed at atmospheric pressure and a temperature of 450 K. Figure 5.5 shows that both SSE and ASE version slightly over-predict flame speed, especially as the equivalence ratio increases. However, the SSE version is observed to have a better agreement with the predictions of the
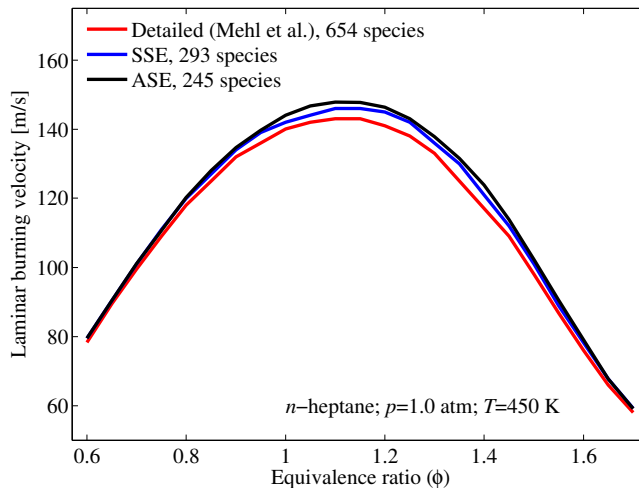
Figure 5.5: Comparison of laminar burning velocity predictions by the detailed, SSE and ASE reduced versions of the n-heptane model by Mehl et al. [10] at a pressure of 1.0 atm, a temperature of 450 K, and an Ar/O_2 ratio of 3.76.

detailed model than the ASE version.

The previous comparisons show that the SSE method is effective in both obtaining reduced versions that are efficient in terms of the predictive performance, and also more efficient in terms of the computational time required to finish the reduction process. While the effectiveness of the SSE method has been demonstrated for relatively small models (300 to 650 species), the method needs to be tested for larger systems to evaluate its performance under this condition.

5.2   Skeletal models of *iso*-octane using ASE and SSE

The SSE method is now utilized and tested for the reduction of a relatively larger chemical kinetic model. The method is used to reduce the recently published *iso*-octane model by Mehl et al. [102], which contains 874 species and 7522 reactions. Both methods are applied at a temperature of 1050 K, a pressure of 12 atm, and an Ar/O_2 ratio of 3.76. A fixed threshold value of 3×10^{-4} is used in the ASE reduction process, and the same value is used as the initial threshold value in the SSE reduction process. The SSE method resulted in a reduced model with 240 species, while the ASE reduced model has 234 species. The computational time reduction is similar to that of the previous *n*-heptane model.

The predictive performance of the detailed, SSE, and ASE versions of the *iso*-octane model is then compared. First, Figure 5.6 shows the comparison of ignition delay time predictions of the three versions at stoichiometric conditions, an Ar/O_2 ratio of 3.76, and various pressures of 10, 20, and 30 atm, to evaluate the ability of the SSE model to capture the pressure effect on the ignition delay times. As shown in Figure 5.6, all three versions capture the expected pressure effect; as ignition delay times decrease with increasing pressure. The predictions of the SSE version agree reasonably well with those of the detailed and ASE versions at higher temperatures. While the SSE and the ASE versions show excellent agreement all over the tested temperature range for the three pressures, both versions start to deviate from the predictions of the detailed model at temperatures below 950 K. This deviation becomes more obvious at higher pressures. The detailed version seems to capture a possible Negative Temperature Coefficient (NTC) behavior, which is not captured by both SSE and ASE versions. This could be improved by using a lower temperature than 1050 K in the reduction.

The effect of dilution ratio is then tested. Figure 5.7 shows ignition delay time predictions using the detailed, SSE, and ASE *iso*-octane models at stoichiometric conditions for a dilution
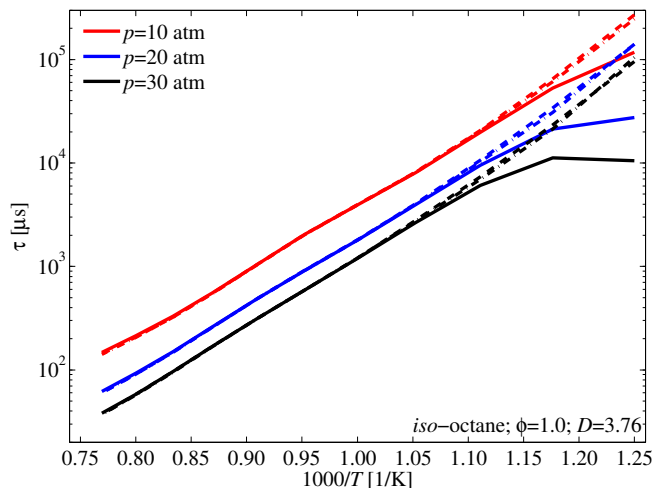
Figure 5.6: Comparison of pressure effect on the prediction of ignition delay time by the detailed, SSE and ASE reduced versions of the iso-octane model by Mehl et al. [102] at stoichiometric conditions and an Ar/O_2 ratio of 3.76. Solid lines: Detailed model. Dashed lines: SSE version. Dash dot lines: ASE version.

ratio of 3.76 at pressures of 10 and 30 atm, as well as for a dilution ratio of 10.0 for a pressure of 30 atm. The three versions predict the qualitative dilution ratio effect, where the ignition delay times increase with higher dilution ratios. The data set at a pressure of 30 atm and a dilution ratio of 10.0 has an intermediate reactivity between the two data sets at a dilution ratio of 3.76 and pressures of 10 and 30 atm. The three versions continue to show excellent agreement at temperatures above 950 K. As shown in the previous case, the ASE and SSE versions have almost identical predictions in general, and both versions over-predict ignition delay times at temperatures than 950 K, compared to the predictions of the detailed version. The deviation is more pronounced for the data set at a pressure of 30 atm and a dilution ratio of 3.76. NTC behavior is only captured by the detailed version.

In terms of equivalence ratio effect, the ignition delay time predictions of the detailed, SSE, and ASE versions of the *iso*-octane model are compared at a pressure of 30 atm, a dilution ratio of 3.76, an equivalence ratios of 0.5, 1.0, and 2.0. As in the previous two cases, the equivalence ratio effect is qualitatively captured by the three versions, where the ignition delay times decrease with increasing equivalence ratio. Quantitatively, the SSE and ASE versions
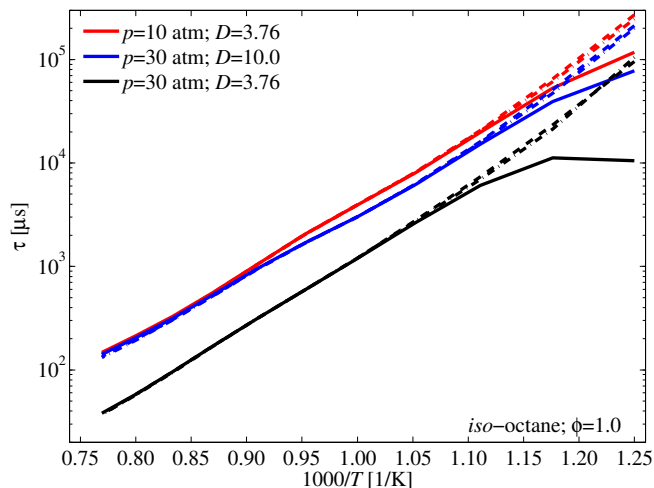
Figure 5.7: Comparison of dilution ratio effect on the prediction of ignition delay time by the detailed, SSE and ASE reduced versions of the iso-octane model by Mehl et al. [102] at stoichiometric conditions and pressures of 10 and 30 atm. Solid lines: Detailed model. Dashed lines: SSE version. Dash dot lines: ASE version.

continue to have excellent agreement with each other, except for a very slight deviation at the rich condition for temperatures below 830 K. Both reduced versions continue to agree reasonably with the detailed version at temperatures above 950 K, where they start to over-predict ignition delay times compared to the predictions of the detailed version, with
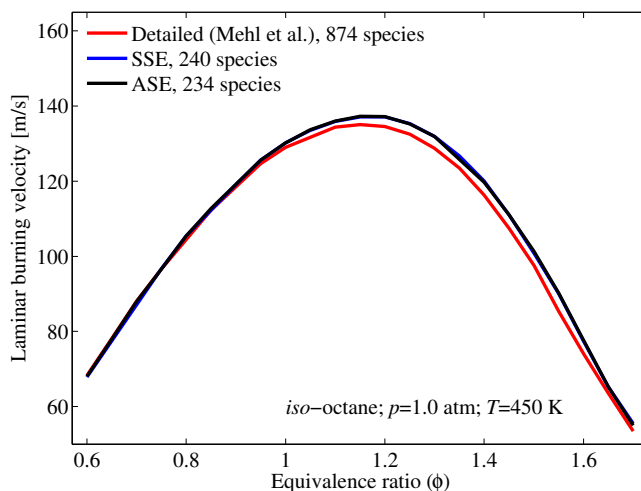
Figure 5.8: Comparison of laminar burning velocity predictions by the detailed, SSE and ASE reduced versions of the iso-octane model by Mehl et al. [102] at a pressure of 1.0 atm, a temperature of 450 K, and an Ar/O_2 ratio of 3.76.

the largest deviations observed at the rich condition.

Laminar burning velocity simulations are performed using the detailed, SSE, and ASE versions of the *iso*-octane model at atmospheric pressure and a temperature of 450 K, as shown in Figure 5.8. The SSE and ASE reduced versions have excellent agreement in general. Both reduced versions agree reasonably with the detailed version at lean and stoichiometric conditions. At higher equivalence ratios, i.e. rich conditions, the SSE and ASE versions slightly over-predict the flame speed compared to the detailed version.

The previous results show that the SSE method is able to reproduce the predictive performance of the existing ASE method, while the time consumed to perform the reduction process is significantly reduced. However, the need for further time and computational requirement reduction arises as the computational time of the SSE reduction process of the *iso*-octane model is approximately 2 days. For larger mechanisms with more than 1000 species the time required to perform SSE reduction is expected to be much longer. This calls for a modification in the SSE method to accommodate larger models with more than a thousand species.

5.3   Skeletal models of n-octanol using SSE with multi-species sampling

Based on the observed time requirement for SSE reduction process, the reduction of the n-octanol model by Cai et al. [103] is expected to take much longer time. The model contains 1281 species and 5537 reactions. The relatively large size of the mechanism and the time taken to reduce shorter models prompted the modification of the SSE approach to better suit the reduction of such large systems. For this purpose, a multi-stage, multi-species sampling SSE approach is adopted, as discussed in the model reduction approach section.

The reduction procedure of the n-octanol model by Cai et al. [103] starts with a 3-species sampling SSE process, where the model size is reduced to 1137 species. This is followed by a 2-species sampling SSE process, which further reduces the model to 810 species. Finally, a standard SSE process is performed. All reduction stages are performed at a pressure of 12 atm, a temperature of 1050 K, a dilution ratio of 3.76, and an initial threshold value of 3×10^{-4}, which dynamically increases up to approximately 1×10^{-2} at the end of the reduction process. This approach produces the final reduced model containing 450 species. The total time of the 3 reduction stages is 5 days and 7 hours. If a standard SSE approach is employed as in the reduction of the iso-octane and n-heptane models, the computational time is expected to be significantly longer.

The ignition delay time predictions of the detailed and SSE reduced versions of the n-octanol model are compared at stoichiometric conditions, a dilution ratio of 3.76, and pressures of 10, 20, and 30 atm, as shown in Figure 5.9. The expected pressure effect on the ignition delay times is captured by both versions, where ignition delay times increase with decreasing pressure. A reasonable agreement between the detailed and the SSE versions is observed for the three pressures investigated. A slight deviation between both versions is observed at lower temperatures, which is more pronounced at 30 atm for temperatures below 950 K. Moreover, a very slight deviation is observed at temperatures above 1110 K for all three pressures.
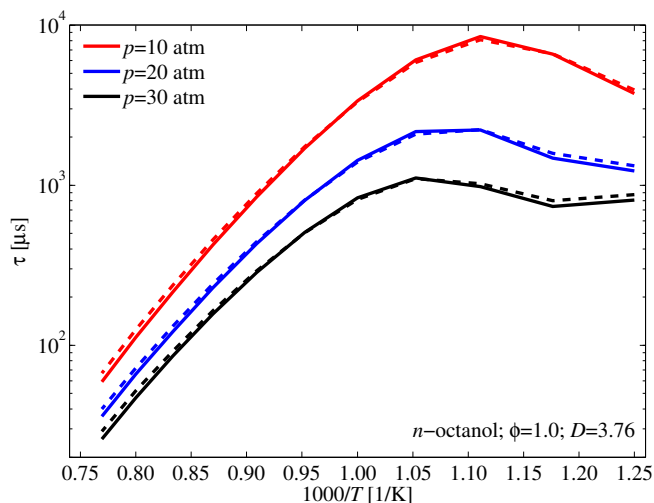
Figure 5.9: Comparison of pressure effect on the prediction of ignition delay time by the detailed and SSE reduced versions of the n-octanol model by Cai et al. [103] at stoichiometric conditions and an Ar/O_2 ratio of 3.76. Solid lines: Detailed model. Dashed lines: SSE version.

The dilution ratio effect on the ignition delay time predictions is also investigated through the comparison between predictions of the detailed and SSE versions of the n-octanol model at a dilution ratio of 3.76 for pressures of 10 and 30 atm, and at a dilution ratio of 10.0 for a pressure of 30 atm, as shown in Figure 5.10. The expected ignition behavior is captured, where
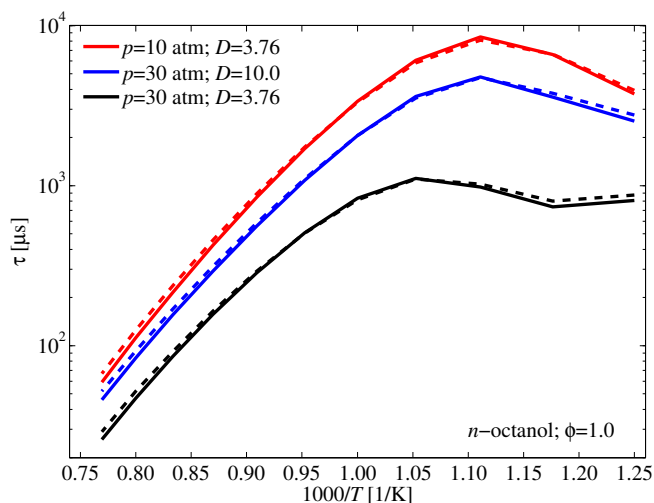
Figure 5.10: Comparison of dilution ratio effect on the prediction of ignition delay time by the detailed and SSE reduced versions of the n-octanol model by Cai et al. [103] at stoichiometric conditions and pressures of 10 and 30 atm. Solid lines: Detailed model. Dashed lines: SSE version.
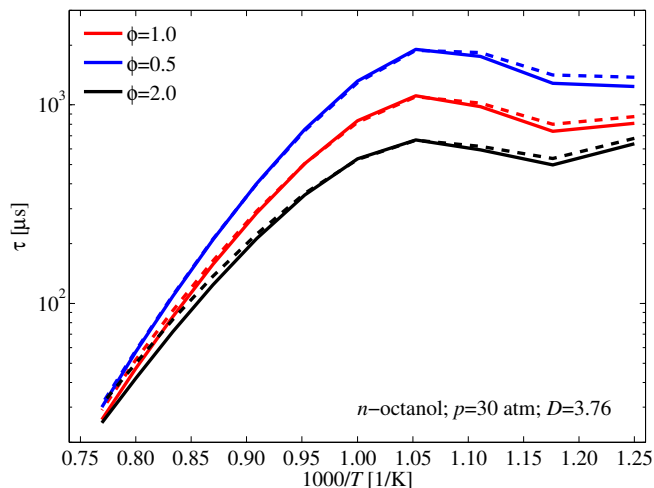
Figure 5.11: Comparison of equivalence ratio effect on the prediction of ignition delay time by the detailed and SSE reduced versions of the n-octanol model by Cai et al. [103] at a pressure of 30 atm and an Ar/O_2 ratio of 3.76. Solid lines: Detailed model. Dashed lines: SSE version.

the condition at 30 atm and dilution ratio of 10.0 has longer ignition delay time than the condition at the same pressure and dilution ratio of 3.76, where it has shorter ignition delay time than the condition at 10 atm and dilution ratio of 3.76. Quantitatively, the agreement between both versions is similar to that in the previous comparison, where good agreement is observed in general, with slight deviations at both higher and lower temperature ends.

Finally, the ignition predictions of the detailed and SSE reduced versions of the n-octanol model at various equivalence ratios are compared in Figure 5.11 to test the ability of the SSE version to capture the equivalence ratio effect predicted by the detailed model. The ignition delay simulations are performed at a pressure of 30 atm, a dilution ratio of 3.76, and equivalence ratios of 0.5, 1.0, and 2.0. The agreement between both versions is generally reasonable, with some deviations observed. At an equivalence ratio of 0.5, a good agreement is observed at temperatures above 925 K, where some deviations occur at lower temperatures. At stoichiometric conditions, a similar deviation is observed below 925 K, as well as a very slight deviation at temperatures above 1110 K. At an equivalence ratio of 2.0, a more significant deviation is observed at temperatures above 1050 K, which becomes more pronounced as the temperature increases. A slight deviation, similar to those observed at the other two

equivalence ratios, is shown at temperatures below 950 K.

Therefore, the multi-species sampling SSE approach is shown to be effective in large model reduction. The predictive performance of the resulting reduced model is generally reasonable, with the most significant deviations shown at rich condition and higher pressures. The time consumed is reasonable, and this extended SSE approach is believed to be more time efficient than the standard SSE approach, and therefore much more time efficient that the existing ASE method.

In this work, the existing Alternate Species Elimination (ASE) method [96] is extended to a stochastic species sampling approach, referred to as the Stochastic Species Elimination (SSE) method. The new SSE method features dynamic mechanism sizing and dynamic threshold determination to help reduce the time and computational requirements of the reduction process. The SSE approach also enables the user to track the real-time reduction progress, so that the process can be terminated when a reasonable number of species is attained.

The SSE method is observed to provide similar reduction efficiency to that of the ASE method in terms of the number of retained species, with a significantly reduced computational time; up to 34% in the case of n-heptane model [10] reduction. Results from different randomization processes are shown to be consistent in terms of the reduced model size.

The SSE approach is used for the reduction of the n-heptane model by Mehl et al.[10]. The SSE reduced version is observed to be in a better agreement with the detailed model than the ASE version for both ignition delay time simulations and flame speed simulations. Very slight deviations are observed in ignition delay simulations at the lower temperature end for lean and rich conditions, but these deviations are still less pronounced than those exhibited by the ASE model.

Moreover, the SSE approach is employed to reduce the relatively larger iso-octane model by Mehl et al. [102]. In general, the SSE model was successful in reproducing the predictions

of the ASE version for both ignition delay and flame simulations. For ignition delay time simulations, both versions start to significantly deviate from the predictions of the detailed model at lower temperatures, which suggests that possible NTC behavior is not captured by the reduced versions, unlike the detailed model.

Finally, the standard SSE approach is extended to increase its efficiency for the reduction of larger chemical kinetic models with over 1000 species. A 3-stage, multi-species sampling SSE approach is proposed and adopted to reduce the large n-octanol model by Cai et al. [103]. The resulting SSE version has a good agreement in general with the ignition delay predictions of the detailed model, with the most pronounced deviations observed at higher temperature for an equivalence ratio of 2.0, which suggests that the chemical kinetics at rich conditions are not sufficiently captured by the reduced model.

This work contributes into the ongoing model reduction efforts, and is aimed at providing a simple, easy-to-use, and time-efficient model reduction approach that yields reduced models with reasonable predictive accuracy. Possible improvements of SSE method include the use of pre-sized stochastic sampled submechanisms in the detailed model reduction instead of investigating one species or a few species at a time as a means of further reducing the computational time required in the reduction process.

Chapter 6

Conclusion and outlook

The present work addresses the ignition behavior of selected oxygenated and non-oxygenated hydrocarbons which are of relevance to combustion systems. It is a combination of experiments, chemical kinetic modeling, and model analyses aimed at rationalizing the observed experimental trends. The approach is comparative, seeking to reveal trends, similarities and differences in ignition behavior of the selected fuel classes, which can be used in the development of detailed and reduced chemical kinetic models.

The ignition of furans, a class of oxygenated cyclic hydrocarbons, is studied. A detailed study of the ignition of DMF, 2-MF, and furan over a wide range of conditions provides information on the dependence of their ignition delay times on the equivalence ratio, dilution, pressure and temperature. Important trends are revealed with respect to the ignition behavior of furans. The results show a non-monotonic trend with respect to chemical structure, whereby DMF is the least reactive while 2-MF is the most readily ignitable. Two chemical models also predict 2-MF to be more reactive than DMF, although quantitative agreement varies over the range of conditions investigated. With regards to equivalence ratio effect on the ignition behavior of each furan, ignition delay times generally decrease with increasing equivalence ratios, except for DMF which exhibits reduced reactivity at lower temperatures for rich mixtures. The trends in the ignition behavior of these three furans are partially explained by differences

in their molecular structure. Chemical kinetic analyses, including sensitivity analysis and reaction pathway analysis, are performed to explain the differences in predictive performance between existing chemical kinetic models of furans. The main contribution of this part of this work is to reveal trends that could not be revealed by experimental, modeling, and theoretical chemical investigations of individual fuels.

Isomer effects on furan ignition is revealed by comparing DMF ignition behavior to that of its isomer 2-EF, which is found to ignite up to 6 times faster than DMF, indicating much higher chemical reactivity. For combustion systems with the need to avoid ignition, DMF is better suited, while 2-EF could be a better fuel for diesel engines.

The ignition behavior of the least reactive furan in this work, DMF, is compared to that of *iso*-octane, a representative gasoline surrogate, to reveal the comparative reactivity trends of the two fuel classes and to evaluate the suitability of DMF for use in spark ignition engines, especially in terms of auto ignition resistance. It is observed that *iso*-octane ignites faster than DMF, in line with their reactivity trends revealed through the Research Octane Numbers (RON). Ignition delay time measurements reveal important reactivity trends, showing that *iso*-octane is more reactive than DMF under all conditions. This confirms that DMF is well-suited for use in spark-ignition engines where auto ignition is best avoided.

The effect of blending DMF and *iso*-octane is studied through ignition delay time measurements of equal liquid proportion blends of the pure fuels. Blend reactivity falls between the two pure fuels, closer to *iso*-octane, indicating reduced impact of the DMF fraction in the blend. A chemical kinetic model for the fuel blend is assembled from literature models of the pure fuels. Reaction rate modifications and reaction pathway additions are performed to improve predictive performance of DMF ignition. The blend model shows improved performance with respect to DMF ignition prediction and reasonable prediction of the ignition of the fuel blend. Further chemical kinetic analyses are performed using the combined DMF/*iso*-octane model, such as reaction pathway analysis, to explore the interaction of the pure fuels chemistries

during blend combustion.

Regarding saturated furans, THF is shown to be generally more reactive than MTHF at all conditions. Ignition delay times of MTHF, are compared to those of the similar unsaturated furan, 2-MF, at different conditions of pressure, temperature, and equivalence ratio. It is observed that under stoichiometric conditions, MTHF has longer ignition delay times than 2-MF, with differences of about a factor of 2 at 3 atm. The differences are less pronounced for lean mixtures and a complex behavior is observed for rich mixtures where MTHF can be more reactive at lower temperatures. For MTHF it is observed that ignition delay times generally decrease with increasing equivalence ratios. The reactivity difference is tentatively attributed to differences in the rates of radical attack on side methyl groups, such that they are faster for 2-MF. Current models of MTHF under predict the ignition delay times and consequently lead to much faster fuel consumption rates than observed in experiments.

Further exploration of the effect of molecular structure on ignition propensity of ring compounds involves the ignition behavior of the dimethyl and ethyl isomers of cyclohexane, DMCH and ECH. It is observed that the ignition delay times of DMCH are generally longer than those of ECH under similar experimental conditions. A difference of up to a factor of 2 is observed between DMCH and ECH, compared to a more pronounced difference between the ignition delay times of the similar furans, DMF and 2-EF, where a difference of up to a factor of 5 is observed. These observations are in line with the established reactivity trend of m-xylene and ethyl benzene, where ignition delay times can differ from those of ethyl benzene by up to a factor of 3, or 5 under some conditions. The equivalence ratio effect on the ignition behavior of DMCH is studied. A reversed trend is observed, where DMCH ignites more readily at lean conditions, while the longest ignition delay times are observed at rich conditions. The reversed equivalence ratio effect is partially explained by experimental temperature range differences.

A new chemical kinetic model of DMCH is tested against ignition delay times of DMCH

and ECH obtained in this work. The model predictions are in reasonable agreement with the experimental data of DMCH over a wide range of conditions with the most pronounced deviation observed to be up to a factor of 2.2. Good agreement is also observed overall between the experimental data and the predictions of both models.

With regards to chemical kinetic model reduction methods, a computationally cheaper stochastic species sampling approach, referred to as the Stochastic Species Elimination (SSE) method, a variant of ASE [96], is presented. The SSE method is observed to produce reduced models of similar size to those produced by the ASE method with a significant reduction of computational time up to 34%. The SSE approach is used for the reduction of selected models.

This work contributes toward improving energy efficiencies and developing advanced engine technologies by the following:

- Shedding light on the ignition behavior of important classes of hydrocarbons, such as furans, furan/gasoline blends, and cyclohexanes.

- Presenting relative ignition studies, experimental data, and proposing models that can be useful in the further optimization and reduction of chemical kinetic models, which is vital in the design and improvement of advanced combustion systems.

- Contributing to ongoing model reduction efforts with the proposed reduction approach.

This thesis highlights the need for further experimental measurements against which model predictions can be compared. Extending ignition delay measurements to include concentration measurements of fuels and other important species such as CO_2 will further constrain proposed models. Species concentration measurements during shock tube ignition and pyrolysis have been identified as further validation targets for chemical kinetic models. However, research efforts focused on the characterization of furan combustion have not yet exploited this additional shock tube capability. Concentration profiles during ignition and pyrolysis of

furans can be obtained using mid-infrared laser absorption technique. Other laser diagnostic techniques, such as laser extinction, can be used to obtain time histories of soot formation during the shock tube ignition of furans to evaluate the environmental impacts of this class of biofuels. Finally, the work in this thesis highlights the need to develop analytic expressions which summarize the performance of given detailed chemical kinetic models. Ignition delay correlations can be developed from chemical kinetic models, through ignition delay time simulations using literature models over a range of conditions. The simulation results can be used to develop ignition delay time correlations which enable the prediction of simulated ignition delay times at a wide range of conditions. In summary, this thesis prompts further experimental and modeling research efforts that are aimed at further improvement of chemical kinetic model performance.

Appendices

Appendix A

Representative ignition data

Ignition delay data set for 2,5-dimethyl furan (DMF), 2-methyl furan (2-MF), furan, 2-ethyl furan (2-EF), *iso*-octane, DMF/*iso*-octane 50-50 blends, methyltetrahydrofuran (MTHF), tetrahydrofuran (THF), dimethylcyclohexane (DMCH), and ethylcyclohexane (ECH). Mixtures are identified by the equivalence ratio, ϕ, and the argon/oxygen ratio, D.

Table A.1: Ignition delay times of DMF

ϕ	D	Diluent	p [atm]	T [K]	τ [μs]
			5.4	1157	1223
			5.3	1179	1074
0.5	3.76	Ar	5.2	1200	792
			4.8	1203	696
			4.8	1204	767
			5.3	1292	251
			5.1	1333	179
			4.7	1363	119
			12.1	1009	2503
			12.5	1033	2024
			11.5	1042	1885

Table A.1 – *DMF, continued from previous page*

ϕ	D	Diluent	p [atm]	T [K]	τ [μs]
			11.9	1054	1659
			11.5	1089	1267
			11.2	1096	1224
			11.4	1129	929
			10.7	1149	780
			10.8	1191	518
			10.7	1227	354
			10.2	1255	312
			10.6	1272	221
			3.4	1252	1498
			3.8	1266	1245
1	12.2	Ar	3.7	1308	829
			3.9	1315	874
			4.0	1329	694
			4.0	1347	586
			4.0	1349	569
			3.9	1367	428
			3.9	1377	500
			3.6	1401	365
			4.1	1440	219
			3.4	1466	197
			3.5	1497	129
			3.6	1515	98
			3	1265	1713
			2.9	1338	680
1	16.6	Ar			

Table A.1 – *DMF, continued from previous page*

ϕ	D	Diluent	p [atm]	T [K]	τ [μs]
			3.2	1345	969
			3.5	1366	769
			5.2	1371	667
			5.4	1399	547
			3.1	1405	536
			5.2	1408	481
			3.3	1442	315
			3.2	1443	189
			3.2	1463	236
			5.7	1467	128
			3.2	1475	259
			3.3	1503	140
			3.1	1581	161
			3.2	1530	123
			1.7	1538	349
			1.9	1549	299
			3.3	1552	78
			1.3	1570	130
			1.7	1641	28
			1.9	1191	1668
			1.9	1206	1451
1	3.76	Ar	1.8	1237	1065
			2.0	1253	865
			1.8	1303	528
			1.9	1305	482

Table A.1 – *DMF, continued from previous page*

ϕ	D	Diluent	p [atm]	T [K]	τ [μs]
			2.0	1314	424
			2.0	1322	403
			2.0	1368	252
			1.9	1384	150
			1.7	1398	152
			4.6	1133	1928
			4.8	1144	1376
			4.5	1151	1455
			5.0	1159	1250
			4.4	1162	1254
			4.5	1182	1039
			4.4	1203	892
			4.9	1227	733
			4.3	1229	772
			5.0	1231	568
			4.2	1253	540
			5.2	1280	374
			4.8	1313	255
			4.9	1322	221
			4.2	1327	218
			4.4	1331	205
			5.1	1332	219
			4.2	1361	189
			4.3	1392	128
			11.6	1007	1138

Table A.1 – *DMF, continued from previous page*

ϕ	D	Diluent	p [atm]	T [K]	τ [μs]
			12.1	1031	1213
			11.2	1039	1388
			12.0	1041	1137
			9.8	1044	1265
			12.0	1059	1144
			9.9	1061	913
			11.5	1062	1277
			11.3	1065	1161
			11.3	1076	1176
			11.3	1095	876
			7.7	1100	996
			10.4	1103	892
			11.8	1103	965
			11.4	1106	798
			10.6	1107	969
			10.8	1126	916
			11.3	1130	732
			11.3	1135	670
			9.8	1143	636
			13.1	1157	404
			11.1	1161	526
			11.0	1163	552
			9.2	1175	478
			10.7	1179	523
			9.9	1198	466

Table A.1 – *DMF, continued from previous page*

ϕ	D	Diluent	p [atm]	T [K]	τ [μs]
			10.7	1200	403
			10.9	1201	383
			10.6	1208	368
			10.3	1226	331
			9.9	1227	372
			10.7	1230	296
			9.4	1232	306
			9.2	1256	233
			10.6	1256	224
			8.7	1264	240
			10.2	1270	206
			10.3	1302	136
			4.9	1133	1013
			4.6	1156	889
2	3.76	Ar	5.2	1199	650
			4.5	1206	512
			4.7	1244	418
			5.2	1265	283
			4.8	1265	607
			4.4	1266	312
			5.1	1273	294
			4.3	1292	291
			4.3	1304	240
			12.0	1024	1871
			11.9	1026	2043

Table A.1 – *DMF, continued from previous page*

ϕ	D	Diluent	p [atm]	T [K]	τ [μs]
			10.9	1032	1926
			11.7	1032	1927
			11.6	1062	1417
			10.8	1064	1588
			10.7	1080	1370
			11.5	1118	801
			11.1	1126	734
			10.9	1166	445
			10.7	1205	358
			10.9	1265	162
			9.2	1342	81

Table A.2: *Ignition delay times of 2-MF*

ϕ	D	Diluent	p [atm]	T [K]	τ [μs]
			10.7	977	2063
			12.2	997	2071
0.5	3.76	Ar	11.7	1014	1431
			11.9	1054	1228
			11.6	1056	1307
			12.3	1081	969
			10.9	1093	949
			10.9	1114	775
			12.6	1130	480

Table A.2 – *2-MF, continued from previous page*

ϕ	D	Diluent	p [atm]	T [K]	τ [μs]
			11.1	1153	444
			10.5	1195	254
			10.9	1226	180
			10.6	1291	89
1	15.5	Ar	1.8	1357	546
			2.0	1420	222
			1.8	1440	226
			2.0	1467	244
			1.9	1475	156
			1.8	1489	163
			1.7	1503	118
			8.9	1144	1551
			9.1	1144	1346
			9.7	1224	667
			9.4	1262	449
			1.8	1281	815
			9.7	1306	262
			11.0	1316	252
			10.6	1327	172
			8.5	1330	287
1	3.76	Ar	1.9	1183	1090
			2.0	1205	804
			1.8	1230	605
			2.1	1261	331
			1.9	1278	368

Table A.2 – *2-MF, continued from previous page*

ϕ	D	Diluent	p [atm]	T [K]	τ [μs]
			1.7	1286	373
			1.7	1308	357
			1.9	1309	283
			1.8	1311	297
			2.0	1336	219
			2.0	1352	184
			3.7	1075	2208
			3.7	1080	1995
			3.6	1097	1768
			3.6	1130	1338
			3.7	1148	1008
			3.5	1177	707
			3.5	1221	448
			3.3	1265	345
			3.4	1286	224
			4.9	1077	1741
			4.5	1099	980
			4.8	1110	684
			5.3	1143	783
			5.3	1144	570
			5.1	1149	770
			4.9	1171	582
			5.5	1175	410
			4.9	1200	407
			5.4	1215	301

Table A.2 – *2-MF, continued from previous page*

ϕ	D	Diluent	p [atm]	T [K]	τ [μs]
			4.6	1222	318
			4.6	1227	293
			4.5	1257	249
			4.3	1282	156
			4.3	1291	142
			10.3	1038	1246
			8.7	1055	957
			9.3	1068	987
			10.0	1077	843
			9.9	1099	497
			9.7	1116	611
			9.9	1133	490
			9.7	1169	287
			10.8	1180	234
			10.6	1191	207
			9.3	1197	208
			12.3	979	2115
			12.7	1026	1027
2	3.76	Ar	10.9	1052	668
			11.7	1059	760
			10.6	1060	885
			10.9	1093	568
			11.7	1147	243
			10.1	1149	264
			11.5	1154	214

Table A.2 – *2-MF, continued from previous page*

ϕ	D	Diluent	p [atm]	T [K]	τ [μs]
			10.8	1180	178

Table A.3: Ignition delay times of furan

ϕ	D	Diluent	p [atm]	T [K]	τ [μs]
			12.5	1006	2173
			12.1	1012	2050
0.5	3.76	Ar	11.9	1026	1978
			11.9	1034	1841
			11.9	1068	1374
			12.6	1084	1274
			11.8	1094	1139
			12.1	1132	879
			11.7	1150	762
			11.4	1169	615
			11.1	1214	375
			11.6	1218	352
			11.2	1234	285
			11.0	1317	103
			1.8	1152	742
			1.9	1185	1338
1	3.76	Ar	1.7	1218	962
			1.9	1224	827
			1.9	1272	544

Table A.3 – *furan, continued from previous page*

ϕ	D	Diluent	p [atm]	T [K]	τ [μs]
			1.8	1273	506
			1.8	1316	307
			1.7	1318	402
			1.9	1411	138
			1.9	1412	240
			5.3	1077	1903
			5.2	1083	1506
			5.4	1116	1323
			5.3	1137	1063
			5.3	1174	681
			5.5	1195	550
			4.5	1201	551
			5.0	1268	297
			4.8	1283	233
			5.3	1311	239
			10.7	1033	1354
			10.1	1049	757
			9.7	1051	1420
			10.6	1053	1136
			11.0	1099	688
			10.3	1128	781
			9.9	1138	602
			10.1	1163	493
			9.1	1185	404
			10.2	1196	337

Table A.3 – *furan, continued from previous page*

ϕ	D	Diluent	p [atm]	T [K]	τ [μs]
			9.7	1235	195
			12.3	980	949
			12.8	1008	1233
2	3.76	Ar	12.2	1026	764
			12.9	1088	708
			12.0	1098	652
			10.0	1131	537
			12.1	1147	332
			11.8	1154	341
			10.8	1158	308
			11.0	1167	308
			11.5	1216	137

Table A.4: *Ignition delay times of 2-EF*

ϕ	D	Diluent	p [atm]	T [K]	τ [μs]
			4.7	1065	1435
			4.7	1116	709
1.0	3.76	Ar	4.7	1149	451
			4.5	1172	316
			4.5	1215	190
			4.5	1255	106
			4.6	1274	80
			11.7	1044	877

Table A.4 – *2-EF, continued from previous page*

ϕ	D	Diluent	p [atm]	T [K]	τ [μs]
			11.6	1048	815
			11.4	1061	594
			11.4	1099	370
			11.1	1120	212
			10.6	1122	278
			10.4	1167	145
			11.1	1209	50

Table A.5: Ignition delay times of iso-octane

ϕ	D	Diluent	p [atm]	T [K]	τ [μs]
			5.1	1090	2321
			5.5	1110	1641
0.5	3.76	Ar	5.1	1126	1247
			5.4	1131	1299
			5.1	1151	1088
			4.8	1151	931
			5.4	1161	960
			5.2	1182	690
			5.1	1189	752
			4.9	1204	597
			5.2	1223	484
			5.1	1224	523
			5.0	1242	408

Table A.5 – *iso-octane, continued from previous page*

ϕ	D	Diluent	p [atm]	T [K]	τ [μs]
			5.9	1250	230
			5.1	1274	244
			4.8	1296	184
			4.8	1303	217
			4.8	1304	223
			5.0	1340	140
			4.8	1349	141
			4.8	1350	138
			10.4	1061	1558
			10.3	1073	1581
			12.5	1098	1235
			11.7	1123	814
			10.9	1123	938
			11.7	1128	831
			10.8	1137	738
			10.3	1139	721
			11.9	1169	403
			10.2	1187	393
			9.7	1195	357
			10.7	1211	278
			11.4	1211	269
			9.7	1240	232
			10.9	1251	164
			11.2	1268	148
			8.7	1117	996
1.0	3.76	N_2			

Table A.5 – *iso-octane, continued from previous page*

ϕ	D	Diluent	p [atm]	T [K]	τ [μs]
			8.3	1127	690
			8.8	1137	757
			8.9	1142	717
			8.3	1162	553
			8.3	1173	480
			8.5	1198	365
			8.2	1199	319
			7.8	1220	329
			7.5	1245	260
			8.0	1284	154
			7.9	1308	136
			7.5	1309	132
			5.3	1096	1745
			4.9	1101	1627
1.0	3.76	Ar	4.9	1105	1650
			5.2	1108	1394
			5.0	1110	1442
			5.0	1112	1325
			5.1	1131	1140
			5.3	1135	1098
			5.3	1166	790
			5.1	1196	642
			5.1	1209	447
			4.4	1244	429
			4.8	1258	309

Table A.5 – *iso-octane, continued from previous page*

ϕ	D	Diluent	p [atm]	T [K]	τ [μs]
			4.5	1259	344
			4.7	1285	270
			4.8	1292	270
			4.9	1329	206
			4.8	1351	149
			8.7	1076	1360
			8.0	1077	1451
			7.6	1093	1066
			8.2	1106	1051
			8.1	1127	796
			7.8	1130	852
			7.8	1152	662
			7.9	1192	364
			7.9	1220	310
			7.6	1262	213
			7.2	1303	138
			7.3	1358	103
			12.1	1067	1286
			11.9	1099	827
			10.8	1129	632
			11.5	1130	589
			12.0	1135	515
			10.7	1159	430
			11.2	1185	307
			11.5	1232	177

Table A.5 – *iso-octane, continued from previous page*

ϕ	D	Diluent	p [atm]	T [K]	τ [μs]
			11.1	1236	148
			10.7	1273	97
2.0	3.76	Ar	5.3	1101	1466
			4.9	1150	953
			5.4	1152	824
			5.1	1171	571
			4.8	1198	624
			5.0	1220	435
			4.8	1259	294
			4.7	1259	390
			4.6	1329	202
			4.7	1331	219
			4.6	1371	173
			11.6	1060	1254
			12.4	1078	959
			11.7	1083	895
			11.9	1110	612
			11.4	1112	577
			11.3	1151	392
			11.0	1186	267
			11.0	1213	179
			10.5	1215	181
			10.6	1240	149
			10.7	1251	137
			10.9	1264	123

Table A.5 – *iso-octane, continued from previous page*

ϕ	D	Diluent	p [atm]	T [K]	τ [μs]

Table A.6: *Ignition delay times of DMF/iso-octane 50-50 blends (by volume)*

ϕ	D	Diluent	p [atm]	T [K]	τ [μs]
			11.6	1081	1118
			11.0	1089	1184
1.0	3.76	Ar	10.5	1122	682
			10.7	1129	688
			11.2	1185	331
			10.7	1201	317
			11.3	1202	263
			10.9	1203	294
			10.6	1220	251
			10.7	1254	164
			10.7	1290	91
			11.9	1034	1674
			11.7	1047	1375
2.0	3.76	Ar	11.6	1052	1420
			11.3	1053	1220
			11.2	1085	952
			10.9	1116	650
			10.6	1149	410
			10.1	1169	355
			10.3	1211	238

Table A.6 – *50-50 blends, continued from previous page*

ϕ	D	Diluent	p [atm]	T [K]	τ [μs]
			10.0	1228	205
			10.0	1277	124

Table A.7: Ignition delay times of MTHF

ϕ	D	Diluent	p [atm]	T [K]	τ [μs]
			12.7	1023	1531
			12.3	1037	1312
0.5	3.76	Ar	12.4	1052	1181
			11.9	1084	932
			12.0	1134	586
			11.7	1139	564
			11.4	1168	467
			11.2	1227	232
			11.6	1254	185
			12.4	986	1485
			12.4	1002	1171
1.0	3.76	Ar	12.2	1028	894
			12.2	1034	1000
			12.3	1064	824
			3.7	1068	2410
			11.4	1089	715
			3.5	1105	2221
			3.4	1116	2405

Table A.7 – *MTHF, continued from previous page*

ϕ	D	Diluent	p [atm]	T [K]	τ [μs]
			11.7	1121	531
			3.6	1134	1853
			3.2	1136	1734
			3.5	1138	1754
			11.8	1154	388
			3.4	1156	1551
			11.2	1173	364
			11.4	1193	272
			3.4	1196	1147
			3.3	1224	936
			11.7	1236	158
			3.2	1257	667
			3.2	1296	384
			11.8	957	1565
			11.8	986	1269
2.0	3.76	Ar	12.6	1031	811
			12.1	1071	655
			11.5	1107	525
			10.7	1139	429
			10.7	1146	374
			11.4	1215	215
			11.0	1236	189

Table A.8: Ignition delay times of THF

ϕ	D	Diluent	p [atm]	T [K]	τ [μs]
0.5	3.76	Ar	12.5	988	1775
			13.1	1030	1057
			13.1	1075	774
			11.7	1094	766
			11.2	1114	721
			12.1	1141	539
			11.8	1181	371
			11.7	1228	250
			11.7	1241	230
1.0	3.76	Ar	12.1	1003	1019
			12.6	1005	986
			12.3	1041	794
			11.8	1070	695
			12.0	1111	532
			12.2	1119	536
			11.9	1129	444
			11.2	1158	407
			11.5	1216	261
2.0	3.76	Ar	13.7	998	775
			13.0	1010	750
			12.8	1063	539
			12.0	1141	323
			11.0	1186	255
			10.8	1188	290

Table A.8 – *THF, continued from previous page*

ϕ	D	Diluent	p [atm]	T [K]	τ [μs]
			10.0	1193	288
			11.6	1254	135

Table A.9: Ignition delay times of DMCH

ϕ	D	Diluent	p [atm]	T [K]	τ [μs]
			4.6	1138	1368
			4.5	1163	1171
1.0	3.76	Ar	4.4	1172	934
			4.6	1203	893
			4.5	1210	839
			4.6	1228	620
			4.4	1241	546
			4.7	1244	544
			4.4	1274	379
			4.5	1316	247
			4.5	1369	147
			11.5	1049	1137
			11.7	1097	805
			11.1	1105	768
			10.8	1132	592
			11.5	1207	276
			4.7	1149	2570
0.5	10.0	Ar	4.9	1164	2320

Table A.9 – *DMCH, continued from previous page*

ϕ	D	Diluent	p [atm]	T [K]	τ [μs]
			4.8	1178	2089
			4.7	1193	1831
			4.6	1222	1342
			4.9	1223	1572
			4.4	1305	584
			5	1316	454
			4.2	1344	401
			4.4	1350	323
			4.7	1463	70
			4.4	1503	44
			4.3	1109	3989
			4.4	1150	2920
1.0	10.0	Ar	4.6	1166	2544
			4.8	1180	2439
			4.7	1189	1968
			4.8	1191	1970
			4.7	1201	1665
			4.7	1256	1012
			4.9	1258	986
			4.8	1243	1147
			4.8	1292	847
			4.9	1302	666
			4.7	1321	462
			4.5	1364	339
			4.9	1351	359

Table A.9 – *DMCH, continued from previous page*

ϕ	D	Diluent	p [atm]	T [K]	τ [μs]
			4.7	1370	333
			4.8	1416	203
			4.7	1436	138
			4.3	1445	125
			4.4	1446	125
			4.3	1473	110
			4.4	1513	71
			4.4	1516	67
			4.3	1524	60
			4.6	1131	2923
			5.2	1207	1713
2.0	10.0	Ar	5.1	1233	1492
			4.4	1250	1483
			4.8	1258	1140
			4.7	1342	578
			4.5	1438	234
			4.1	1460	173
			4.1	1523	131
			4.4	1544	84

Table A.10: *Ignition delay times of ECH*

ϕ	D	Diluent	p [atm]	T [K]	τ [μs]
			4.6	1114	1371
1.0	3.76	Ar			

Table A.10 – *ECH, continued from previous page*

ϕ	D	Diluent	p [atm]	T [K]	τ [μs]
			4.5	1128	1286
			4.4	1134	1190
			4.5	1168	833
			4.8	1187	590
			4.8	1231	288
			4.6	1243	259
			4.6	1249	259
			4.6	1302	177
			4.6	1329	114
			11.1	1057	1019
			11.2	1092	796
			11.2	1092	876
			11.4	1119	565
			11.1	1135	455
			10.6	1162	368
			10.6	1198	311
			9.9	1258	176

References

[1]   *Key world energy statistics.* International Energy Agency, 2014 (cit. on p. 1).

[2]   Rajendra K Pachauri and Andy Reisinger. *Climate Change 2007 Synthesis Report: Summary for Policymakers.* IPCC Secretariat, 2007 (cit. on p. 1).

[3]   Shaohua Zhong, Ritchie Daniel, Hongming Xu, Jun Zhang, Dale Turner, Miroslaw L. Wyszynski, and Paul Richards. "Combustion and Emissions of 2,5-Dimethylfuran in a Direct-Injection Spark-Ignition Engine". In: *Energy Fuels* 24.5 (2010), pp. 2891–2899 (cit. on pp. 2, 8).

[4]   Yuriy Román-Leshkov, Christopher J Barrett, Zhen Y Liu, and James A Dumesic. "Production of dimethylfuran for liquid fuels from biomass-derived carbohydrates". In: *Nature* 447.7147 (2007), pp. 982–985 (cit. on pp. 2, 3).

[5]   Xinli Tong, Yang Ma, and Yongdan Li. "Biomass into chemicals: Conversion of sugars to furan derivatives by catalytic processes". In: *Appl. Catal., A* 385.12 (2010), pp. 1–13 (cit. on p. 2).

[6]   Mandan Chidambaram and Alexis T Bell. "A two-step approach for the catalytic conversion of glucose to 2, 5-dimethylfuran in ionic liquids". In: *Green Chem.* 12.7 (2010), pp. 1253–1262 (cit. on p. 2).

[7]   Mark Mascal and EdwardB. Nikitin. "Direct, High-Yield Conversion of Cellulose into Biofuel". In: *Angew. Chem.* 120.41 (2008), pp. 8042–8044 (cit. on p. 2).

[8]   Chih-Jen Sung and Henry J Curran. "Using rapid compression machines for chemical

kinetics studies". In: *Prog. Energy Combust. Sci.* (2014) (cit. on p. 4).

[9]   Wing Tsang and Assa Lifshitz. "Shock tube techniques in chemical kinetics". In: *Ann. Rev. Phys. Chem.* 41.1 (1990), pp. 559–599 (cit. on pp. 4, 21).

[10] Marco Mehl, William J Pitz, Charles K Westbrook, and Henry J Curran. "Kinetic modeling of gasoline surrogate components and mixtures under engine conditions". In: *Proc. Combust. Inst.* 33.1 (2011), pp. 193–200 (cit. on pp. 5, 10, 11, 17, 46, 53, 80–83, 86, 88, 114–119, 127).

[11] Zhenyu Tian, Tao Yuan, Ren Fournet, Pierre-Alexandre Glaude, Baptiste Sirjean, Frdrique Battin-Leclerc, Kuiwen Zhang, and Fei Qi. "An experimental and kinetic investigation of premixed furan/oxygen/argon flames". In: *Combust. Flame* 158.4 (2011), pp. 756–773 (cit. on pp. 5, 9).

[12] Kieran P. Somers, John M. Simmie, Fiona Gillespie, Christine Conroy, Grainne Black, Wayne K. Metcalfe, Frdrique Battin-Leclerc, Patricia Dirrenberger, Olivier Herbinet, Pierre-Alexandre Glaude, Philippe Dagaut, Casimir Togb, Kenji Yasunaga, Ravi X. Fernandes, Changyoul Lee, Rupali Tripathi, and Henry J. Curran. "A comprehensive experimental and detailed chemical kinetic modelling study of 2,5-dimethylfuran pyrolysis and oxidation". In: *Combust. Flame* 160.11 (2013), pp. 2291–2318 (cit. on pp. 5, 8, 16, 17, 35, 53, 56, 59–65, 67, 68, 80, 81, 83, 85–88, 100–102).

[13] Baptiste Sirjean, Rene Fournet, Pierre-Alexandre Glaude, Frederique Battin-Leclerc, Weijing Wang, and Matthew A. Oehlschlaeger. "Shock Tube and Chemical Kinetic Modeling Study of the Oxidation of 2,5-Dimethylfuran". In: *J. Phys. Chem. A* 117.7 (2013), pp. 1371–1392 (cit. on pp. 5, 8, 16, 53, 56, 60–62, 64, 66–68, 87).

[14] K.P. Somers, J.M. Simmie, F. Gillespie, U. Burke, J. Connolly, W.K. Metcalfe, F. Battin-Leclerc, P. Dirrenberger, O. Herbinet, P.-A. Glaude, and H.J. Curran. "A high temperature and atmospheric pressure experimental and detailed chemical kinetic modelling study of 2-methyl furan oxidation". In: *Proc. Combust. Inst.* 34.1 (2013), pp. 225–232 (cit. on pp. 5, 8, 9).

[15]   N Peters and FA Williams. "The asymptotic structure of stoichiometric methane air flames". In: *Combust. Flame* 68.2 (1987), pp. 185–207 (cit. on p. 6).

[16]   N Peters, G Paczko, R Seiser, and K Seshadri. "Temperature cross-over and non-thermal runaway at two-stage ignition of n-heptane". In: *Combust. Flame* 128.1 (2002), pp. 38–59 (cit. on p. 6).

[17]   P Saxena, N Peters, and FA Williams. "An analytical approximation for high-temperature autoignition times of higher alkanes". In: *Combust. Flame* 149.1 (2007), pp. 79–90 (cit. on p. 6).

[18]   PC Anderson, JM Sharkey, and RP Walsh. "Calculation of the research octane number of motor gasolines from gas chromatographic data and a new approach to motor gasoline quality control". In: *J. Inst. Pet* 58.560 (1972), p. 83 (cit. on p. 7).

[19]   *ASTM Manual for Rating Motor, Diesel and Aviation Fuels, 1973-74.* American Society for Testing and Materials, 1973 (cit. on p. 7).

[20]   Mark E Myers Jr, Janis Stollsteimer, and Andrew M Wims. "Determination of gasoline octane numbers from chemical composition". In: *Anal. Chem.* 47.13 (1975), pp. 2301–2304 (cit. on p. 7).

[21]   AM Douaud and P Eyzat. *Four-octane-number method for predicting the anti-knock behavior of fuels and engines.* Tech. rep. SAE Technical Paper, 1978 (cit. on p. 7).

[22]   M Fikri, J Herzler, R Starke, C Schulz, P Roth, and GT Kalghatgi. "Autoignition of gasoline surrogates mixtures at intermediate temperatures and high pressures". In: *Combust. flame* 152.1 (2008), pp. 276–281 (cit. on pp. 7, 11).

[23]   BM Gauthier, DF Davidson, and RK Hanson. "Shock tube determination of ignition delay times in full-blend and surrogate fuel mixtures". In: *Combust. Flame* 139.4 (2004), pp. 300–311 (cit. on pp. 7, 11).

[24]   M Chaos, Z Zhao, A Kazakov, P Gokulakrishnan, M Angioletti, and FL Dryer. "A PRF+ toluene surrogate fuel model for simulating gasoline kinetics". In: *5th US Combustion Meeting.* 2007, pp. 25–28 (cit. on pp. 7, 11).

[25] M Yahyaoui, N Djebaili-Chaumeix, P Dagaut, C-E Paillard, and S Gail. "Experimental and modelling study of gasoline surrogate mixtures oxidation in jet stirred reactor and shock tube". In: *Proc. Combust. Inst.* 31.1 (2007), pp. 385–391 (cit. on pp. 7, 11).

[26] Katharina Kohse-Höinghaus, Patrick Oßwald, Terrill A Cool, Tina Kasper, Nils Hansen, Fei Qi, Charles K Westbrook, and Phillip R Westmoreland. "Biofuel combustion chemistry: from ethanol to biodiesel". In: *Angew. Chem. Int. Ed.* 49.21 (2010), pp. 3572–3597 (cit. on p. 7).

[27] Charles K Westbrook. "Biofuels Combustion". In: *Ann. Rev. Phys. Chem.* 64 (2013), pp. 201–219 (cit. on p. 7).

[28] Jeffrey M. Bergthorson and Murray J. Thomson. "A review of the combustion and emissions properties of advanced transportation biofuels and their impact on existing and future engines". In: *Renew. Sust. Energ. Rev.* 42.0 (2015), pp. 1393 –1417 (cit. on p. 7).

[29] Jeffrey T Moss, Andrew M Berkowitz, Matthew A Oehlschlaeger, Joffrey Biet, Valérie Warth, Pierre-Alexandre Glaude, and Frédérique Battin-Leclerc. "An experimental and kinetic modeling study of the oxidation of the four isomers of butanol". In: *J. Phys. Chem. A* 112.43 (2008), pp. 10843–10855 (cit. on p. 8).

[30] G Black, HJ Curran, S Pichon, JM Simmie, and V Zhukov. "Bio-butanol: Combustion properties and detailed chemical kinetic model". In: *Combust. Flame* 157.2 (2010), pp. 363–373 (cit. on p. 8).

[31] K.A. Heufer, R.X. Fernandes, H. Olivier, J. Beeckmann, O. Röhl, and N. Peters. "Shock tube investigations of ignition delays of n-butanol at elevated pressures between 770 and 1250 K". In: *Proc. Combust. Inst.* 33.1 (2011), pp. 359–366 (cit. on p. 8).

[32] S Vranckx, KA Heufer, C Lee, H Olivier, L Schill, WA Kopp, K Leonhard, CA Taatjes, and RX Fernandes. "Role of peroxy chemistry in the high-pressure ignition of n-butanol–Experiments and detailed kinetic modelling". In: *Combust. Flame* 158.8 (2011), pp. 1444–1455 (cit. on p. 8).

[33]   Ivo Stranic, Deanna P Chase, Joseph T Harmon, Sheng Yang, David F Davidson, and Ronald K Hanson. "Shock tube measurements of ignition delay times for the butanol isomers". In: *Combust. Flame* 159.2 (2012), pp. 516–527 (cit. on p. 8).

[34]   Roberto Grana, Alessio Frassoldati, Tiziano Faravelli, Ulrich Niemann, Eliseo Ranzi, Reinhard Seiser, Robert Cattolica, and Kalyanasundaram Seshadri. "An experimental and kinetic modeling study of combustion of isomers of butanol". In: *Combust. Flame* 157.11 (2010), pp. 2137–2154 (cit. on p. 8).

[35]   Ritchie Daniel, Lixia Wei, Hongming Xu, Chongming Wang, Miroslaw L. Wyszynski, and Shijin Shuai. "Speciation of Hydrocarbon and Carbonyl Emissions of 2,5-Dimethylfuran Combustion in a DISI Engine". In: *Energy Fuels* 26.11 (2012), pp. 6661–6668 (cit. on p. 8).

[36]   David A. Rothamer and Jamie H. Jennings. "Study of the knocking propensity of 2,5-dimethylfurangasoline and ethanolgasoline blends". In: *Fuel* 98.0 (2012), pp. 203–212 (cit. on p. 8).

[37]   S. Gouli, E. Lois, and S. Stournas. "Effects of Some Oxygenated Substitutes on Gasoline Properties, Spark Ignition Engine Performance, and Emissions". In: *Energy Fuels* 12.5 (1998), pp. 918–924 (cit. on p. 8).

[38]   Earl Christensen, Janet Yanowitz, Matthew Ratcliff, and Robert L. McCormick. "Renewable oxygenate blending effects on gasoline properties". In: *Energy Fuels* 25.10 (2011), pp. 4723–4733 (cit. on p. 8).

[39]   Xiao Ma, Hongming Xu, Changzhao Jiang, and Shijin Shuai. "Ultra-high speed imaging and OH-LIF study of {DMF} and {MF} combustion in a {DISI} optical engine". In: *Appl. Energy* 122 (2014), pp. 247–260 (cit. on p. 8).

[40]   Mingzhang Pan, Gequn Shu, Jiaying Pan, Haiqiao Wei, Dengquan Feng, Yubin Guo, and Youcai Liang. "Performance comparison of 2-methylfuran and gasoline on a spark-ignition engine with cooled exhaust gas recirculation". In: *Fuel* 132 (2014), pp. 36–43 (cit. on p. 8).

[41] Zhanjun Cheng, Lili Xing, Meirong Zeng, Weile Dong, Feng Zhang, Fei Qi, and Yuyang Li. "Experimental and kinetic modeling study of 2,5-dimethylfuran pyrolysis at various pressures". In: *Combust. Flame* 161.10 (2014), pp. 2496–2511 (cit. on p. 8).

[42] Katiuska Alexandrino, Ángela Millera, Rafael Bilbao, and María U. Alzueta. "Novel aspects in the pyrolysis and oxidation of 2,5-dimethylfuran". In: *Proc. Combust. Inst.* (2014) (cit. on p. 8).

[43] Liangjie Wei, Chenglong Tang, Xingjia Man, and Zuohua Huang. "Shock-Tube Experiments and Kinetic Modeling of 2-Methylfuran Ignition at Elevated Pressure". In: *Energy Fuels* 27.12 (2013), pp. 7809–7816 (cit. on pp. 8, 9, 35).

[44] Yasar Uygun, Sakiko Ishihara, and Herbert Olivier. "A high pressure ignition delay time study of 2-methylfuran and tetrahydrofuran in shock tubes". In: *Combust. Flame* 161.10 (2014), pp. 2519–2530 (cit. on pp. 9, 55).

[45] Liangjie Wei, Chenglong Tang, Xingjia Man, Xue Jiang, and Zuohua Huang. "High-Temperature Ignition Delay Times and Kinetic Study of Furan". In: *Energy Fuels* 26.4 (2012), pp. 2075–2081 (cit. on p. 9).

[46] John M Simmie. "Kinetics and thermochemistry of 2,5-dimethyltetrahydrofuran and related oxolanes: next next-generation biofuels". In: *J. Phys. Chem. A* 116.18 (2012), pp. 4528–4538 (cit. on p. 9).

[47] Kai Moshammer, Stijn Vranckx, Harish K Chakravarty, Prajakta Parab, Ravi X Fernandes, and Katharina Kohse-Höinghaus. "An experimental and kinetic modeling study of 2-methyltetrahydrofuran flames". In: *Combust. Flame* 160.12 (2013), pp. 2729–2743 (cit. on pp. 9, 17, 100–102).

[48] Alena Sudholt, Liming Cai, Joshua Heyne, Francis M Haas, Heinz Pitsch, and Frederick L Dryer. "Ignition characteristics of a bio-derived class of saturated and unsaturated furans for engine applications". In: *Proc. Combust. Inst.* 35.3 (2015), pp. 2957–2965 (cit. on pp. 9, 56, 96).

[49] Alena Sudholt, Liming Cai, Joshua Heyne, Francis M Haas, Heinz Pitsch, and Frederick

L Dryer. "Ignition characteristics of a bio-derived class of saturated and unsaturated furans for engine applications". In: *Proc. Combust. Inst.* (2014) (cit. on pp. 9, 74).

[50]   William J Pitz and Charles J Mueller. "Recent progress in the development of diesel surrogate fuels". In: *Prog. Energy and Combust. Sci.* 37.3 (2011), pp. 330–350 (cit. on p. 10).

[51]   K. Fieweger, Ro Blumenthal, and G. Adomeit. "Self-ignition of SI engine model fuels: a shock tube investigation at high pressure". In: *Combust. Flame* 109.4 (1997), pp. 599–619 (cit. on p. 10).

[52]   DF Davidson, BM Gauthier, and RK Hanson. "Shock tube ignition measurements of *iso*-octane/air and toluene/air at high pressures". In: *Proc. Combust. Inst.* 30.1 (2005), pp. 1175–1182 (cit. on p. 10).

[53]   Hsi-Ping S Shen, Jeremy Vanderover, and Matthew A Oehlschlaeger. "A shock tube study of iso-octane ignition at elevated pressures: The influence of diluent gases". In: *Combust. Flame* 155.4 (2008), pp. 739–755 (cit. on p. 10).

[54]   Benjamin Akih-Kumgeh and Jeffrey M Bergthorson. "Shock tube study of methyl formate ignition". In: *Energy Fuels* 24.1 (2009), pp. 396–403 (cit. on p. 10).

[55]   X He, MT Donovan, BT Zigler, TR Palmer, SM Walton, MS Wooldridge, and A Atreya. "An experimental and modeling study of iso-octane ignition delay times under homogeneous charge compression ignition conditions". In: *Combust. Flame* 142.3 (2005), pp. 266–275 (cit. on p. 10).

[56]   SM Walton, X He, BT Zigler, MS Wooldridge, and A Atreya. "An experimental investigation of iso-octane ignition phenomena". In: *Combust. flame* 150.3 (2007), pp. 246–262 (cit. on p. 10).

[57]   Henry J Curran, P Gaffuri, WJ Pitz, and CK Westbrook. "A comprehensive modeling study of iso-octane oxidation". In: *Combust. flame* 129.3 (2002), pp. 253–280 (cit. on p. 10).

[58]   Eliseo Ranzi, Tiziano Faravelli, Paolo Gaffuri, Angelo Sogaro, Andrea D'Anna, and

Anna Ciajolo. "A wide-range modeling study of iso-octane oxidation". In: *Combust. Flame* 108.1 (1997), pp. 24–42 (cit. on p. 10).

[59]   Meredith Colket, Tim Edwards, Skip Williams, Nicholas P Cernansky, David L Miller, Fokion Egolfopoulos, Peter Lindstedt, Kalyanasundaram Seshadri, Frederick L Dryer, Chung K Law, et al. "Development of an experimental database and kinetic models for surrogate jet fuels". In: *45th AIAA Aerospace Sciences Meeting and Exhibit*. 2007, pp. 8–11 (cit. on p. 11).

[60]   William J Pitz, CV Naik, T Ní Mhaoldúin, Charles K Westbrook, Henry J Curran, John P Orme, and JM Simmie. "Modeling and experimental investigation of methyl-cyclohexane ignition in a rapid compression machine". In: *Proc. Combust. Inst.* 31.1 (2007), pp. 267–275 (cit. on p. 11).

[61]   Subith S Vasu, David F Davidson, Zekai Hong, and Ronald K Hanson. "Shock tube study of methylcyclohexane ignition over a wide range of pressure and temperature". In: *Energy Fuels* 23.1 (2008), pp. 175–185 (cit. on p. 11).

[62]   B Sirjean, E Dames, DA Sheen, FN Egolfopoulos, H Wang, DF Davidson, RK Hanson, H Pitsch, CT Bowman, CK Law, et al. *A high-temperature chemical kinetic model of n-alkane, cyclohexane, and methyl-, ethyl-, n-propyl and n-butyl-cyclohexane oxidation at high temperatures, JetSurF version 1.1, September 15, 2009* (cit. on p. 11).

[63]   Zekai Hong, King-Yiu Lam, David F Davidson, and Ronald K Hanson. "A comparative study of the oxidation characteristics of cyclohexane, methylcyclohexane, and *n*-butylcyclohexane at high temperatures". In: *Combust. Flame* 158.8 (2011), pp. 1456–1468 (cit. on p. 11).

[64]   Jeremy Vanderover and Matthew A Oehlschlaeger. "Ignition time measurements for methylcylcohexane-and ethylcyclohexane-air mixtures at elevated pressures". In: *Int. J. Chem. Kinet.* 41.2 (2009), pp. 82–91 (cit. on p. 11).

[65]   Houliang Li, David L Miller, and Nicholas P Cernansky. *Development of a reduced chemical kinetic model for prediction of preignition reactivity and autoignition of*

primary reference fuels. Tech. rep. SAE Technical Paper, 1996 (cit. on p. 11).

[66] Shigeyuki Tanaka, Ferran Ayala, and James C Keck. "A reduced chemical kinetic model for HCCI combustion of primary reference fuels in a rapid compression machine". In: *Combust. flame* 133.4 (2003), pp. 467–481 (cit. on p. 11).

[67] Youngchul Ra and Rolf D Reitz. "A reduced chemical kinetic model for IC engine combustion simulations with primary reference fuels". In: *Combust. Flame* 155.4 (2008), pp. 713–738 (cit. on p. 11).

[68] Stephen D. Klotz, Kenneth Brezinsky, and Irvin Glassman. "Modeling the combustion of toluene-butane blends". In: *Symp. Int. Combust.* 27.1 (1998). Twenty-Seventh Sysposium (International) on Combustion Volume One, pp. 337 –344 (cit. on p. 11).

[69] JT Farrell, NP Cernansky, FL Dryer, CK Law, DG Friend, CA Hergart, RM McDavid, AK Patel, Charles J Mueller, and H Pitsch. *Development of an experimental database and kinetic models for surrogate diesel fuels.* Tech. rep. 2007-01-0201. SAE Technical Paper, 2007 (cit. on pp. 11, 104).

[70] Johan CG Andrae, P Björnbom, RF Cracknell, and GT Kalghatgi. "Autoignition of toluene reference fuels at high pressures modeled with detailed chemical kinetics". In: *Combust. Flame* 149.1 (2007), pp. 2–24 (cit. on p. 11).

[71] Frédérique Battin-Leclerc. "Detailed chemical kinetic models for the low-temperature combustion of hydrocarbons with application to gasoline and diesel fuel surrogates". In: *Prog. Energy Combust. Sci.* 34.4 (2008), pp. 440–498 (cit. on p. 11).

[72] Henry J Curran, Elizabeth M Fisher, P-A Glaude, Nick M Marinov, WJ Pitz, CK Westbrook, DW Layton, Patrick F Flynn, Russell P Durrett, AO Zur Loye, et al. *Detailed chemical kinetic modeling of diesel combustion with oxygenated fuels.* Tech. rep. SAE Technical Paper, 2001 (cit. on p. 12).

[73] Youngchul Ra and Rolf D Reitz. "A combustion model for IC engine combustion simulations with multi-component fuels". In: *Combust. flame* 158.1 (2011), pp. 69–90 (cit. on p. 12).

[74] Tianfeng Lu and Chung K Law. "A directed relation graph method for mechanism reduction". In: *Proc. Combust. Inst.* 30.1 (2005), pp. 1333–1341 (cit. on pp. 12, 13).

[75] Perrine Pepiot-Desjardins and Heinz Pitsch. "An efficient error-propagation-based reduction method for large chemical kinetic mechanisms". In: *Combust. Flame* 154.1 (2008), pp. 67–81 (cit. on p. 12).

[76] XL Zheng, TF Lu, and CK Law. "Experimental counterflow ignition temperatures and reaction mechanisms of 1, 3-butadiene". In: *Proc. Combust. Inst.* 31.1 (2007), pp. 367–375 (cit. on p. 12).

[77] Tianfeng Lu and Chung K Law. "Strategies for mechanism reduction for large hydrocarbons: n-heptane". In: *Combust. Flame* 154.1 (2008), pp. 153–163 (cit. on p. 12).

[78] Kyle E Niemeyer, Chih-Jen Sung, and Mandhapati P Raju. "Skeletal mechanism generation for surrogate fuels using directed relation graph with error propagation and sensitivity analysis". In: *Combust. Flame* 157.9 (2010), pp. 1760–1770 (cit. on p. 12).

[79] Tianfeng Lu, Max Plomer, Zhaoyu Luo, SM Sarathy, WJ Pitz, Sibendu Som, and Douglas E Longman. "Directed relation graph with expert knowledge for skeletal mechanism reduction". In: *7th US national combustion meeting, Atlanta, GA*. 2011 (cit. on p. 12).

[80] Kalyanasundaram Seshadri, Tianfeng Lu, Olivier Herbinet, Stefan Humer, Ulrich Niemann, William J Pitz, Reinhard Seiser, and Chung K Law. "Experimental and kinetic modeling study of extinction and ignition of methyl decanoate in laminar non-premixed flows". In: *Proc. Combust. Inst.* 32.1 (2009), pp. 1067–1074 (cit. on p. 12).

[81] Zhaoyu Luo, Tianfeng Lu, Matthias J Maciaszek, Sibendu Som, and Douglas E Longman. "A reduced mechanism for high-temperature oxidation of biodiesel surrogates". In: *Energy Fuels* 24.12 (2010), pp. 6283–6293 (cit. on p. 12).

[82] Jessica L Brakora, Youngchul Ra, and Rolf D Reitz. "Combustion model for biodiesel-fueled engine simulations using realistic chemistry and physical properties". In: *SAE*

Int. J. Engines 4.2011-01-0831 (2011), pp. 931–947 (cit. on p. 12).

[83] W Liu, R Sivaramakrishnan, Michael J Davis, S Som, DE Longman, and TF Lu. "Development of a reduced biodiesel surrogate model for compression ignition engine modeling". In: *Proc. Combust. Inst.* 34.1 (2013), pp. 401–409 (cit. on p. 12).

[84] Harun Mohamed Ismail, Hoon Kiat Ng, Suyin Gan, Tommaso Lucchini, and Angelo Onorati. "Development of a reduced biodiesel combustion kinetics mechanism for CFD modelling of a light-duty diesel engine". In: *Fuel* 106 (2013), pp. 388–400 (cit. on p. 12).

[85] Hoon Kiat Ng, Suyin Gan, Jo-Han Ng, and Kar Mun Pang. "Development and validation of a reduced combined biodiesel–diesel reaction mechanism". In: *Fuel* 104 (2013), pp. 620–634 (cit. on p. 12).

[86] H An, WM Yang, A Maghbouli, J Li, and KJ Chua. "A skeletal mechanism for biodiesel blend surrogates combustion". In: *Energ. Convers. Manage.* 81 (2014), pp. 51–59 (cit. on p. 12).

[87] Xin Wang, Haifeng Liu, Zunqing Zheng, and Mingfa Yao. "A Skeletal Mechanism of a Biodiesel Surrogate Fuel for Compression Ignition Engines". In: *Energy Fuels* 29.2 (2015), pp. 1160–1171 (cit. on p. 12).

[88] Kyle E Niemeyer and Chih-Jen Sung. "Reduced chemistry for a gasoline surrogate valid at engine-relevant conditions". In: *Energy Fuels* 29.2 (2015), pp. 1172–1185 (cit. on p. 12).

[89] J Revel, JC Boettner, M Cathonnet, and JS Bachman. "Derivation of a global chemical kinetic mechanism for methane ignition and combustion". In: *J. Chim. Phys.* 91.4 (1994), pp. 365–382 (cit. on p. 12).

[90] Ioannis P Androulakis, Jeffrey M Grenda, and Joseph W Bozzelli. "Time-integrated pointers for enabling the analysis of detailed reaction mechanisms". In: *AIChE J.* 50.11 (2004), pp. 2956–2970 (cit. on p. 12).

[91] Kaiyuan He, Ioannis P Androulakis, and Marianthi G Ierapetritou. "On-the-fly re-

duction of kinetic mechanisms using element flux analysis". In: *Chem. Eng. Sci.* 65.3 (2010), pp. 1173–1184 (cit. on p. 12).

[92]   Wenting Sun, Zheng Chen, Xiaolong Gou, and Yiguang Ju. "A path flux analysis method for the reduction of detailed chemical kinetic mechanisms". In: *Combust. Flame* 157.7 (2010), pp. 1298–1307 (cit. on p. 13).

[93]   Hüseyin Karadeniz, Hakan Serhad Soyhan, and Cem Sorusbay. "Reduction of large kinetic mechanisms with a new approach to the necessity analysis method". In: *Combust. Flame* 159.4 (2012), pp. 1467–1480 (cit. on p. 13).

[94]   G Esposito and HK Chelliah. "Skeletal reaction models based on principal component analysis: Application to ethylene–air ignition, propagation, and extinction phenomena". In: *Combust. Flame* 158.3 (2011), pp. 477–489 (cit. on p. 13).

[95]   Peng Zhao, Samuel M Nackman, and Chung K Law. "On the application of betweenness centrality in chemical network analysis: Computational diagnostics and model reduction". In: *Combust. Flame* 162.8 (2015), pp. 2991–2998 (cit. on p. 13).

[96]   Ben Akih-Kumgeh and Jeffrey M Bergthorson. "A Four Component Skeletal Model for the Analysis of Jet Fuel Surrogate Combustion". In: *ASME Turbo Expo 2013: Turbine Technical Conference and Exposition.* American Society of Mechanical Engineers. 2013, V01AT04A060 (cit. on pp. 13, 47, 50, 51, 82, 127, 132).

[97]   Benjamin Akih-Kumgeh and Jeffrey M Bergthorson. "Skeletal chemical kinetic mechanisms for syngas, methyl butanoate, n-heptane, and n-decane". In: *Energy Fuels* 27.4 (2013), pp. 2316–2326 (cit. on pp. 13, 17, 19).

[98]   Nathan D Peters, Ben Akih-Kumgeh, and Jeffrey M Bergthorson. "Comparative Analysis of Chemical Kinetic Models Using the Alternate Species Elimination Approach". In: *J. Eng. Gas Turb. Power* 137.2 (2015), p. 021505 (cit. on p. 13).

[99]   Alain Fossi, Alain DeChamplain, Benjamin Akih-Kumgeh, and RW Lewis. "Unsteady RANS and scale adaptive simulations of a turbulent spray flame in a swirled-stabilized gas turbine model combustor using tabulated chemistry". In: *Int. J. Numer. Method.*

H. 25.5 (2015) (cit. on p. 13).

[100] D. G. Goodwin. "An open-source, extensible software suite for CVD process simula-
tion". In: *Chemical Vapor Deposition XVI and EUROCVD 14, ECS Proc.* Ed. by M.
Allendorf, F. Maury, and F. Teyssandier. Vol. 2003-08. The Electrochemical Society,
2003, pp. 155–162 (cit. on pp. 13, 32, 46, 50, 114).

[101] H Wang, E Dames, B Sirjean, DA Sheen, R Tangko, A Violi, JYW Lai, FN Egolfopoulos,
DF Davidson, and RK Hanson. "A hightemperature chemical kinetic model of n-alkane
(up to n-dodecane), cyclohexane, and methyl-, ethyl-, n-propyl and n-butyl-cyclohexane
oxidation at high temperatures, JetSurF version 2.0; September 19, 2010". In: *URL
(http://melchior.usc.edu/JetSurF/JetSurF2.0).* (2010) (cit. on pp. 17, 111, 113, 115).

[102] M Mehl, HJ Curran, WJ Pitz, and CK Westbrook. "Chemical kinetic modeling of
component mixtures relevant to gasoline". In: *European Combustion Meeting.* 2009
(cit. on pp. 17, 46, 114, 120–122, 127).

[103] Liming Cai, Yasar Uygun, Casimir Togbé, Heinz Pitsch, Herbert Olivier, Philippe
Dagaut, and S Mani Sarathy. "An experimental and modeling study of n-octanol
combustion". In: *Proc. Combust. Inst.* 35.1 (2015), pp. 419–427 (cit. on pp. 18, 46,
114, 124–126, 128).

[104] Mazen A. Eldeeb and Benjamin Akih-Kumgeh. "Reactivity Trends in Furan and Alkyl
Furan Combustion". In: *Energy Fuels* 28.10 (2014), pp. 6618–6626 (cit. on pp. 19, 43).

[105] Mazen A. Eldeeb and Benjamin Akih-Kumgeh. "Investigation of 2,5-dimethyl furan
and iso-octane ignition". In: *Combust. Flame* 162.6 (2015), pp. 2454–2465 (cit. on
pp. 19, 43).

[106] Mazen A. Eldeeb and Benjamin Akih-Kumgeh. "High-temperature auto-ignition
studies of 2,5-dimethylfuran, 2-ethyl furan, and iso-octane". In: *9th US National
Combustion Meeting, Cincinnati, OH.* 2015 (cit. on p. 19).

[107] Mazen A. Eldeeb, Shirin Jouzdani, Lingshu Zhang, and Benjamin Akih-Kumgeh.
"High-temperature autoignition study of 2-methyl furan and 2-methyl tetrahydrofuran".

In: *The 9th International Conference on Chemical Kinetics (ICCK), Ghent, Belgium.* 2015, pp. 76–79 (cit. on p. 19).

[108] Mazen A. Eldeeb and Benjamin Akih-Kumgeh. "Investigation of ignition behavior of dimethyl and ethyl isomers of cycloalkanes and furans". In: *25th International Colloquium on the Dynamics of Explosions and Reactive Systems (ICDERS), Leeds, UK.* 2015 (cit. on p. 19).

[109] A. G. Gaydon and I. R. Hurle. *The Shock Tube in High-temperature Chemical Physics.* Chapman and Hall, 1963 (cit. on pp. 21, 25, 26, 38).

[110] R Liinn Belford and Roger A Strehlow. "Shock tube technique in chemical kinetics". In: *Ann. Rev. Phys. Chem.* 20.1 (1969), pp. 247–272 (cit. on pp. 21, 24).

[111] J V Michael and K P Lim. "Shock Tube Techniques in Chemical Kinetics". In: *Ann. Rev. Phys. Chem.* 44.1 (1993), pp. 429–458 (cit. on p. 21).

[112] K A Bhaskaran and P. Roth. "The shock tube as wave reactor for kinetic studies and material systems". In: *Prog. Energy Combust. Sci.* 28.2 (2002), pp. 151–192 (cit. on p. 21).

[113] Douglas William Holder and Donald Lorimer Schultz. *On the flow in a reflected-shock tunnel.* HM Stationary Office, London, UK, 1962 (cit. on p. 24).

[114] S. Browne, J. Ziegler, and E. Shepherd. *Numerical solution methods for shock and detonation jump conditions.* Tech. rep. FM2006.006. Pasadena, CA USA 91125: Graduate Aeronautics Laboratory, California Institute of Technology, 2008 (cit. on p. 32).

[115] DC Horning, DF Davidson, and RK Hanson. "Study of the high-temperature autoignition of n-alkane/o/ar mixtures". In: *J. Propul. Power* 18.2 (2002), pp. 363–371 (cit. on p. 33).

[116] Eric L Petersen, David F Davidson, and Ronald K Hanson. "Ignition delay times of Ram accelerator CH/O/diluent mixtures". In: *J. Propul. Power* 15.1 (1999), pp. 82–91 (cit. on p. 33).

[117] Eric L. Petersen. "Interpreting endwall and sidewall measurements in shock-tube

ignition studies". In: *Combust. Sci. Technol.* 181.9 (2009), pp. 1123–1144 (cit. on p. 33).

[118]   David Charles Horning. "A study of the high-temperature autoignition and thermal decomposition of hydrocarbons". PhD thesis. Stanford University Stanford, 2001 (cit. on p. 37).

[119]   J.R. Taylor. *An introduction to error analysis: the study of uncertainties in physical measurements.* Series of books in physics. Sausalito, CA: University Science Books, 1982 (cit. on p. 37).

[120]   J.P. Holman. *Experimental Methods for Engineers.* McGraw-Hill series in mechanical engineering. New York, NY: McGraw-Hill, 1994 (cit. on pp. 37, 39).

[121]   Eric L Petersen, Matthew JA Rickard, Mark W Crofton, Erin D Abbey, Matthew J Traum, and Danielle M Kalitan. "A facility for gas-and condensed-phase measurements behind shock waves". In: *Meas. Sci. Technol.* 16.9 (2005), p. 1716 (cit. on pp. 37–39).

[122]   Zihang Zhang, Erjiang Hu, Lun Pan, Yizhen Chen, Jing Gong, and Zuohua Huang. "Shock-Tube Measurements and Kinetic Modeling Study of Methyl Propanoate Ignition". In: *Energy Fuels* 28.11 (2014), pp. 7194–7202 (cit. on p. 40).

[123]   Eric L Petersen and Ronald K Hanson. "Nonideal effects behind reflected shock waves in a high-pressure shock tube". In: *Shock Waves* 10.6 (2001), pp. 405–420 (cit. on p. 40).

[124]   DF Davidson and RK Hanson. "Interpreting shock tube ignition data". In: *Int. J. Chem. Kinet.* 36.9 (2004), pp. 510–523 (cit. on p. 40).

[125]   Yingjia Zhang, Zuohua Huang, Liangjie Wei, Jiaxiang Zhang, and Chung K Law. "Experimental and modeling study on ignition delays of lean mixtures of methane, hydrogen, oxygen, and argon at elevated pressures". In: *Combust. Flame* 159.3 (2012), pp. 918–931 (cit. on p. 40).

[126]   James A Miller, Robert J Kee, and Charles K Westbrook. "Chemical kinetics and combustion modeling". In: *Annu. Rev. Phys. Chem.* 41.1 (1990), pp. 345–387 (cit. on

pp. 44, 46).

[127] RJ Kee, FM Rupley, JA Miller, ME Coltrin, JF Grcar, E Meeks, HK Moffat, AE Lutz, G Dixon-Lewis, MD Smooke, et al. *CHEMKIN collection*. Tech. rep. Reaction Design Inc., San Diego, CA, 2000 (cit. on pp. 46, 90, 111, 114).

[128] Emma J Silke, Henry J Curran, and John M Simmie. "The influence of fuel structure on combustion as demonstrated by the isomers of heptane: a rapid compression machine study". In: *Proc. Combust. Inst.* 30.2 (2005), pp. 2639–2647 (cit. on p. 56).

[129] S Mani Sarathy, Tamour Javed, Florent Karsenty, Alexander Heufer, Weijing Wang, Sungwoo Park, Ahmed Elwardany, Aamir Farooq, Charles K Westbrook, William J Pitz, Matthew A Oehlschalaeger, Guillaume Dayman, Henry J Curran, and Philippe Dagaut. "A comprehensive combustion chemistry study of 2,5-dimethylhexane". In: *Combust. Flame* 161.6 (2014), pp. 1444–1459 (cit. on p. 56).

[130] Chunsheng Ji, S Mani Sarathy, Peter S Veloo, Charles K Westbrook, and Fokion N Egolfopoulos. "Effects of fuel branching on the propagation of octane isomers flames". In: *Combust. Flame* 159.4 (2012), pp. 1426–1436 (cit. on p. 56).

[131] S Mani Sarathy, Ulrich Niemann, Coleman Yeung, Ryan Gehmlich, Charles K West-brook, Max Plomer, Zhaoyu Luo, Marco Mehl, William J Pitz, Kalyanasundaram Seshadri, Murray J Thomson, and Tienfeng Lu. "A counterflow diffusion flame study of branched octane isomers". In: *Proc. Combust. Inst.* 34.1 (2013), pp. 1015–1023 (cit. on p. 56).

[132] Ning Liu, S Mani Sarathy, Charles K Westbrook, and Fokion N Egolfopoulos. "Ignition of non-premixed counterflow flames of octane and decane isomers". In: *Proc. Combust. Inst.* 34.1 (2013), pp. 903–910 (cit. on p. 56).

[133] Kieran Patrick Somers, John M Simmie, Henry Curran, and Wayne K Metcalfe. "The Pyrolysis of 2-Methylfuran: A Quantum Chemical, Statistical Rate Theory and Kinetic Modelling Study". In: *Phys. Chem. Chem. Phys.* (2014) (cit. on p. 56).

[134] John M Simmie and Henry J Curran. "Formation Enthalpies and Bond Dissociation

Energies of Alkylfurans. The Strongest C-X Bonds Known?" In: *J. Phys. Chem. A* 113.17 (2009), pp. 5128–5137 (cit. on pp. 57, 99, 103).

[135] John M Simmie, Kieran P Somers, Kenji Yasunaga, and Henry J Curran. "A Quantum Chemical Study of the Abnormal Reactivity of 2-Methoxyfuran". In: *Int. J. Chem. Kinet.* 45.8 (2013), pp. 531–541 (cit. on p. 58).

[136] H. K. Ciezki, G. Adomeit. "Shock-Tube Investigation of Self-Ignition of *n*-Heptane-Air Mixtures Under Engine Relevant Conditions". In: *Combust. Flame* 26 (1993), pp. 421–433 (cit. on pp. 59, 78).

[137] Hsi-Ping S Shen and Matthew A Oehlschlaeger. "The autoignition of C_8H_{10} aromatics at moderate temperatures and elevated pressures". In: *Combust. Flame* 156.5 (2009), pp. 1053–1062 (cit. on pp. 72, 73, 104).

[138] DL Baulch, CJ Cobos, RA Cox, P Frank, Go Hayman, Th Just, JA Kerr, T Murrells, MJ Pilling, J Troe, et al. "Evaluated kinetic data for combustion modeling. Supplement I". In: *J. Phys. Chem. Ref. Data* 23.6 (1994), pp. 847–848 (cit. on pp. 73, 84, 85).

[139] Marco Mehl, Olivier Herbinet, Patricia Dirrenberger, Roda Bounaceur, Pierre-Alexandre Glaude, Frédérique Battin-Leclerc, and William J Pitz. "Experimental and modeling study of burning velocities for alkyl aromatic components relevant to diesel fuels". In: *Proc. Combust. Inst.* 35.1 (2015), pp. 341–348 (cit. on p. 73).

[140] Jürgen Warnatz. "Rate coefficients in the C/H/O system". In: *Combustion chemistry*. Springer, 1984, pp. 197–360 (cit. on pp. 84, 85).

[141] Richard R Baker, Roy R Baldwin, and Raymond W Walker. "Addition of i-butane to slowly reacting mixtures of hydrogen and oxygen at 480 C". In: *J. Chem. Soc., Faraday Trans. 1* 74 (1978), pp. 2229–2251 (cit. on pp. 84, 85).

[142] W Müller-Markgraf and J Troe. "Thermal decomposition of ethylbenzene, styrene, and bromophenylethane: UV absorption study in shock waves". In: *J. Phys. Chem.* 92.17 (1988), pp. 4914–4922 (cit. on p. 84).

[143] Robert Shaw. "Semi-empirical extrapolation and estimation of rate constants for

abstraction of H from methane by H, O, HO, and O2". In: *J. Phys. Chem. Ref. Data* 7.3 (1978), pp. 1179–1190 (cit. on pp. 84, 85).

[144] Xuesong Wu, Qianqian Li, Jin Fu, Chenglong Tang, Zuohua Huang, Ritchie Daniel, Guohong Tian, and Hongming Xu. "Laminar burning characteristics of 2,5-dimethylfuran and *iso*-octane blend at elevated temperatures and pressures". In: *Fuel* 95 (2012), pp. 234–240 (cit. on pp. 89, 90).

[145] M. J. Frisch, G. W. Trucks, H. B. Schlegel, G. E. Scuseria, M. A. Robb, J. R. Cheeseman, G. Scalmani, V. Barone, B. Mennucci, G. A. Petersson, H. Nakatsuji, M. Caricato, X. Li, H. P. Hratchian, A. F. Izmaylov, J. Bloino, G. Zheng, J. L. Sonnenberg, M. Hada, M. Ehara, K. Toyota, R. Fukuda, J. Hasegawa, M. Ishida, T. Nakajima, Y. Honda, O. Kitao, H. Nakai, T. Vreven, J. A. Montgomery Jr., J. E. Peralta, F. Ogliaro, M. Bearpark, J. J. Heyd, E. Brothers, K. N. Kudin, V. N. Staroverov, R. Kobayashi, J. Normand, K. Raghavachari, A. Rendell, J. C. Burant, S. S. Iyengar, J. Tomasi, M. Cossi, N. Rega, J. M. Millam, M. Klene, J. E. Knox, J. B. Cross, V. Bakken, C. Adamo, J. Jaramillo, R. Gomperts, R. E. Stratmann, O. Yazyev, A. J. Austin, R. Cammi, C. Pomelli, J. W. Ochterski, R. L. Martin, K. Morokuma, V. G. Zakrzewski, G. A. Voth, P. Salvador, J. J. Dannenberg, S. Dapprich, A. D. Daniels, . Farkas, J. B. Foresman, J. V. Ortiz, J. Cioslowski, and D. J. Fox. *Gaussian 09 Revision D.01*. Gaussian Inc. Wallingford CT 2009 (cit. on pp. 102, 103).

[146] Alexander C. Davis and S. Mani Sarathy. "Computational Study of the Combustion and Atmospheric Decomposition of 2-Methylfuran". In: *J. Phys. Chem. A* 117.33 (2013), pp. 7670–7685 (cit. on p. 103).

[147] Harish Kumar Chakravarty and Ravi X Fernandes. "Reaction Kinetics of Hydrogen Abstraction Reactions by Hydroperoxyl Radical from 2-Methyltetrahydrofuran and 2,5-Dimethyltetrahydrofuran". In: *J. Phys. Chem. A* 117.24 (2013), pp. 5028–5041 (cit. on p. 103).

[148] James G Speight. *Environmental analysis and technology for the refining industry.*

Vol. 167. John Wiley & Sons, 2005 (cit. on p. 104).

[149] William J Pitz, Nicholas P Cernansky, Frederick L Dryer, FN Egolfopoulos, JT Farrell, DG Friend, and H Pitsch. *Development of an experimental database and chemical kinetic models for surrogate gasoline fuels*. Tech. rep. 2007-01-0175. SAE Technical Paper, 2007 (cit. on p. 104).

[150] Meredith Colket, Tim Edwards, Skip Williams, Nicholas P Cernansky, David L Miller, Fokion Egolfopoulos, Peter Lindstedt, Kalyanasundaram Seshadri, Frederick L Dryer, Chung K Law, Daniel Friend, David B Lenhert, Heinz Pitsch, Adel Sarofim, Mitchell Smooke, and Wing Tsang. "Development of an experimental database and kinetic models for surrogate jet fuels". In: *45th AIAA Aerospace Sciences Meeting and Exhibit*. 2007, pp. 8–11 (cit. on p. 104).

[151] Shane M Daley, Andrew M Berkowitz, and Matthew A Oehlschlaeger. "A shock tube study of cyclopentane and cyclohexane ignition at elevated pressures". In: *Int. J. Chem. Kin.* 40.10 (2008), pp. 624–634 (cit. on p. 104).

[152] Zhandong Wang, Zhanjun Cheng, Wenhao Yuan, Jianghuai Cai, Lidong Zhang, Feng Zhang, Fei Qi, and Jing Wang. "An experimental and kinetic modeling study of cyclohexane pyrolysis at low pressure". In: *Combust. Flame* 159.7 (2012), pp. 2243–2253 (cit. on p. 108).

[153] Zhandong Wang, Lili Ye, Wenhao Yuan, Lidong Zhang, Yizun Wang, Zhanjun Cheng, Feng Zhang, and Fei Qi. "Experimental and kinetic modeling study on methylcyclohexane pyrolysis and combustion". In: *Combust. Flame* 161.1 (2014), pp. 84–100 (cit. on p. 108).

[154] Zhandong Wang, Long Zhao, Yu Wang, Huiting Bian, Lidong Zhang, Feng Zhang, Yuyang Li, S Mani Sarathy, and Fei Qi. "Kinetics of ethylcyclohexane pyrolysis and oxidation: An experimental and detailed kinetic modeling study". In: *Combust. Flame* (2015) (cit. on p. 108).

[155] Edward R Ritter. "THERM: A computer code for estimating thermodynamic properties

for species important to combustion and reaction modeling". In: *J. Chem. Inform. Comput. Sci.* 31.3 (1991), pp. 400–408 (cit. on p. 108).

[156]   Dongil Kang, Gregory Lilik, Vernon Dillstrom, John Agudelo, Magín Lapuerta, Khalid Al-Qurashi, and André L Boehman. "Impact of branched structures on cycloalkane ignition in a motored engine: Detailed product and conformational analyses". In: *Combust. Flame* 162.4 (2015), pp. 877–892 (cit. on p. 108).

[157]   N Cohen. "Revised group additivity values for enthalpies of formation (at 298 K) of carbon–hydrogen and carbon–hydrogen–oxygen compounds". In: *J. Phys. Chem. Ref. Data* 25.6 (1996), pp. 1411–1481 (cit. on p. 108).

Vita

Author's Name: Mazen A. Eldeeb

Place of Birth: Giza, Egypt

Date of Birth: January 4, 1987

Degrees Awarded:

Bachelor of Science, Cairo University, 2008

Master of Science, Cairo University, 2010

Professional Experience:

Teaching and Research Assistant, Syracuse University, Department of MAE, 2012-2015

Assistant Lecturer, Cairo University, Department of Mech. Power Eng., 2010-2015

Research Assistant, The American University in Cairo, Department of Physics, 2009-2010

Teaching Assistant, Cairo University, Department of Mech. Power Eng., 2008-2010